MATERIAL BEHAVIOR OF MIXED FORMULATION SOLDERS

by

Nalini Kanth Kurumaddali

A thesis submitted to the Graduate Faculty of
Auburn University
in partial fulfillment of the
requirements for the Degree of
Master of Science

Auburn, Alabama
May 14, 2010

Keywords: Creep, Mixed Formulation Solders,
Sn-Pb Content, Temperature Dependent Tensile Properties

Approved by

Jeffrey C. Suhling, Chair, Quina Distinguished Professor of Mechanical Engineering
Pradeep Lall, Thomas Walter Professor of Mechanical Engineering
Michael J. Bozack, Professor of Physics

Abstract

The transition from tin-lead to lead free soldering in the electronics manufacturing industry has been in progress for the past 10 years. In the interim period before lead free assemblies are uniformly accepted, mixed formulation solder joints are becoming commonplace in electronic assemblies. For example, area array components (BGA/CSP) are frequently available only with lead free Sn-Ag-Cu (SAC) solder balls. Such parts are often assembled to printed circuit boards using traditional 63Sn-37Pb solder paste. The resulting "mixed" solder joints contain unusual quaternary alloys of Sn, Ag, Cu, and Pb. In addition, the alloy composition can vary across the solder joint based on the paste to ball solder volumes and the reflow profile utilized. The mechanical and physical properties of such Sn-Ag-Cu-Pb alloys have not been explored extensively in the literature. In addition, the reliability of mixed formulation solder joints is poorly understood.

In this work, the creep properties of mixed formulation solder materials were explored. Seven different mixture ratios of 63Sn-37Pb and SAC305 solder materials have been formed, which include five carefully controlled mixtures of the two solder alloys (by weight percentage) and the two extreme cases (pure Sn-Pb and pure SAC 305). For the various percentage mixtures, the melting point, pasty range, and creep curves have been characterized. The variations of the mechanical properties and creep rates with

aging at room temperature (25 ^{o}C) and elevated temperature (100 ^{o}C) have also been measured. Finally, the microstructures realized with the various mixtures have been studied for laboratory specimens and actual mixed formulation BGA solder joints. The results for the mechanical and physical properties show a very complicated dependence on the mixture ratio.

In a second study on microelectronic solders, the temperature dependent tensile properties of SAC 305 and 63Sn-37Pb solder have been measured over a wide temperature range from -175 ^{o}C to +150 ^{o}C. The extracted material properties exhibit a linear variations with temperature, and lead free SAC 305 solder was found more sensitive to variations in temperature than Sn-Pb solder. This data provides the baseline input properties for finite element simulations of electronic packages.

Acknowledgements

I would like to acknowledge my deep and sincere gratitude towards my advisor Dr. Jeffrey C. Suhling, for his immense support, patience and continuous encouragement. Sincere gratitude and appreciation are also extended to my committee members, Dr. Pradeep Lall and Dr. Michael Bozack, for their invaluable guidance and help during the course of this study. The author acknowledges and extends gratitude for financial support received from the NSF Center for Advanced Vehicle and Extreme Environment Electronics (CAVE^3).

I would also like to express my deep gratitude and gratefulness to my father Mr. Kurumaddali Jagan Mohan Rao, mother Mrs. Kurumaddali Padma Priya, and my brother Mr. Kurumaddali Naveen for their love and support. I thank Dr. Hongtao Ma for passing on his knowledge and guidance in data collection and analysis. I have collaborated with many colleagues during this work, I want to acknowledge their support and friendship special and sincere thanks go to Mr. Yifei Zhang for his continuous help and support during this work. I also want to thank my co-workers Zijie Cai, Chang Lin, and Jordan Roberts.

Table of Contents

List of Tables

List of Figures

CHAPTER 1

INTRODUCTION

1.1 Electronic Packaging

Electronic Packaging is the art (based on science) of establishing interconnections between various levels of electronic devices, components, modules and systems. Packaging of electronics refers to the placement and connection of many electronic and electromechanical components in an enclosure that protects the system from the environment and provides easy access for routine maintenance. Packaged electronics consists of the active components (e.g. Integrated Circuit (IC) chips, displays, loudspeakers etc.), which are interconnected, supplied with electric power, and housed in a system. Functions of electronic packaging include signal distribution, power distribution, heat dissipation, protection (mechanical, chemical, electromagnetic).

1.2 Electronic Packaging Hierarchy

Figure 1.1 shows the hierarchy of electronic packaging. The bare silicon chip is at the zeroth level. The silicon chip consists of electronic devices (example: transistors and resistors) that are connected in a pattern to form an IC that performs a desired function.

The chip carrier is the first level of packaging and the interconnections of the chip carrier are referred to as the first level interconnects. The second level of packaging is the Printed Circuit Board (PCB), which contains several first level packages assembled onto it. The third level of packaging is the motherboard, which incorporates the connection between PCBs. The fourth level of packaging is the connection between two subassemblies.

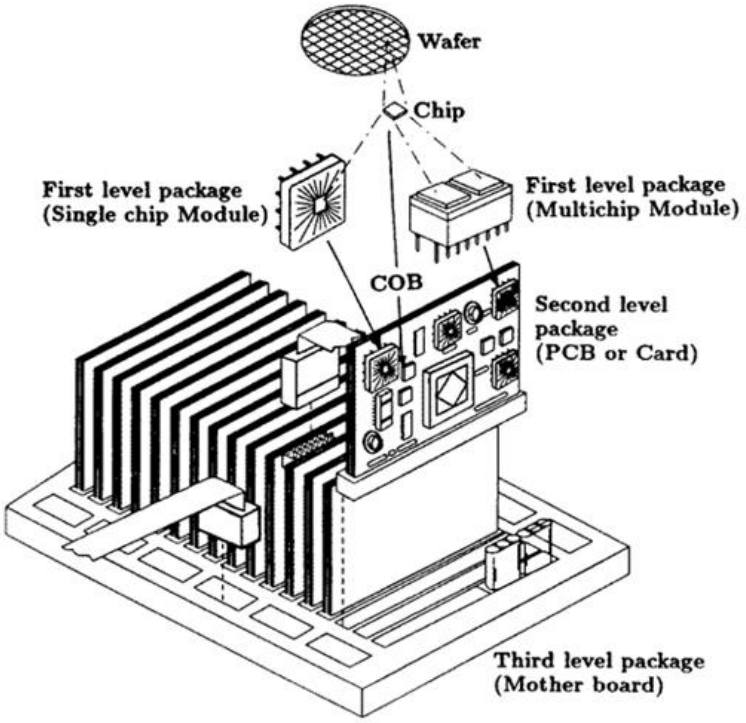

Figure 1.1 - Hierarchy of Electronic Packaging

There are two technologies available for mounting components on printed circuit board, Plated Through Hole (PTH) and Surface Mount Technology (SMT). In surface

mount technology the components are directly mounted on the printed circuit board (PCB). This technology has largely replaced the plated through hole (PTH) in the recent years. The advantages of SMT over through hole are reliable assemblies at reduced weight, volume and cost, whereas the plated through hole (PTH) technology provides more robust and strong mechanical bonds compared to SMT.

1.3 Lead-Free Solders in Electronics

Solder joints provide both electrical and mechanical connection in electronic packaging modules. Eutectic or near eutectic (Sn-Pb) solder has been the predominant choice of solders in electronics industry due to its outstanding solderability and reliability. However, legislation that mandates the banning of lead in electronics has been actively pursued worldwide during the last 15 years due to the environmental and health concerns. Although the implementation deadlines and products covered by such legislation continue to evolve, it is clear that laws requiring conversion to lead-free electronics are becoming a reality.

A large number of research studies are currently underway in the lead-free solder area. Although no “drop in” replacement has been identified for all applications; Sn-Ag, Sn-Ag-Cu (SAC), and other alloys involving elements such as Sn, Ag, Cu, Bi, In, and Zn have been identified as potential replacements for standard 63Sn-37Pb eutectic solder [Zhang 2009]. Several SAC alloys have been the proposed by various user groups and industry experts. These include 96.5Sn-3.0Ag-0.5Cu (SAC305), 95.5Sn-3.8Ag-0.7Cu (SAC387), 95.5Sn-3.9Ag-0.6Cu (SAC396) and 95.5Sn-4.0Ag-0.5Cu (SAC405). For enhanced reliability during high strain rate exposures (e.g. shock and drop), several alloys

with lower silver content have been recommended including 98.5Sn-1.0Ag-0.5Cu (SAC105) and 99Sn-0.3Ag-0.7Cu (SAC0307) [Suh 2007]. The main benefits of the various SAC alloy systems are their relatively low melting temperatures (217^{o}C) compared with the 96.5Sn-3.5Ag (221^{o}C) binary eutectic alloy, as well as their superior mechanical and solderability properties when compared to other lead free solders.

1.4 Mixed Formulation Solders

Even though many countries have stated deadlines for the completion of the tin-lead to lead free soldering transition, many critical issues have not been resolved due to the incomplete infrastructure for lead free soldering technology, as well as the timing and technical readiness in the various sectors of the electronics manufacturing industry. Therefore, companies often face an interim period of "mixed assembly" where lead free components are used with tin-lead solder paste, or tin-lead plated components or printed circuit boards are used with lead-free solder paste. The presence of so-called "mixed formulation" solder joints or "mixed solders" is often unavoidable due to unavailability of components with the desired finish or careless suppliers providing components that do not meet the specifications of the manufacturer doing the SMT assembly.

There are two kinds of mixed assemblies defined by the conditions that the solder balls, platings, and pastes are combined [Nandagopal 2006, Evans 2005, Handwerker 2005, Hua 2005, Kannabiran 2006, McCormick 2006]. When the older "standard" Sn-Pb pastes and processes are mixed with components with SAC solder balls or component leads with SAC finishes, the process is referred to as a "backward compatible" process (see Figure 1.2). Likewise, when SAC pastes and processes are mixed with components

with Sn-Pb solder balls or components/PCBs with Sn-Pb surface finishes, the process is referred to as a “forward compatible” process.

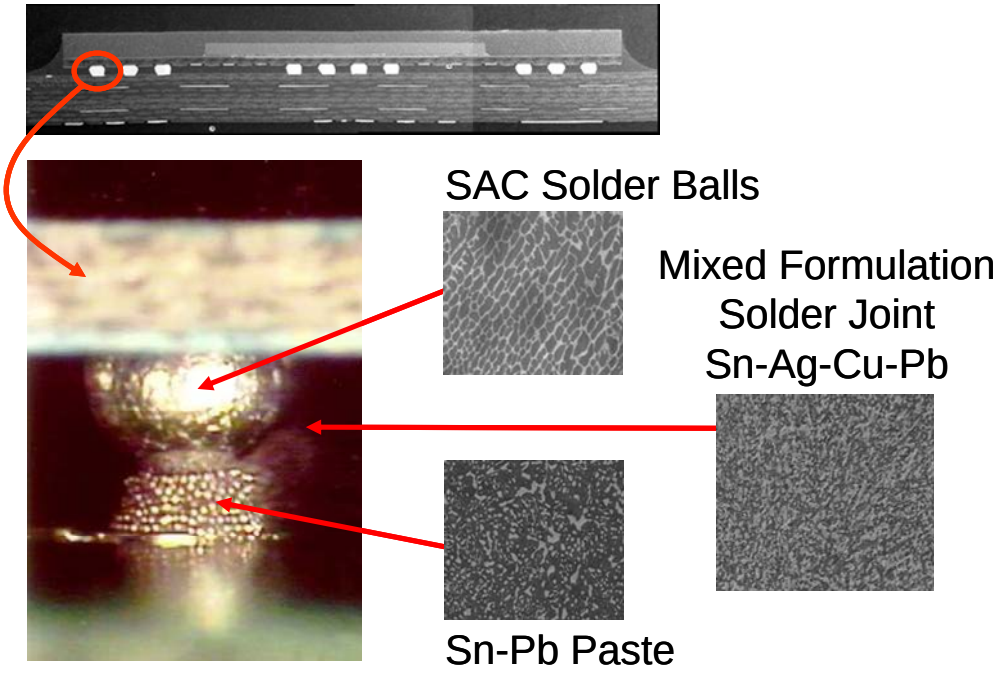

Figure 1.2 - Mixed Assembly (Backward Compatibility)

The metallurgical reaction of Sn-Ag-Cu and Sn-Pb is a secondary alloying process and two different micro-structural scenarios typically result: (1) fully-mixed joint, and (2) partially mixed joint. There is a 34 °C temperature difference between the melting temperature of the Sn-Ag-Cu system (217 °C) and the melting temperature of the Sn-Pb system (183 °C). The homogeneity of a mixed Pb and Sn-Ag-Cu structure is driven by Pb diffusion in the solder joint and determined by such factors as Pb concentration, peak reflow temperature and dwell time, soldering environment, and lead-

free solder composition [Abtew 2006]. For example, SEM microstructures of cross-sectioned mixed formulation BGA solder joints that are well mixed and poorly mixed are shown in Figures 1.3 and 1.4, respectively. In these cases, the degree of mixing was controlled by adjusting the peak reflow temperature and the dwell at the peak temperature. Further examples of poor mixing can be found in the literature [Chatterji 2006, Zbrzezny 2006, Hillman 2005].

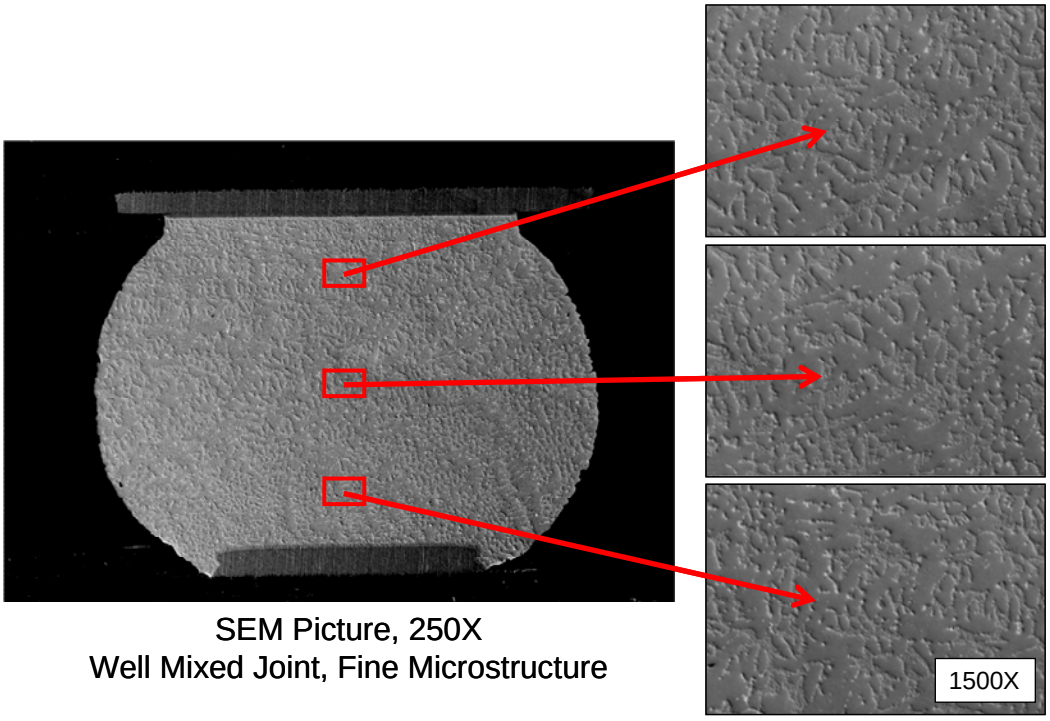

Figure 1.3 - SEM Micrograph of Well-Mixed BGA Joint

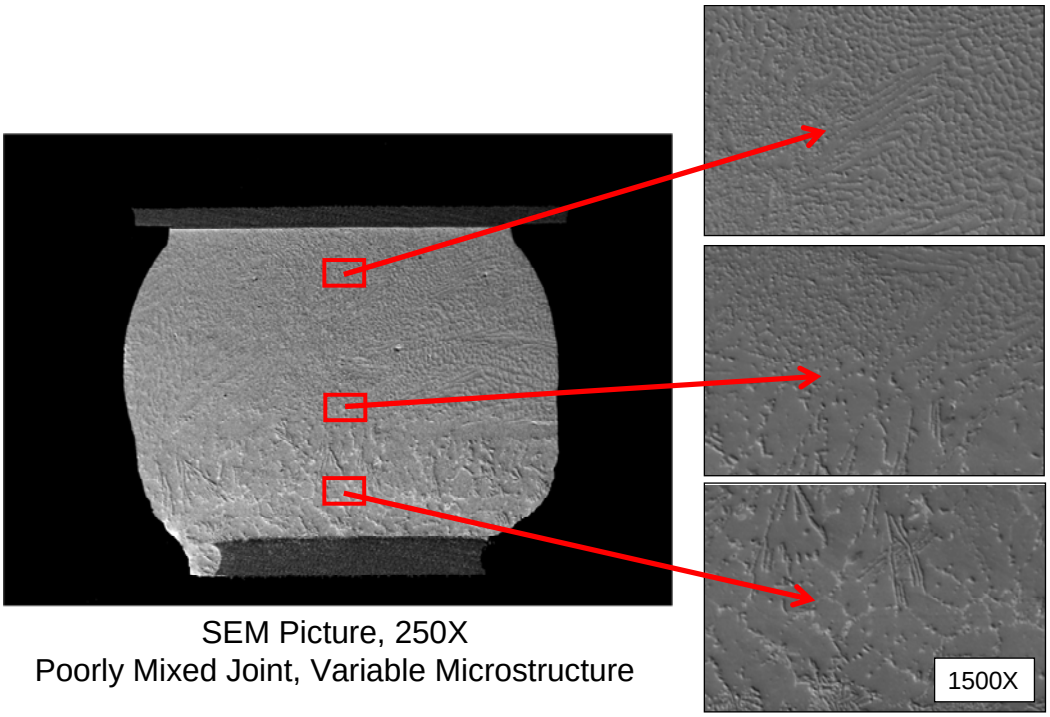

Figure 1.4 - SEM Micrograph of Poorly Mixed BGA Joint

1.5 Mechanical Properties of Solders

Solder joints provide electrical and mechanical connection in electronic packages, and the mechanical properties of solders are of paramount importance in producing reliable products. In assessing the mechanical properties of solders, creep and tensile properties are of particular interest and have been extensively investigated.

1.5.1 Tensile Properties

Tensile properties are generally determined by stress-strain curves. In practice engineering stress and engineering strain are described as follows [Hertzberg 1996]:

$$\sigma = \frac{P}{A_0} \tag{1.1}$$

$$\varepsilon = \frac{l_f - l_o}{l_o} \tag{1.2}$$

where P is the load, A_o is the initial cross-sectional area, l_f is the final gage length and l_o is the initial gage length.

A typical tensile stress-strain curve for solder with labeled standard material properties is shown in Figure 1.5. The notation "E" is taken to be the effective elastic modulus, which is the initial slope of the stress-strain curve. In the elastic region, the engineering stress is linear, with engineering strain in conformance to Hooke's law as follows [Thornton 1985]:

$$\sigma = E\varepsilon \tag{1.3}$$

The yield stress σ_Y (YS) is taken to be the standard .2% yield stress (upon unloading, the permanent strain is equal to $\varepsilon = .002$). Finally, the ultimate tensile strength σ_u (UTS) is taken to be the maximum stress realized in the stress-strain data.

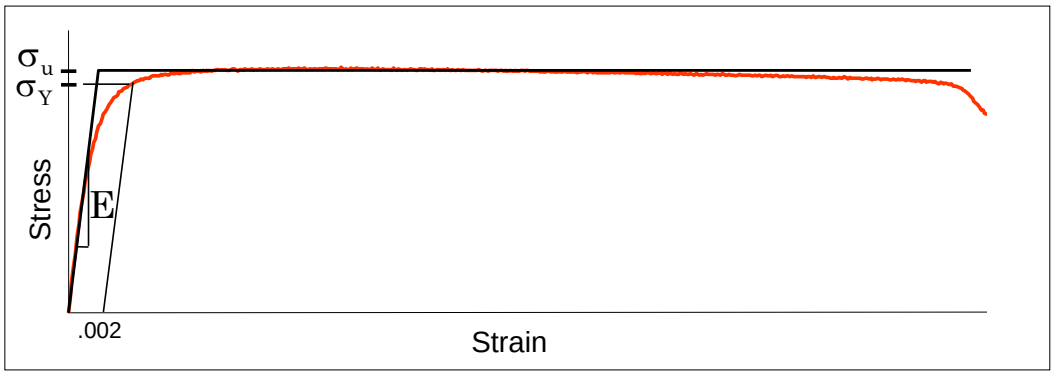

Figure 1.5 - Typical Solder Stress-Strain Curve

1.5.2 Creep

Creep generally refers to the time-independent strain plastic deformations at constant uniaxial stress [Garofalo 1966]. Creep deformation tends to be rapid when the homologous temperature is above 0.5 T_m. The homologous temperature is the ratio of the temperature of the material and its melting temperature in degrees Kelvin [Cadek 1988].

$$T_h = \frac{T}{T_m} \tag{1.4}$$

The homologous temperature is an empirical value. When T_h is greater than 0.5 T_m, creep deformations will be the dominate deformation mode in metallic materials [Cadek 1988]. Figure 1.6 shows a typical creep curve, which generally consists of three stages after the initial instantaneous strain when a constant load is applied [Garofalo 1966]. The initial strain may consist of elastic or time-independent plastic deformation as soon as load is applied. In the first stage, which is referred to as primary creep, the strain rate decreases rapidly over time. This is caused by work hardening, which restricts the deformation. The secondary stage, or steady-state creep region is typically characterized by a very long duration of nearly constant slope. This slope is referred to as the "steady state" secondary creep rate or creep compliance, and it is often used by practicing engineers as one of the key material parameters for solder in finite element simulations used to predict solder joint reliability. In this stage, the strain rate is retarded by strain-hardening, which decreases the deformation speed, while the associated recovery and recrystallization (softening) tend to accelerate the creep rate [Hertzberg 1996]. The third stage is Tertiary creep, where nucleation and growth of cavities has been induced

[Garofalo 1966]. Necking and micro-cracking will subsequently occur, which will eventually lead to creep rupture of the specimen.

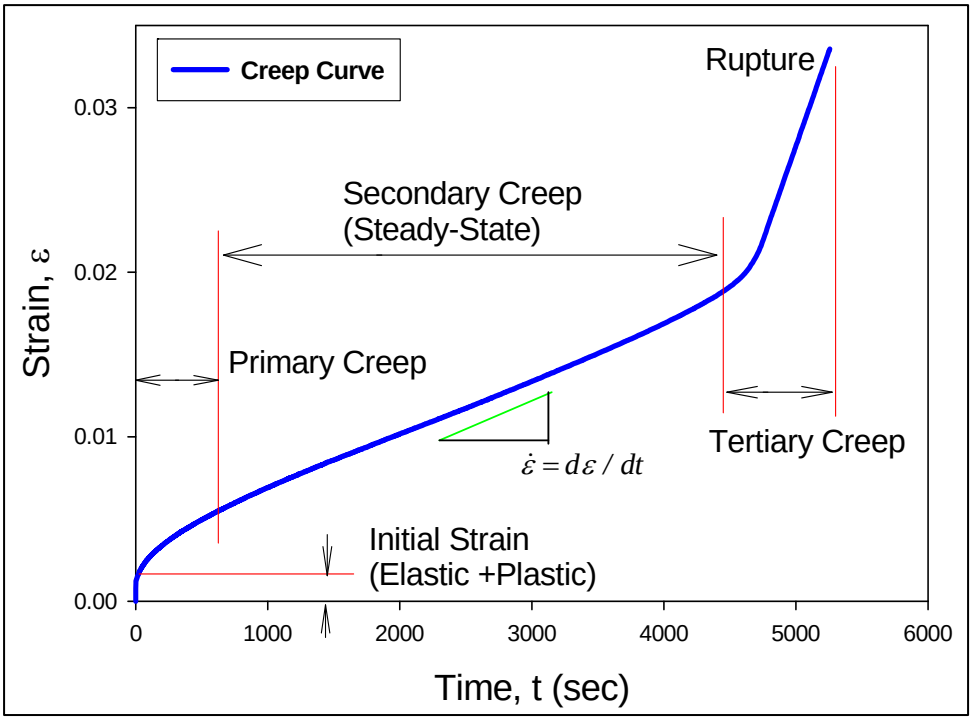

Figure 1.6 - Typical Creep Curve

1.6 Creep of Solders

Electronic packaging components are under constant stress due to continuous CTE (Coefficient of Thermal Expansion) mismatches in packaging modules. Creep deformation is one of the dominant deformation modes that cause failure modes solder joints, due to its high homologous temperature [Ma 2009]. Solders have a very high homologous temperature, even at room temperatures. The T_h of eutectic 63Sn-37Pb is 0.65 T_m at room temperature (T_m = 183 ^oC), while the T_h of SAC305 alloy is at 0.61T_m at room temperature (T_m = 217 ^oC). Both of these homologous temperatures are well above 0.5T_m, and are considered "hot". Consequently, solder alloys will undergo significant creep even at room temperature. In actual electronic applications, where the operating temperatures are typically in the range of -40 to 125 ^oC, eutectic Sn-Pb solder is at 0.51-0.87T_m, while SAC305 solder is at 0.48-0.81T_m. Both of these ranges are within the rapid creep deformation range when the devices are under stress.

1.7 Thesis Organization

Chapter 2 presents a detailed literature review on reliability of mixed formulation solders, the processing conditions which influence the formation of mixed solder joints, the effects of lead content on performance of mixed formulation solder joints. The effects of thermal aging on solder material behavior has also been discussed. In Chapter 3 the experimental procedure followed for uniaxial preparation is described, and the Micro-Testing machine is introduced. The test matrix of experiments performed and empirical model to average the experimental measurements have also been described in detail.

In Chapter 4, the physical properties of mixed formulation solders formed have been presented. The microstructure, tensile, and creep properties, and the effects of aging on creep rates of mixed formulation solders are discussed. Chapter 5 gives detailed insight into the temperature dependent tensile properties of SAC 305 and 63Sn-37Pb solders. Chapter 6 summarizes the entire study and offers conclusions.

CHAPTER 2

LITERATURE REVIEW

2.1 Introduction

Solder joint fatigue is one of the predominant failure mechanisms in electronics exposed to thermal cycling and steady state conditions. Reliable, consistent, and comprehensive solder constitutive equations and material properties are needed for use in mechanical design, reliability assessment and process optimization. There are numerous technical research reports and articles in the area mechanical characterization of lead-free solders, however very little work has been published on physical and mechanical properties of mixed formulation solders.

2.2 Mixed Formulation Solders

Ever since the European Union initiated the ban of Lead in electronic products, there has been a steady transformation in the electronics industry from conventional SnPb solder to Pb-free. As the transformation is progressing steadily, an interim stage characterized by mixed application of tin-lead and lead free solders has been widely acknowledged within the industry. This interim stage has been prevalent because of several reasons. First of all, some area array packages are now manufactured

with only SAC solder balls, with no Sn-Pb versions available. As a result, it has become necessary to integrate SAC balled area array components onto tin/lead assemblies [McCormick 2006]. Secondly, processing and reliability issues with Pb-free manufacturing have forced exemption of certain product categories from the legislations banning the use of lead. These include electronic products designed to meet long-term field reliability or survive harsh environments such as those used in telecommunications, military, avionics, and high-end computer servers. These exemptions have been incorporated into ROHS directive to allow more time to understand and characterize the long-term reliability of Pb-free interconnect technologies and minimize any potential impacts to critical, high reliability product applications [Nandagopal 2005].

2.3 Reliability of Mixed Formulation Solders

Maintaining solder joint reliability is the key challenge in the transition to lead free, and questions always occur when the mixing of tin-lead and lead free materials and processes occur. Contradictory research results regarding mixed soldering have been found in the literature [Chatterji 2006]. Some studies have showed enhanced mechanical properties and reliabilities in solder joints formed by mixing Sn-Ag-Cu and Pb, whereas other studies reported deteriorated performance. Two topics that are often debated include: (1) the minimum peak temperature and dwell time above liquidous (TAL) required for reliable backward assembly, and (2) the best methods to achieve optimal homogeneity and reliability of mixed solder joints. High peak temperatures are usually used in reflowing lead-free solder joints due to the high SAC melting temperature in

order to obtain a homogenous microstructure. However, high reflow temperatures will often cause assembly challenges and reliability concerns.

Hua, et al. [Hua 2001, 2005] have concluded that reliability and process risks are high for backward solder joints formed with a reflow profile with peak temperature less than 217 °C. Low reflow peak temperatures resulted in inhomogeneous microstructures and partially collapsed Sn-Ag-Cu solder balls. The same phenomenon was also observed by Zbrzezny, et al. [Zbrzezny 2006]. Theuss and coworkers [Theuss 2003] further stated that a peak temperature of at least 235 ºC is needed to obtain acceptable reliability of backward compatible solder joints. On the contrary, Nandagopal, et al. [Nandagopal 2005, 2006] found that backward solder joints with fully mixed microstructure could be achieved with a peak reflow temperature of about 210 °C with 20-30 second dwell times, for certain paste to ball weight ratios. Nguyen, et al. [Nguyen 2007] found that complete mixing of SnPb solder with SnAgCu depends on the volume of the SnPb solder paste relative to that of the SnAgCu ball, and the soldering temperature. They concluded that proper mixing can result for reflow temperatures below 217 ºC if the right amount of SnPb solder paste is used. Finally, Sun and coworkers [Sun 2006], reported good reliability and relatively homogenous microstructure with reflow peak temperatures between 183-220 ºC.

Several other investigations on backward compatibility processes have been undertaken including: (1) evaluating Pb diffusion and the phases formed in solder mixtures containing Sn-Pb and Sn-Ag-Cu alloys [Chung 2002, Hunt 2002]; (2) evaluation of the reliability of mixed solder joints for various components under different accelerated thermal cycling environments [Evans 2005, Kannabiran 2006, McCormick

2006, Bath 2005, Clech 2004]; (3) measurement of the properties and failure modes of mixed solder joints under mechanical and shock loadings [Bath 2005, Nguyen 2006, Choubey 2006]; and (4) use of finite element analysis to predict mixed solder joint reliability [Jiang 2007].

2.4 Influence of Pb Content on Reliability of Mixed Solder Joints

Abtew, et. al. [Abtew 2006] have experimentally investigated the effects of Pb content and inert atmosphere reflow conditions on the mechanical strength and fatigue resistance of joints formed with mixing Sn-Ag-Cu and Pb. Their study suggested that solder joints with 10% Pb content by weight had the lowest shear strength. Appreciable increase in strength was found when the Pb content of the joints was increased beyond 15%. Oliver, et. al. [Oliver 2002] and Wable, et. al. [Wable 2005] have explained that at low lead concentration, 5% wt or less, the Pb will exist as a larger Pb phases located in the last solidified inter-dendritic regions unevenly distributed throughout the joint as shown in Figure 2.1. This uneven distribution of lead in the Sn/Ag/Cu system forms an inhomogeneous microstructure which is susceptible to inhomogeneous deformation under stress. The low shear strength for low lead concentrations (10% wt or less), is likely the result of the formation of this inhomogeneous microstructure. When Pb concentration in the mixed the solder joints is increased to 20%, the Pb was found to be evenly distributed throughout the solder joint and exhibited finer macrostructure as shown in Figure 2.1.

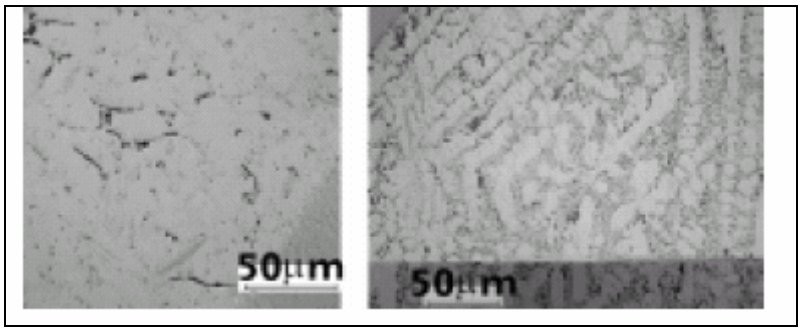

Figure 2.1 - Microstructure of Mixed Solder Joints with 5% (left) and 20% (right) Pb concentration [Oliver 2002]

Abtew, et. al. [Abtew 2006], Kime, et. al. [Kim 2004], and Watanabe, et. al. [Wtanabe 1998] have explained the effect of Pb distribution on fatigue mechanisms in mixed solder joints. When low concentrations of Pb are present, the small amounts of Pb precipitates tend to reside at energetically favorable locations near grain boundaries. This interface of the Sn grain and Pb phase is weak, and can be a potential crack initiation site when solder joints are subjected to cyclic stress. Seeling, et. al. [Seeling 2002] and Zbrzezny, et. al. [Zbrzezny 2006] have found that lead rich phases tend to accumulate at the interfaces in mixture solders as they represent the last areas to cool. Such an inhomogeneous Pb distribution offers a very convenient path for crack propagation, especially when lead forms a continuous layer just above the intermetallic layer.

2.5 Effects of Thermal Aging on Solder Joint Reliability

The microstructure, mechanical response, and failure behavior of lead free solder joints in electronic assemblies are constantly evolving when exposed to isothermal aging and/or thermal cycling environments [Hsuan 2007, Xiao 2004a and 2004b, Ding 2004

and 2007, Pang 2004, Darveaux 2005, Wiese 2007, Dutta 2005, Medvedev 1956, Lampe 1976, Miyazawa 1999 and 2001, Chilton 1989, Gagliano 1999, Coyle 2000, Tsui 2002, Lee 2002, Hasegawa 2001, Li 2002, Chou 2002, Law 2004, Chiu 2004, Ding 2004, Ma 2006 and 2007 and 2008, and Zhang 2008 and 2009]. The observed material behavior variation during thermal aging/cycling is universally detrimental to reliability and includes reductions in stiffness, yield stress, ultimate strength, and strain to failure, as well as highly accelerated creep. Such aging effects are greatly exacerbated at higher temperatures typical of thermal cycling qualification tests. However, significant changes occur even with aging at room temperature [Xiao 2004a and 2004b, Pang 2004, Darveaux 2005, Medvedev 1956, Lampe 1976, Miyazawa 1999 and 2001, Chilton 1989, Gagliano 1999, Coyle 2000, Tsui 2002, Lee 2002, Chiu 2004].

As early as 1956, Medvedev [Medvedev 1956] observed a 30% loss of tensile strength for bulk solder Sn/Pb solder stored for 450 days at room temperature. In addition, he reported 4-23% loss of tensile strength for solder joints subjected to room temperature storage for 280-435 days. In 1976, Lampe [Lampe 1976] found losses in shear strength and hardness of up to 20% in Sn-Pb and Sn-Pb-Sb solder alloys stored for 30 days at room temperature. Miyazawa, et. al. [Miyazawa 1999 and 2001] measured significant hardness losses and microstructural coarsening for Sn-Pb, Sn-Ag, and Sn-Zn eutectic solders stored at 25 °C for 1000 hours, while Chilton, et. al. and [Chilton 1989] observed a 10-15% decrease in fatigue life of single SMD joints after room temperature aging. Several studies [Gagliano 1999, Coyle 2000, Tsui 2002, Lee 2002] have also documented the degradation of Sn-Pb and SAC solder ball shear strength (10-35%) in area array packages subjected to room temperature aging.

The effects of room temperature aging on the mechanical properties and creep behavior of SAC alloys have been extensively discussed by Ma, et. al. [Ma 2006, 2007, 2008, 2009] and Zhang, et. al. [Zhang 2008 and 2009]. Zhang, et. al. [Zhang 2008,2009] have further showed the effects of aging on mechanical behavior of lead free solders by performing creep tests on four different SAC (SAC105, SAC205, SAC305, SAC405) alloys that were aged for various durations (0-6 months) at different temperatures (25, 50, 75, 100 and 125 ^{o}C). Analogous tests were performed with Sn-Pb solders for comparison purposes. The results indicated a significant increase in creep rates of lead free solders, and the effects of aging were more pronounced at aging temperatures above 50 ^{o}C. The recorded data also demonstrated that the creep rates of lead free solders experience a "cross over point" where lead free solder begins to creep at higher rates than standard 63Sn-37Pb solder for the same stress level. The cross over points were observed for all the SAC alloys and for all aging temperatures except room temperature (25 ^{o}C).

In addition, they have also examined the effects of aging for doped SAC alloy (SACX consisting of SAC0307+0.1%Bi) and compared it with SAC105 and SAC205. The recorded results indicated that, without aging the creep rates for solders were ordered in the manner:

$$\dot{\varepsilon}_{SACX} > \dot{\varepsilon}_{SAC105} > \dot{\varepsilon}_{SAC205} \quad \text{(no aging)} \tag{2.1}$$

However, as the aging progressed the creep rates get ordered as:

$$\dot{\varepsilon}_{SACX} > \dot{\varepsilon}_{SAC105} > \dot{\varepsilon}_{SAC205} \quad \text{(with aging)} \tag{2.2}$$

2.6 Effects of Temperature and Strain Rate on Tensile Properties

Mechanical properties are temperature and strain rate dependent for most metal alloys, especially for metals with low melting temperature and high homologous temperatures. High temperatures induce transitions in macroscopic fracture, and these transitions parallel the changes in the strength and ductility of materials [Hertzberg 1996]. Materials lose strength at higher temperatures. Hertzberg stated that the material strength increases with the testing strain rate, following a form similar to Holloman's Equation [Hertzberg 1996]:

$$\sigma = C\dot{\varepsilon}^m \tag{2.3}$$

where m is the strain-rate sensitivity factor, or strain hardening exponent; $\dot{\varepsilon}$ is the strain rate; C is the material constant; and σ is the stress.

Solder alloys possess very high homologous temperatures. The properties of solder alloys are strongly dependent on both the temperature and strain rate. Jones, et al. have observed an approximately linear relationship between the strength and temperature [Jones 1997a and 1997b]:

$$\sigma = \alpha T + \beta \tag{2.4}$$

where α is temperature strengthening coefficient; β is the strength at 0 °C in MPa, and T is the testing temperature in °C. Pang [Pang 1998] and Shi [Shi 1999] have observed similar experimental results, with a near linear relationship with temperature and a power law relation (Eq. 2.3) with the strain rate. Several other studies have also observed similar material behavior for both Sn-Pb eutectic and lead-free solder alloys [Nose 2003, Plumbridge 1999, Lang 2005, Dai 2001].

2.7 Summary

A survey of the literature has shown that much of the research in the mixed formulation solder area has focused on developing the conditions appropriate for the processing of mixed solder joints, understanding the composition of the solder joints obtained by reflowing Sn-Ag-Cu solder balls with Pb-Sn solder paste in certain fixed mass ratios, and evaluating the reliability of these mixed solder joints in thermo-mechanical and shock testing. Some studies suggest that mixed solder joints have lower reliability relative to lead free solder joints, but the conclusions depend very much on the details of the joint, processing and testing conditions. The key issue that has to be addressed is the lack of understanding of the fundamental mechanical and physical properties, and the effect of Pb content on the deformation behavior of mixed solder joints. In this work, the basic physical properties and mechanical behavior of mixed formulation solder materials were explored. Seven different mixture ratios of 63Sn-37Pb and SAC305 solder materials have been formed, which include five carefully controlled mixtures of the two solder alloys (by weight percentage) and the two extreme cases (pure Sn-Pb and pure SAC). For the various percentage mixtures, the melting point, pasty range, and creep curves have been characterized. The variations of the creep rates with aging at room temperature (25 ^{o}C) and elevated temperature (100 ^{o}C) have also been measured. Finally, the microstructures realized with the various mixtures have been studied for laboratory specimens and actual mixed formulation BGA solder joints.

There has also been very little work published in the literature on extreme low temperature behavior of solders. In a second solder study in this work, the tensile

properties of two solder alloys (Sn-Pb and SAC 305) have been explored over a wide temperature range from -175 ^{o}C to +150 ^{o}C.

CHAPTER 3

EXPERIMENTAL PROCEDURE

3.1 Uniaxial Test Sample Preparation Procedure

The solder samples used in this study were prepared in a rectangular cross-section glass tubes using a vacuum suction process. The solder is first melted in a quartz crucible using a pair of circular heating elements (see Figure 3.1). A thermocouple attached on the crucible and a temperature control module is used to direct the melting process. One end of the glass tube is inserted into the molten solder, and suction is applied to the other end via a rubber tube connected to the house vacuum system. The suction forces are controlled through a regulator on the vacuum line so that only a desired amount of solder is drawn into the tube. The specimens were then cooled to room temperature by a user selected cooling profile.

In order to observe the extreme variations possible in the mechanical behavior and microstructure, a large spectrum of cooling rates can be explored including water quenching of tubes (fast cooling rate), air cooling with natural and forced convection (slow cooling rates), and controlled cooling using a surface mount technology solder reflow oven. Typical temperature versus time plots for water quenching and air cooling of the test samples are shown in Figure 3.2. For the reflow oven controlled cooling, the

solder in the tubes is first cooled by water quenching, and then sent through a reflow oven (9 zone Heller 1800EXL) to re-melt the solder in the tubes and subject them to the desired temperature profile. Thermocouples are attached to the glass tubes and monitored continuously using a radio-frequency KIC temperature profiling system to ensure that the samples are formed using the desired temperature profile, to match that of the actual solder joints. Figure 3.3 illustrates the reflow temperature profiles used in this work for the SAC and Sn-Pb solder specimens.

3.2 Preparation of Mixed Formulation Solders

Solders with seven different mixture ratios of 63Sn-37Pb and SAC305 solder materials have been formed. Two of these were the pure solder alloys (63Sn-37Pb and SAC305), and five were mixtures controlled by the weight percentages of the two alloys. In this work, the mixed solder alloys are referred with nomenclature MIX A-B, where A and B are the weight percentages of 63Sn-37Pb and SAC305, respectively, in the mixture. For example, MIX 30-70 is a solder mixture of 30% wt 63Sn-37Pb and 70% wt SAC305. The chemical compositions of the seven solder alloys are listed in table 3.1. Since the melting temperatures of all the mixed alloys are quite different, a water quenching cooling profile was used during the specimen preparation (see Figure 3.2).

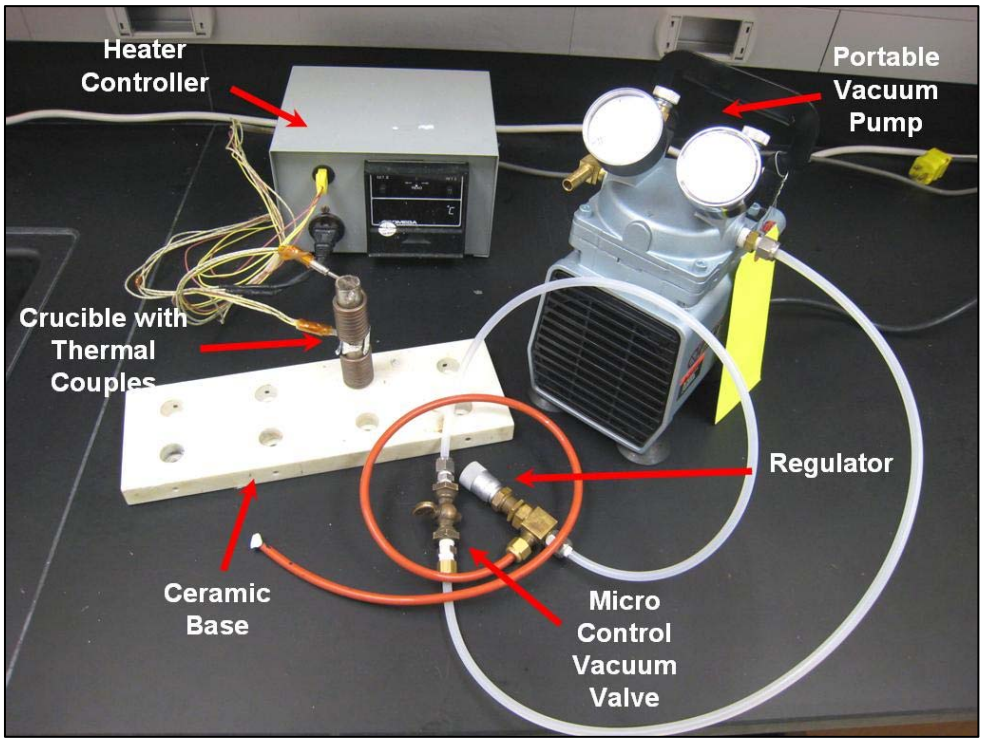

Figure 3.1 - Specimen Preparation Hardware

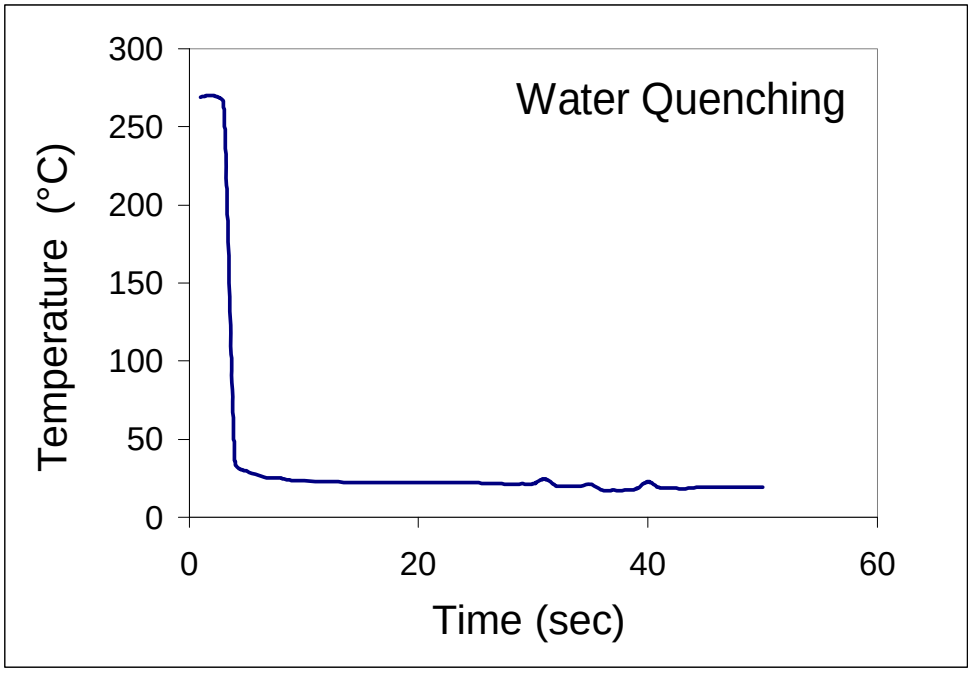

Figure 3.2 - Sample Cooling Profiles

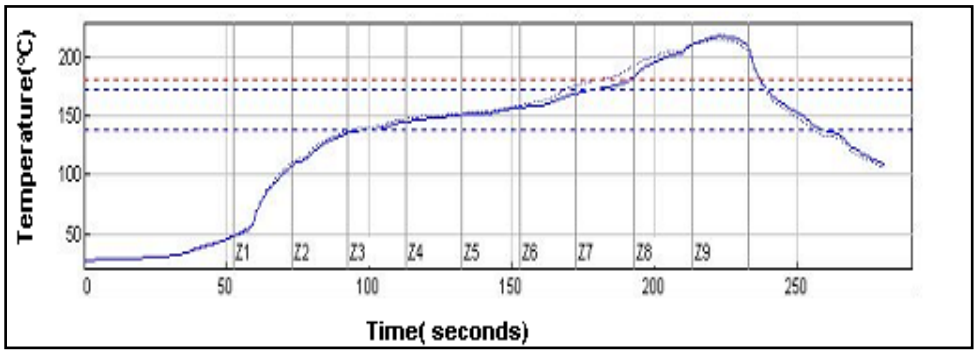

(a) Sn-Pb

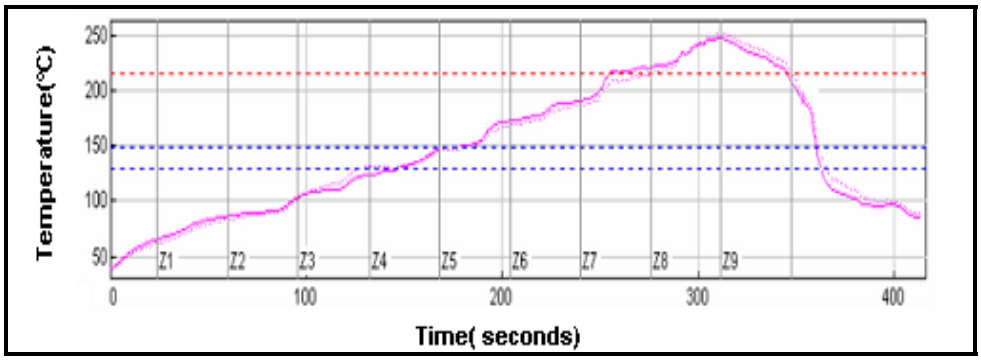

(b) SAC 305

Figure 3.3 - Solder Reflow Temperature Profiles

Solder Type	%Sn	%Pb	%Ag	%Cu
MIX 0-100 (SAC305)	96.50	0	3.00	0.50
MIX 10-90	93.15	3.70	2.70	0.45
MIX 30-70	86.45	11.10	2.10	0.35
MIX 50-50	79.75	18.50	1.50	0.25
MIX 70-30	73.05	25.90	0.90	0.15
MIX 90-10	66.35	33.30	0.30	0.05
MIX 100-0 (63Sn-37Pb)	63.00	37.00	0	0

Table 3.1 - Composition of Mixed Formulation Solder alloys

Typical glass tube assemblies filled with solder and a final extracted specimen are shown in Figure 3.3. For some cooling rates and solder alloys, the final solidified solder samples can be easily pulled from the tubes due to the differential expansions that occur when cooling the low CTE glass tube and higher CTE solder alloy. Other options for more destructive sample removal involve breaking the glass or chemical etching of the glass. The final test specimen dimensions are governed by the useable length of the tube that can be filled with solder, and the cross-sectional dimensions of the hole running the length of the tube. In the current work, uniaxial samples with nominal dimensions of 80 x 3 x 0.5 mm were formed. A thickness of 0.5 mm was chosen because it matches the height of typical BGA solder balls. The specimens were stored in the aging oven immediately after solidification and water quenching to eliminate possible room temperature aging effects.

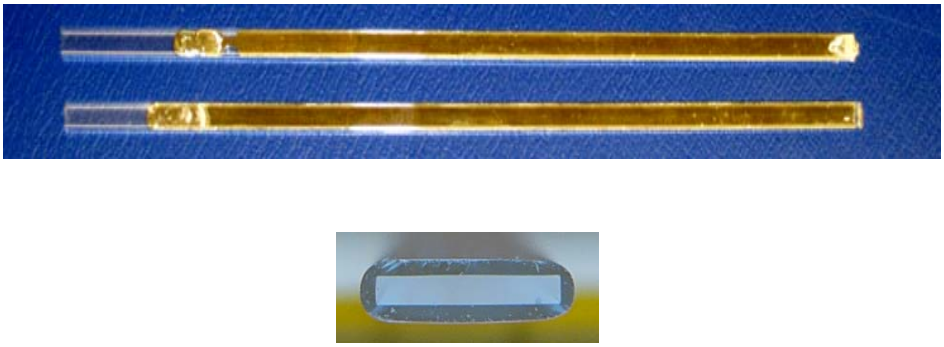

(a) Within Glass Tubes

(b) After Extraction

Figure 3.4 - Solder Uniaxial Test Specimens

The described sample preparation procedure yielded repeatable samples with controlled cooling profile (i.e. microstructure), oxide free surface, and uniform dimensions. By extensively cross-sectioning several specimens and observing under the SEM, it has been verified that the microstructure of any given sample is consistent throughout the volume of the sample, as shown in Figure 3.5. In addition, it has been established that this method of specimen preparation yields repeatable sample microstructures for a given solidification temperature profile. Samples were inspected using a micro-focus x-ray system to detect flaws (e.g. notches and external indentations) and/or internal voids (non-visible). Figure 3.6 illustrates results for good and poor specimens. With proper experimental techniques, samples with no flaws and voids were generated.

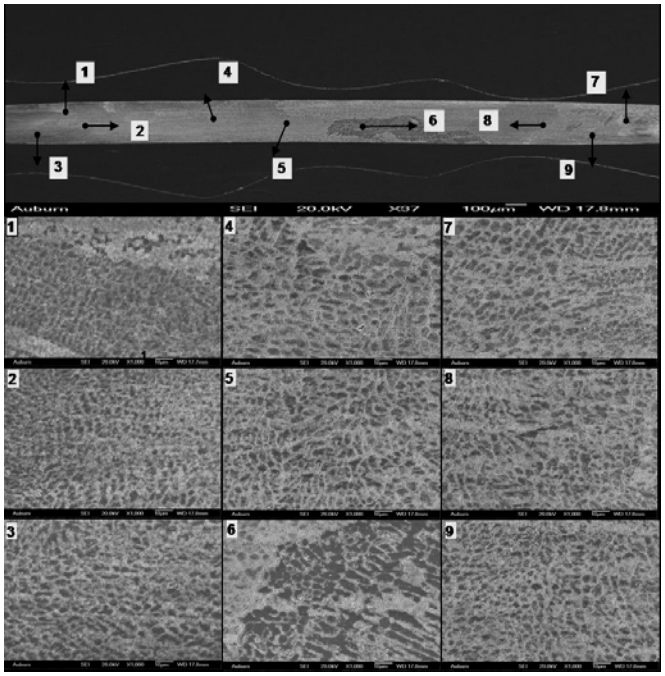

Fig. 3.5 - Uniformity of Specimen Cross-Section (SAC305)

Figure 3.6 - X-Ray Inspection of Solder Test Specimens (Good and Bad Samples)

3.3 Mechanical Testing System

A MT-200 tension/torsion thermo-mechanical test system from Wisdom Technology, Inc., as shown in Figure 3.7, has been used to test the samples in this study. The system provides an axial displacement resolution of 0.1 micron and a rotation resolution of 0.001°. Testing can be performed in tension, shear, torsion, bending, and in combinations of these loadings, on small specimens such as thin films, solder joints, gold wire, fibers, etc. Cyclic (fatigue) testing can also be performed at frequencies up to 5 Hz. In addition, a universal 6-axis load cell was utilized to simultaneously monitor three forces and three moments/torques during sample mounting and testing. Environmental chambers added to the system allow samples to be tested over a temperature range of -185 to +300 °C.

During uniaxial testing, forces and displacements were measured. The axial stress and axial strain were calculated from the applied force and measured cross-head displacement using

$$\sigma = \frac{F}{A} \qquad \varepsilon = \frac{\Delta L}{L} = \frac{\delta}{L} \tag{3.1}$$

where σ is the uniaxial stress, ε is the uniaxial strain, F is the measured uniaxial force, A

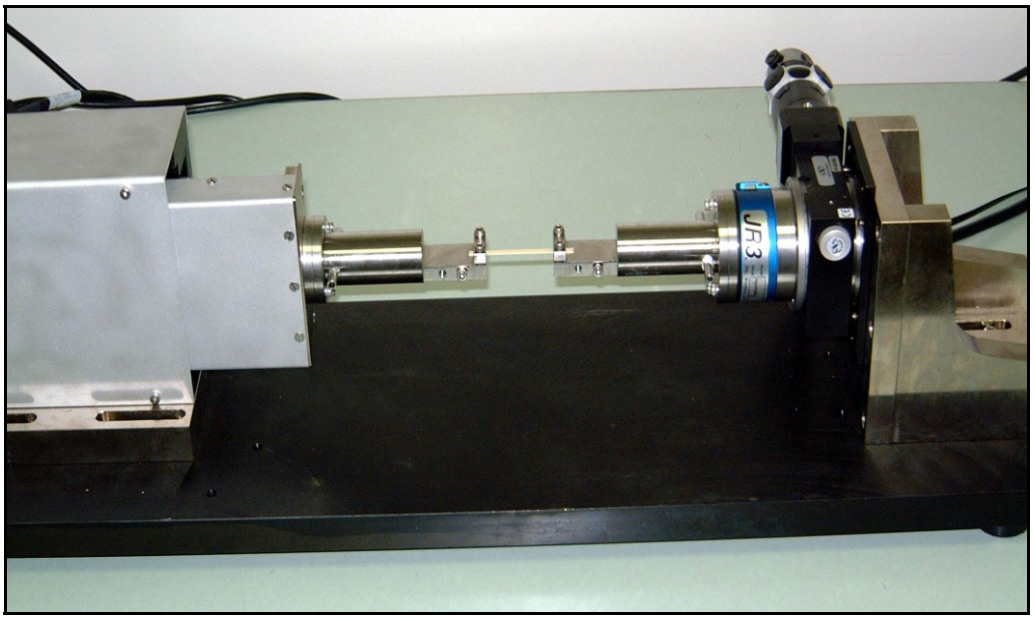

(a) Testing System with Sample

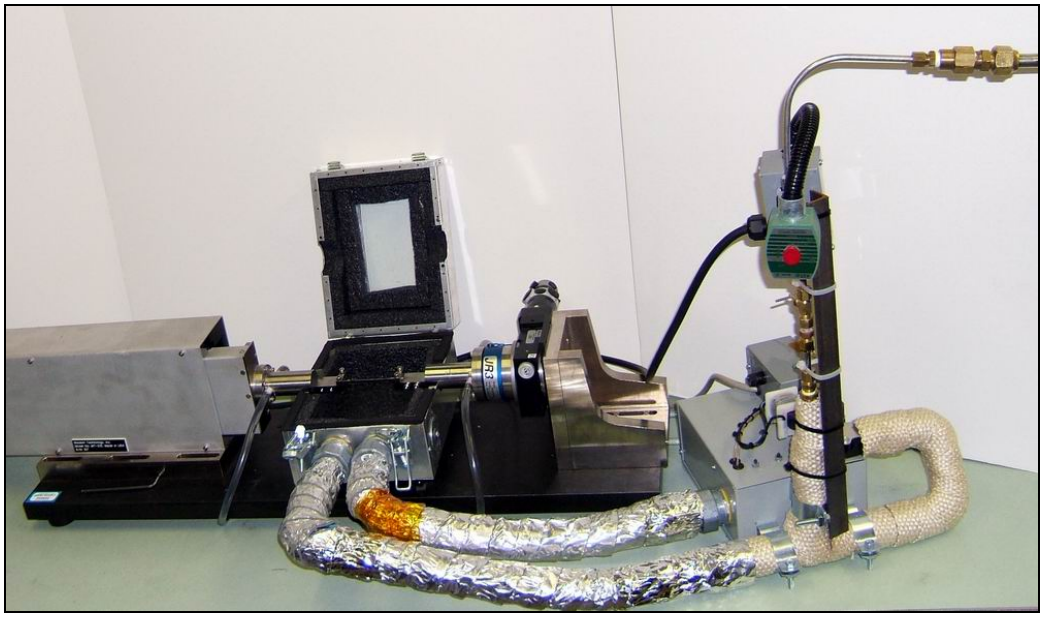

(b) with Environmental Chamber

Figure 3.7 - MT-200 Testing System with Solder Sample

is the original cross-sectional area, δ is the measured crosshead displacement, and L is the specimen gage length (initial length between the grips). The gage length of the specimens in this study was 60 mm, so that the specimen length to width aspect ratio was 20 to 1 (ensuring true uniaxial stress states). All creep tests in this work were conducted at room temperature (25 °C) with an applied stress of σ = 15 MPa.

3.4 Test Matrix Description

Using specimens fabricated with the casting procedure described above, thermal aging effects and creep behavior have been characterized for all the mixed formulations solder alloys. Analogous experiments were also performed with 63Sn-37Pb eutectic and SAC 305 solders samples for comparison purposes. Uniaxial creep curves have been characterized for samples subjected to two different aging temperatures including T = 25 (RT) and 100 °C, with aging durations up to 60 days. The test matrix of aging temperatures and aging times for the creep experiments performed is shown in Table 3.2. All creep tests were conducted on the aged samples at room temperature (25 °C).

	Aging Temperatures	
Aging Time (days)	Room Temperature (25°C)	Elevated Temperature (100 °C)
0	X	X
5	X	X
10	X	X
15	X	X
20	X	X
30	X	X
45	X	X
60	X	X

Table 3.2 - Aging Test Matrix for Creep Tests

3.5. Typical Stress-Strain Data and Empirical Model

Figure 3.8 illustrates a set of typical solder stress-strain curves for solder at T = 0 °C. In this case, 10 curves were recorded for Sn-Pb samples prepared with the same cooling profile (water quenching and reflow) and subjected to the same elevated temperature aging at 125 °C for 50 hours. In this study, the analysis of tensile properties focuses on the portions of the stress-strain curves before extensive visible necking occurs (typically $\varepsilon < 2$-3%). The curves in Figure 3.8 are closely distributed, and well suited for mathematical representation.

In this study, the object was to replace the set of 10 recorded stress-strain curves for a certain testing configuration with a single "average" curve that accurately represents the observed response for all strain levels. Several different mathematical models could be used to represent the recorded data. In this work, a linear model was used for extremely small strains ($\varepsilon << 0.0001$), and a four parameter empirical representation called the Weibull model for larger strains:

$$\sigma(\varepsilon) = E\varepsilon \qquad \varepsilon \le \varepsilon^*$$
$$\sigma(\varepsilon) = C_0 - C_1 e^{-C_2 \varepsilon^{C_3}} \qquad \varepsilon \ge \varepsilon^* \tag{3.2}$$

where E is the initial elastic modulus; C_0, C_1, C_2, C_3 are material constants to be determined; and ε^* is the strain level where the two functions intersect (become equal). The two function approach is typical for elastic-plastic materials, where it is desirable to model the initial portion of the stress-strain curve as perfectly linear (elastic), and the remaining portion of the curve as nonlinear. The fitted model provides an excellent average representation for the 10 recorded stress-strain curves (see Figure 3.9).

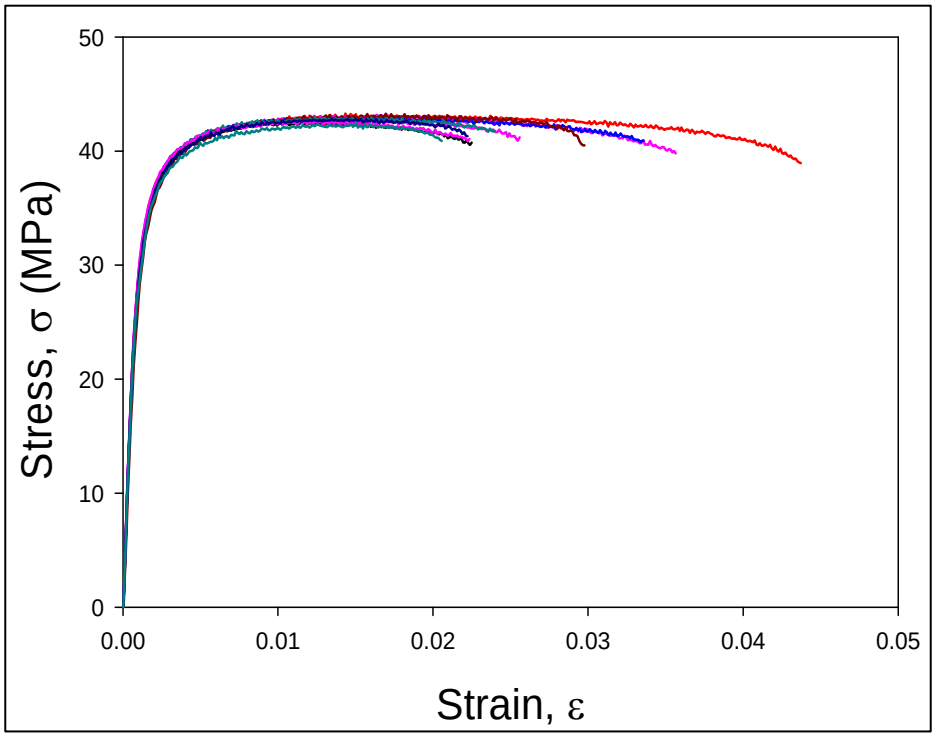

Figure 3.8 - Typical Set of Truncated Stress-Strain Curves for a Given Set of Conditions

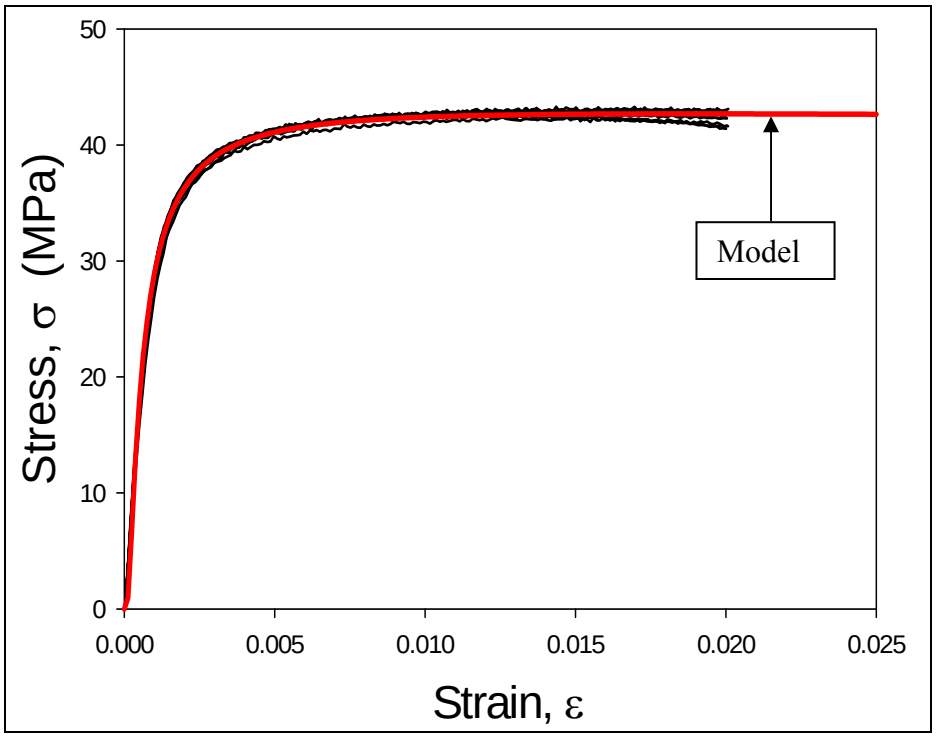

Figure 3.9 - Typical Set of Truncated Stress-Strain Curves and Fitting Model

3.6 Typical Creep Data and Empirical Model

Figure 3.10 illustrates a typical solder creep curve (strain vs. time response for a constant applied stress). The response begins with a quick transition to the initial "elastic" strain level, followed by regions of primary, secondary, and tertiary creep. Depending on the applied stress level, the primary creep region can be more extensive for the SAC alloys relative to Sn-Pb solders. The secondary creep region is typically characterized by a very long duration of nearly constant slope. This slope is referred to as the "steady state" secondary creep rate or creep compliance, and it is often used by practicing engineers as one of the key material parameters for solder in finite element simulations used to predict solder joint reliability. In this work, the measured creep rates were taken to be the minimum slope values in the secondary creep regions of the observed $\dot{\varepsilon}$ versus t responses. The tertiary creep region occurs when rupture is imminent, and typically features an abrupt change to a nearly constant but significantly increased creep rate.

In the solder creep experiments in this research, constant stress levels on the order of 25-50% of the observed UTS are being applied. For the data presented in this work, the applied stress was σ = 15 MPa, which is approximately 25%-35% of the non-aged UTS values for the various alloys tested. Due to the long test times involved, only 5 specimens were tested for each alloy for any given set of aging conditions. The curves for each set of testing conditions were fit with an empirical strain-time model to generate an "average" representation of the creep response for those conditions. For the range of test conditions considered in this work, the raw strain versus time data in the primary and

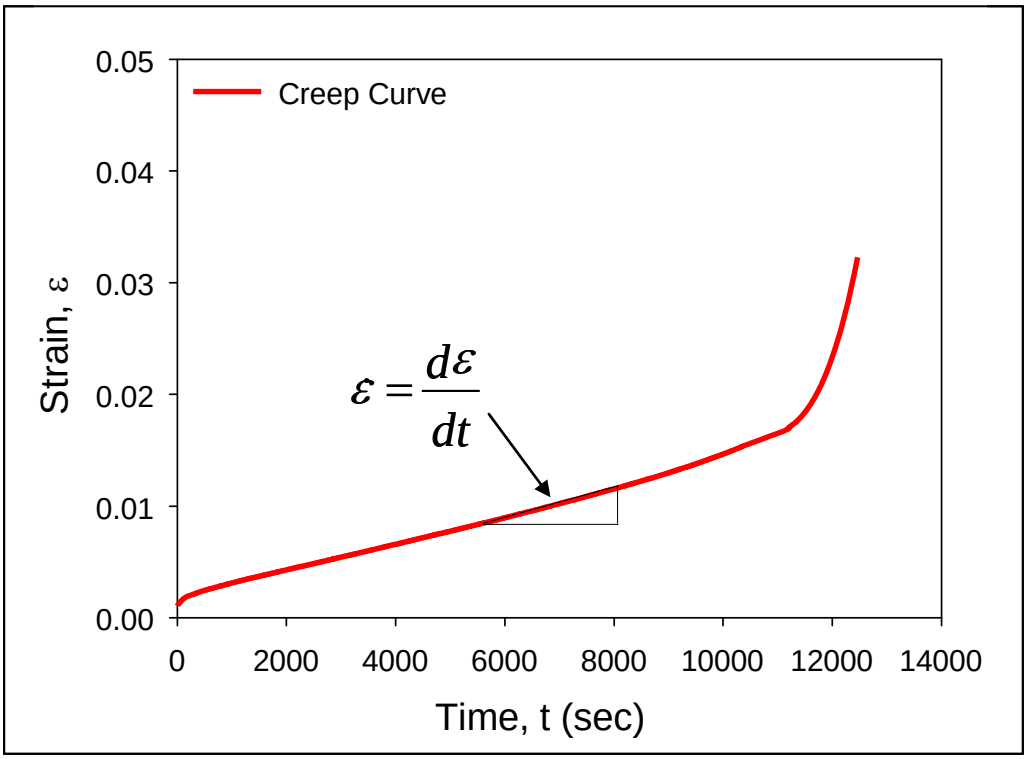

Figure 3.10 - Typical Creep Strain vs Time Curve

secondary creep regions were found to be well fit by creep response of the four parameter Burger's (spring-dashpot) model:

$$\varepsilon = \varepsilon(t) = k_0 + k_1 t + k_2\left(1 - e^{-k_3 t}\right) \tag{3.3}$$

From the recorded strain vs time curves under constant stress, the "steady state" creep strain rates (k_1) have been extracted. In practice, the measured creep rate for each curve was evaluated numerically by calculating the minimum slope value in the secondary creep region of the observed $\dot{\varepsilon}$ versus t response (see Figure 3.11). Variations of the average creep rates with aging were determined and then modeled as a function of aging time.

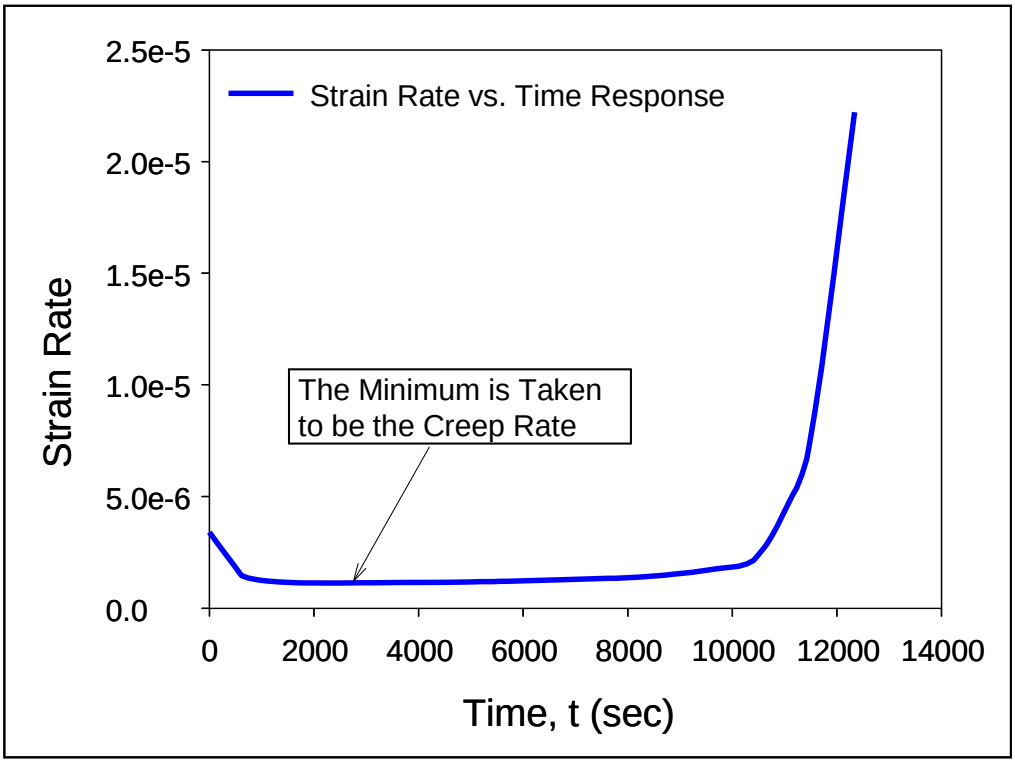

Figure 3.11 - Evaluation of the Creep Strain Rate

CHAPTER 4

MATERIAL BEHAVIOR OF MIXED FORMULATION SOLDERS

4.1 Introduction

Solder alloys have a high operating temperature for most normal operating conditions of electronic components, being greater than $0.5T_m$ (T_m is the melting temperature) even at room temperature. At room temperature (25 ^oC), the homologous temperature is 0.65 T_m for 63Sn-37Pb eutectic solder and 0.61 T_m for SAC 305 solder. The unique properties of solder cause significant aging effects on creep properties of solder alloys even at room temperature. As suggested in the literature review, there is no work in the literature on creep behavior of mixture solders alloys. In this chapter, the physical properties and mechanical behavior of mixed solder alloys are documented, and the effects of room temperature and elevated temperature aging are explored.

4.2 Physical Properties

The variations of solidification properties such as melting temperature and pasty range for the solders of different mixture ratios have been evaluated by DSC analysis (Figure 4.1). Results are plotted in Figures 4.2-4.3, with the horizontal axes in each graph indicating the wt% of Sn-Pb (0% = SAC305 is on the left, and 100% = Sn-Pb is on the right). As the level of Sn-Pb in the mixture is increased, it is observed that the melting temperature of mixed solders decreases as expected until 30% of the alloy is Sn-

Pb. At that point, the melting temperature is approximately constant (at or slightly below the Sn-Pb level of 183 ^{o}C). It also can be seen that the pasty range of mixed formulation solders becomes large as the mixture nears the two extreme compositions of pure SAC or pure Sn-Pb. For mixtures between 30-70% Sn-Pb, the pasty range is very small (less than 2 ^{o}C).

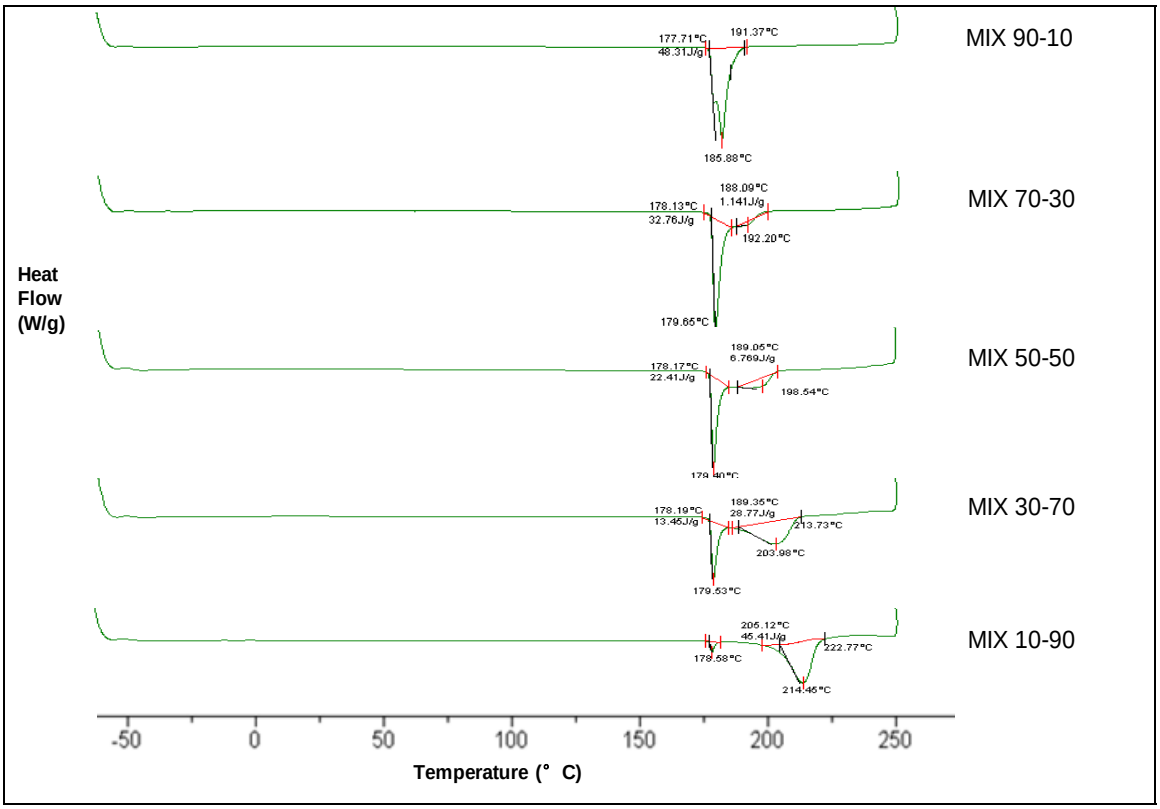

Figure 4.1 - DSC Analysis

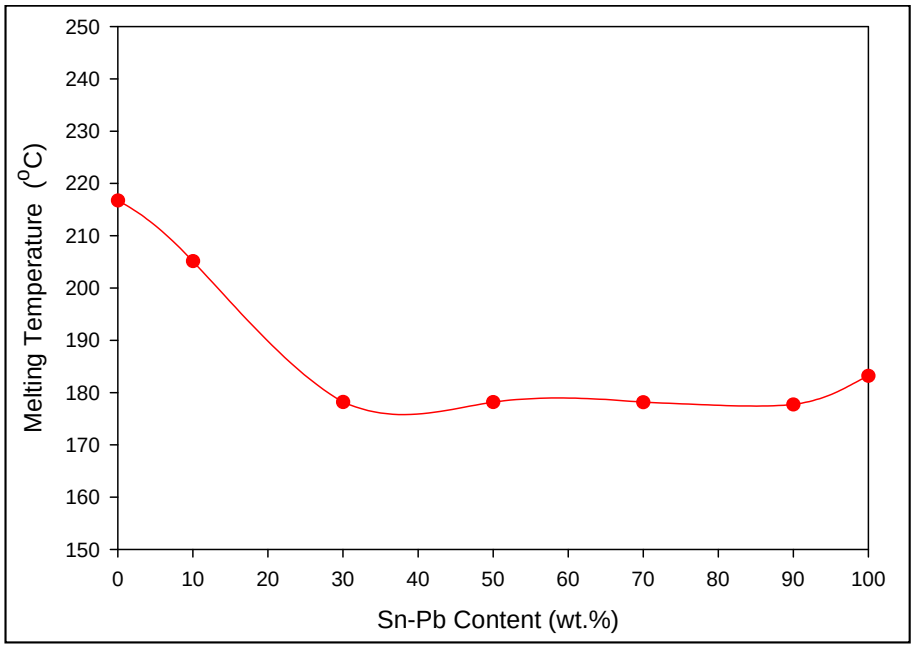

Figure 4.2 - Melting Temperature vs. Sn-Pb Content

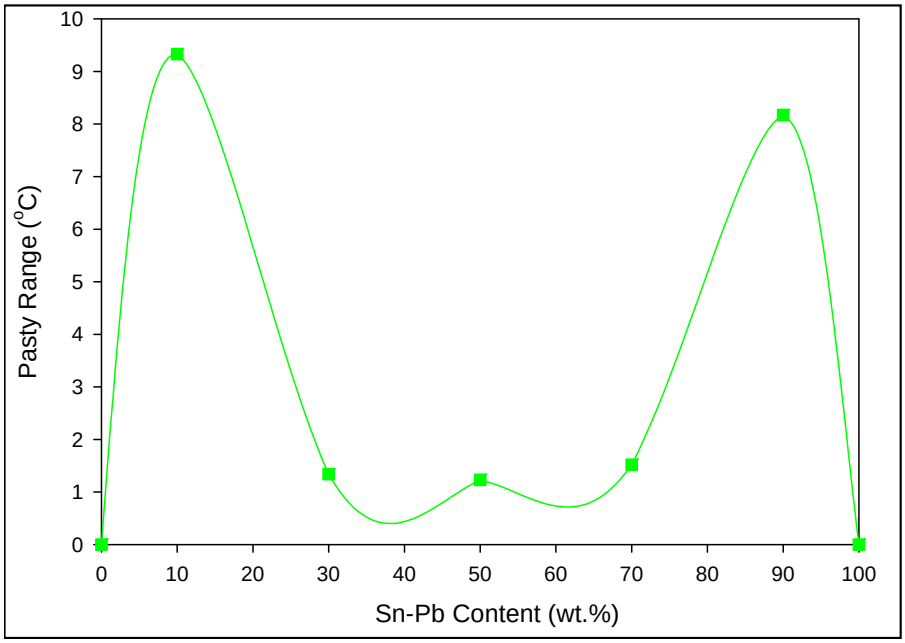

Figure 4.3 - Pasty Range vs. Sn-Pb Content

4.3 Microstructural Evolution

The microstructural changes occurring with different mixture ratios have been evaluated by optical and Scanning Electronic Microscopy [Zhang 2009b]. Figure 4.4 contains micrographs of the seven mixed formulations solders recorded at 1000X and 3500X. The well-known microstructure of pure SAC305, i.e. bundles of needle-shaped Ag_3Sn particles distributed on Sn matrix can be found in the first picture of the series. However, as the content of Sn-Pb increases in the mixtures, the Ag_3Sn particles change dramatically into thin and bone-shaped precipitates distributed across the Sn matrix. EDX analysis (see Figure 4.5) shows that these precipitates are rich in Ag and Pb. As the Sn-Pb content increases from 10% to 90%, the precipitates in the mixed formulation solders evolve from thin bone-shaped to thick bone-shaped to coarse bone-shaped to pie-shaped, and finally, to coarse pie-shaped particles. Eventually, as the Sn-Pb content reaches 100%, the typical eutectic structure is observed (last picture of the series). Since mechanical properties are ultimately determined by microstructure, the distinctive microstructures of mixed formulation solder alloys will have determinative effects on their mechanical performance.

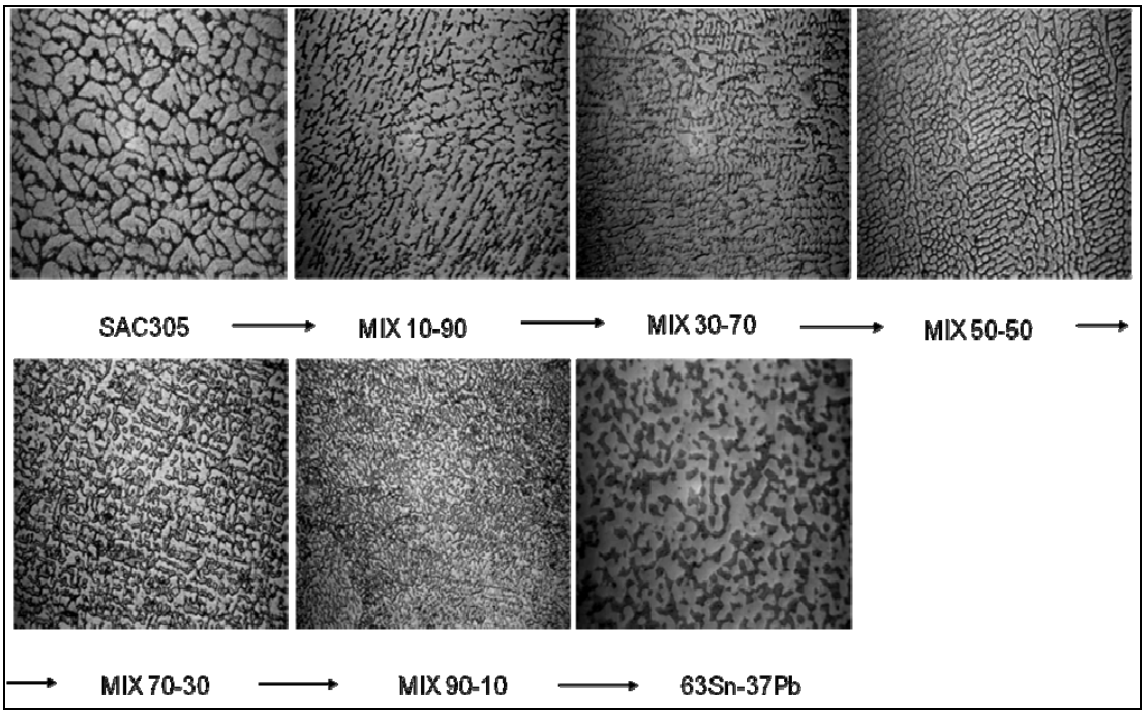

(a) Optical Microscope Magnification: 1000X

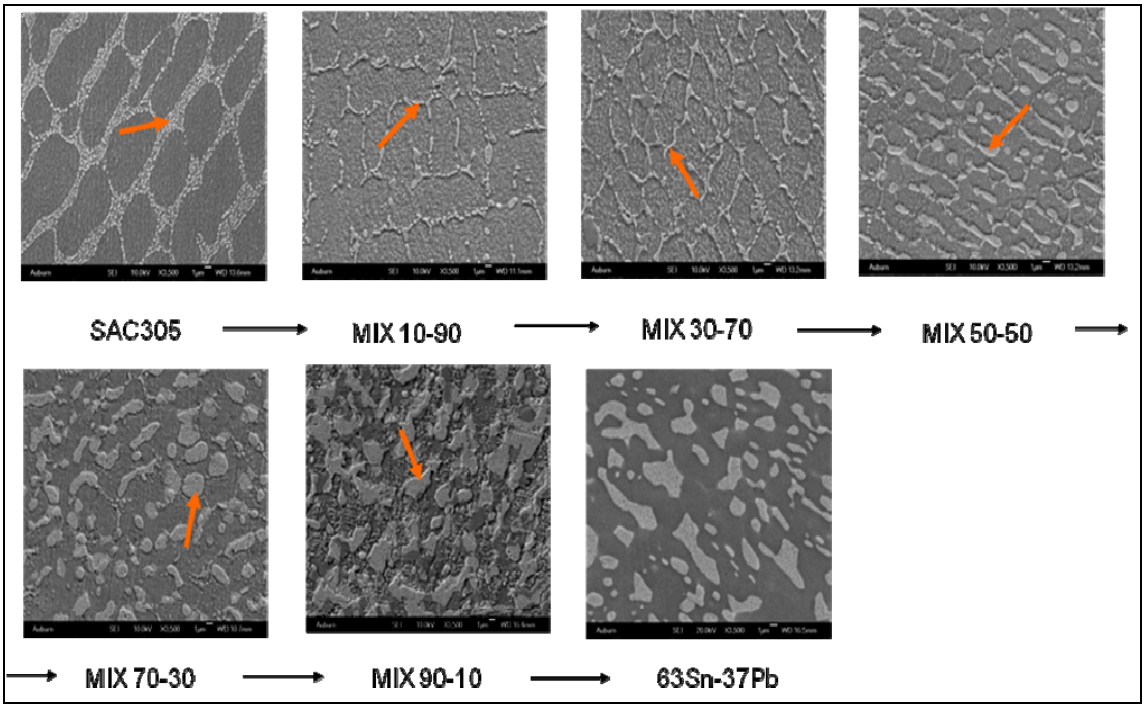

(b) SEM Magnification: 3500X, Arrow: EDX spot

Figure 4.4 - Microstructure of Mixed Formulation Solder Alloys

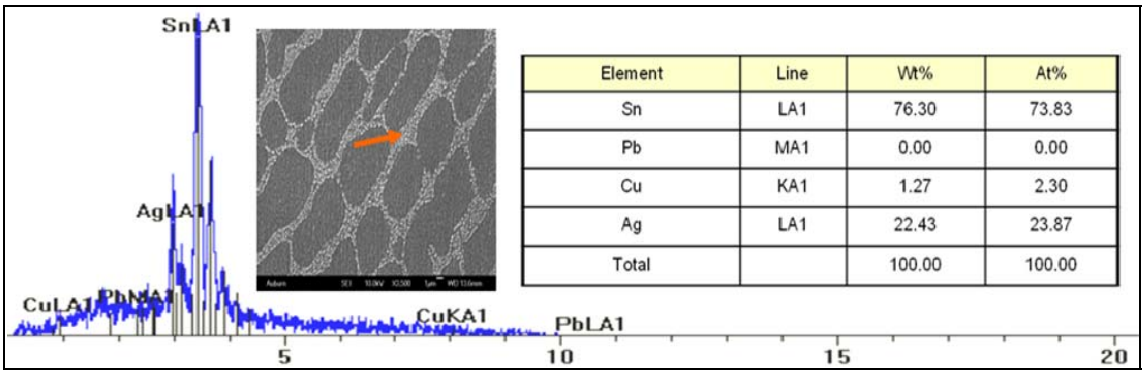

Element	Line	Wt%	At%
Sn	LA1	76.30	73.83
Pb	MA1	0.00	0.00
Cu	KA1	1.27	2.30
Ag	LA1	22.43	23.87
Total		100.00	100.00

(a) SAC305

Microstructure: needle-shaped, Ag_3Sn (white) particles distributed on Sn matrix

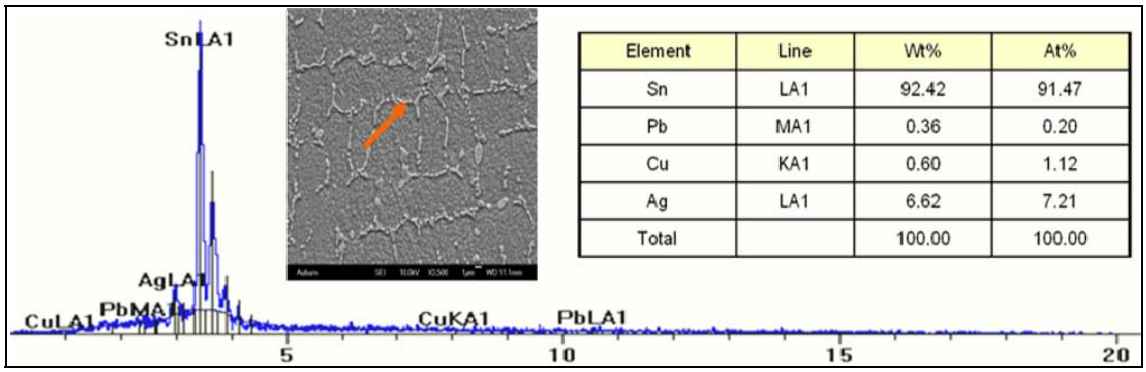

Element	Line	Wt%	At%
Sn	LA1	92.42	91.47
Pb	MA1	0.36	0.20
Cu	KA1	0.60	1.12
Ag	LA1	6.62	7.21
Total		100.00	100.00

(b) MIX 10-90

Microstructure: Ag-rich, thin bone-shaped Precipitates distributed on Sn matrix

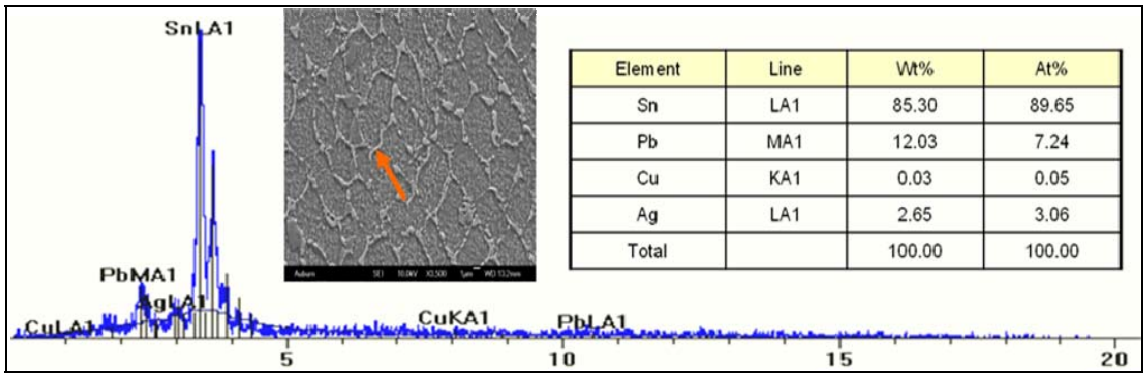

Element	Line	Wt%	At%
Sn	LA1	85.30	89.65
Pb	MA1	12.03	7.24
Cu	KA1	0.03	0.05
Ag	LA1	2.65	3.06
Total		100.00	100.00

(c) MIX 30-70

Microstructure: Pb, Ag-rich, grown bone-shaped precipitates distributed on Sn matrix

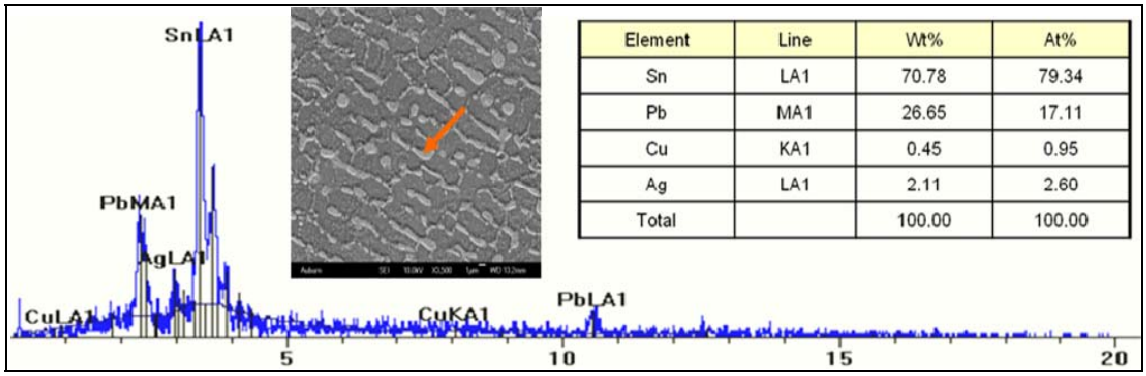

Element	Line	Wt%	At%
Sn	LA1	70.78	79.34
Pb	MA1	26.65	17.11
Cu	KA1	0.45	0.95
Ag	LA1	2.11	2.60
Total		100.00	100.00

(d) MIX 50-50

Microstructure: Pb-rich, coarse bone-shaped precipitates distributed on Sn matrix

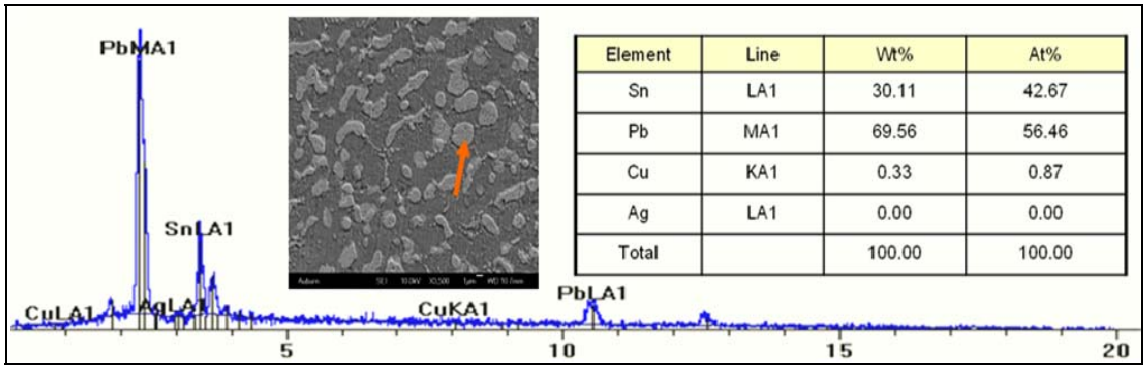

Element	Line	Wt%	At%
Sn	LA1	30.11	42.67
Pb	MA1	69.56	56.46
Cu	KA1	0.33	0.87
Ag	LA1	0.00	0.00
Total		100.00	100.00

(e) MIX 70-30

Microstructure: Pb-rich, pie-shaped precipitates distributed on Sn matrix

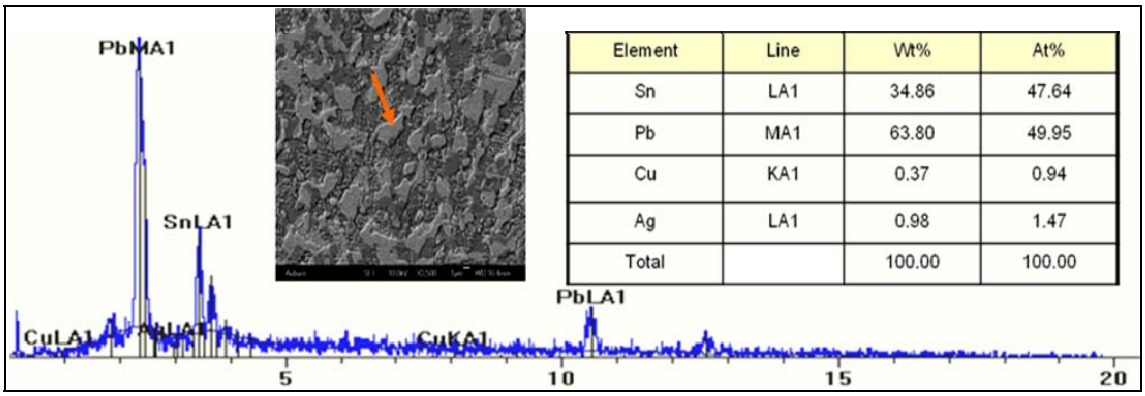

Element	Line	Wt%	At%
Sn	LA1	34.86	47.64
Pb	MA1	63.80	49.95
Cu	KA1	0.37	0.94
Ag	LA1	0.98	1.47
Total		100.00	100.00

(f) MIX 90-10

Microstructure: Pb-rich, coarse pie-shaped precipitates distributed on Sn matrix

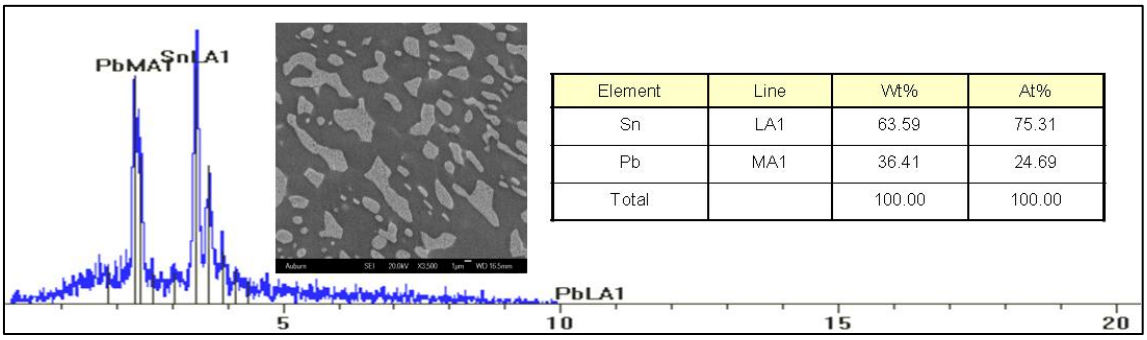

Element	Line	Wt%	At%
Sn	LA1	63.59	75.31
Pb	MA1	36.41	24.69
Total		100.00	100.00

(g) 63Sn-37Pb

Microstructure: Eutectic distribution of Sn and Pb (white) particles

Figure 4.5 - EDX Analysis of Mixed Formulation Solder Alloys

4.4 Tensile Properties of Mixed Formulation Solders

Zhang, et al. [Zhang 2009b] have explored the tensile properties of mixed formulation solders. The test matrix for their tensile tests was similar to the creep tests conducted in this study, i.e seven different mixture ratios of 63Sn-37Pb and SAC305 solder materials which include five carefully controlled mixtures of the two solder alloys (by weight percentage) and the two extreme cases (pure Sn-Pb and pure SAC). Figures 4.6-4.8 show the measured variations of elastic modulus (Figure 4.6), yield strength (Figure 4.7), and UTS (Figure 4.8) with Sn-Pb content and aging time.

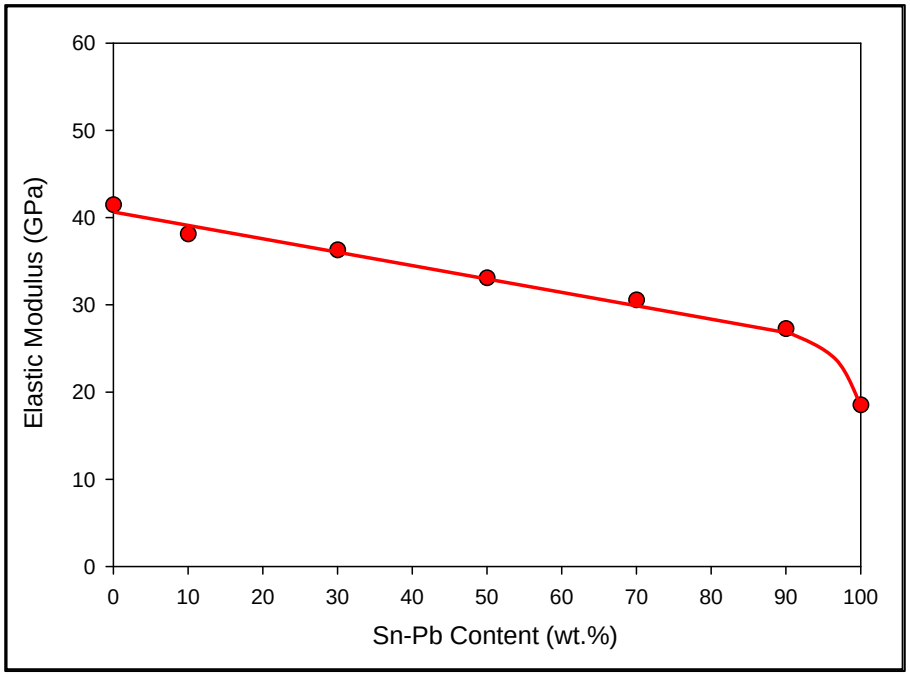

(a) Variation of Elastic Modulus with Sn-Pb content [Zhang 2009b]

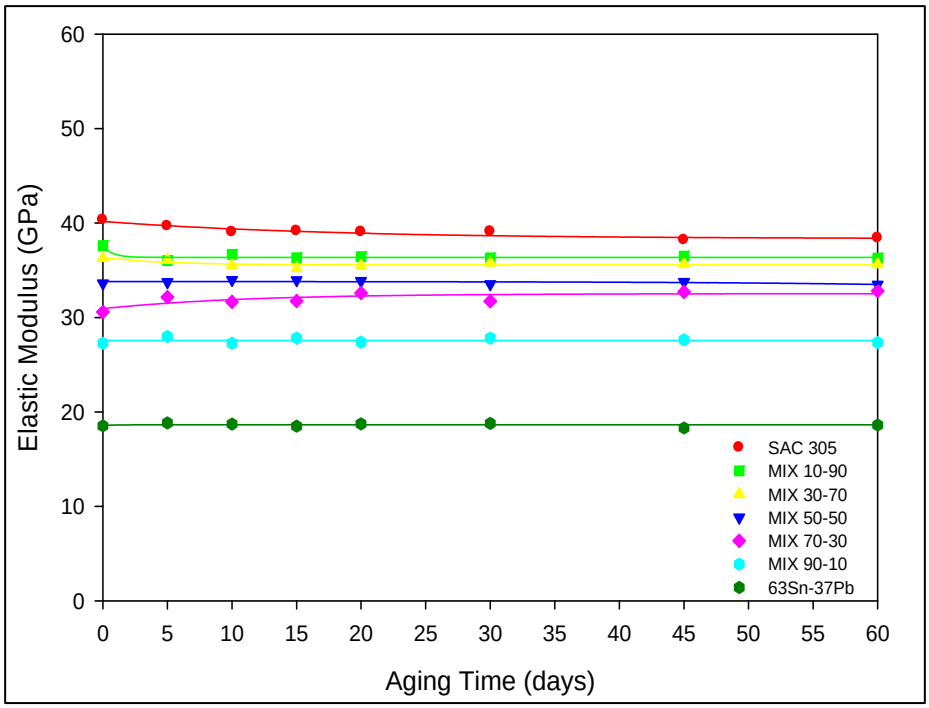

(b) Variation of Elastic Modulus with Room Temperature Aging [Zhang 2009b]

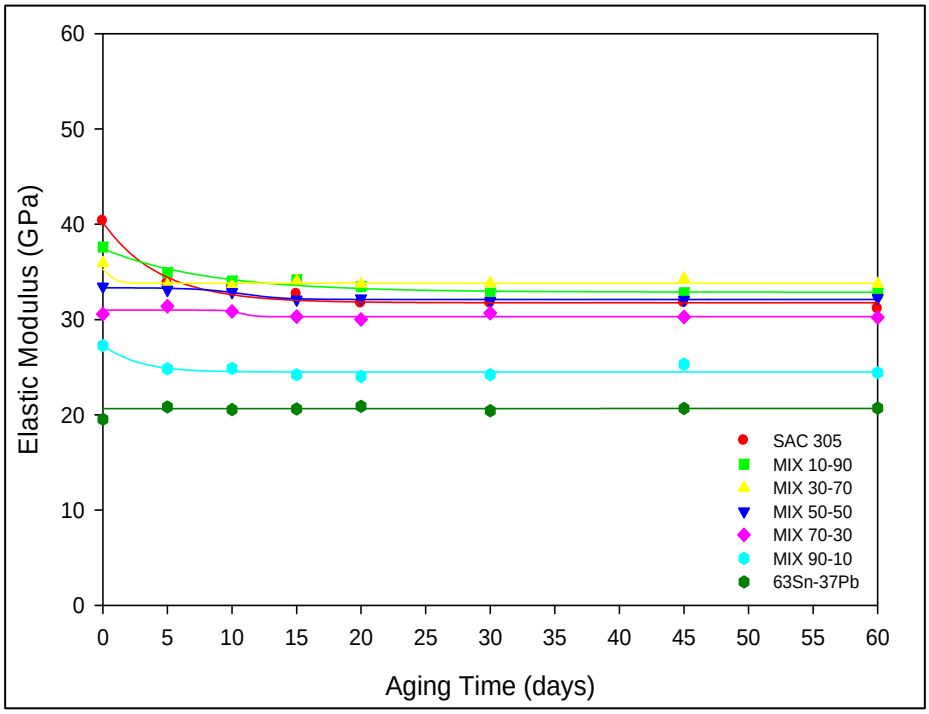

(c) Variation of E with Elevated Temperature Aging (100 ^{o}C) [Zhang 2009b]

Figure 4.6 - Variation of Elastic Modulus of Mixed Formulation Solders

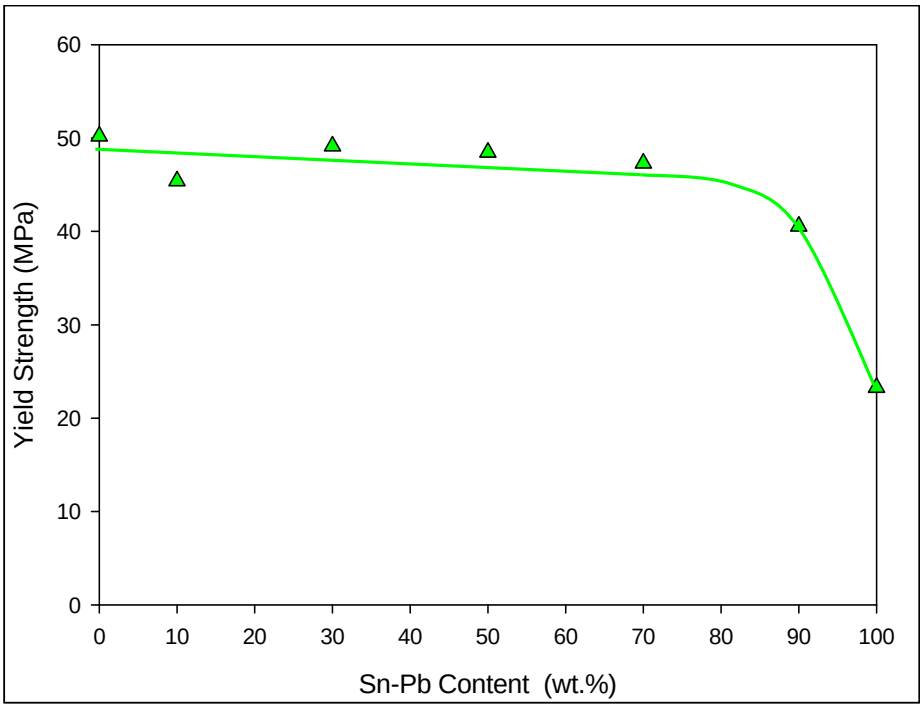

(a) Variation of Yield Strength with Sn-Pb content [Zhang 2009b]

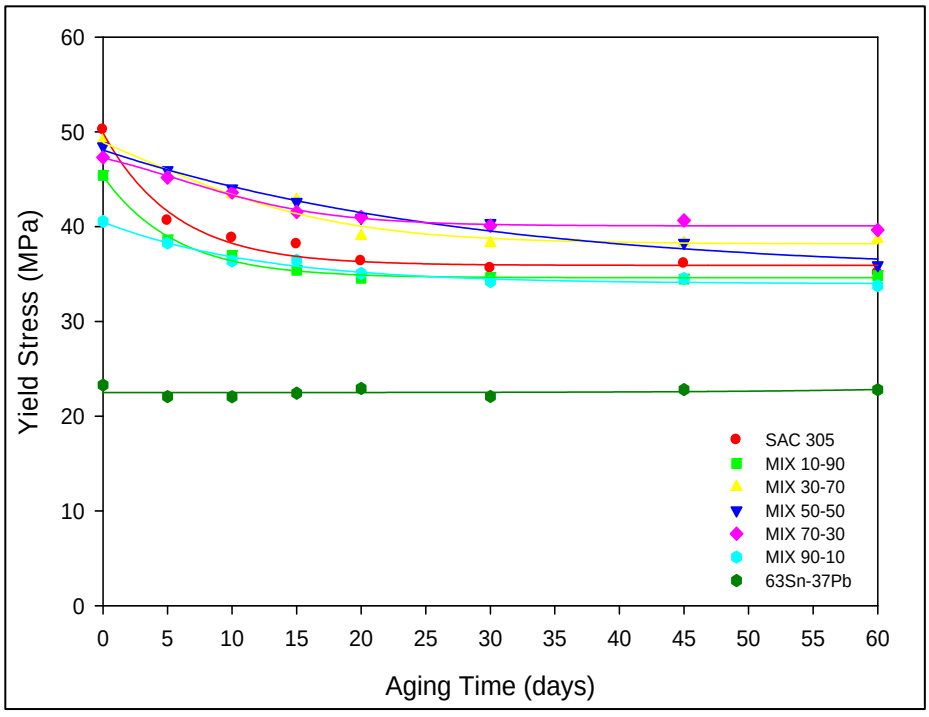

(b) Variation of Yield Strength with Room Temperature Aging [Zhang 2009b]

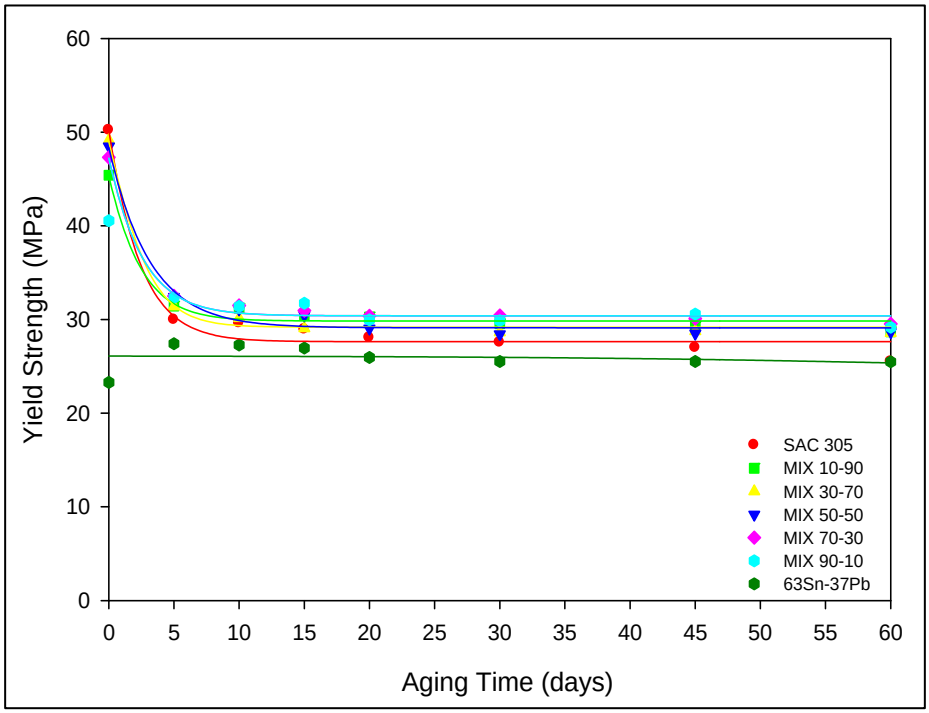

(c) Variation of YS with elevated temperature aging (100 ^{o}C) [Zhang 2009b]

Figure 4.7 - Variation of Yield Strength of Mixed formulation solders

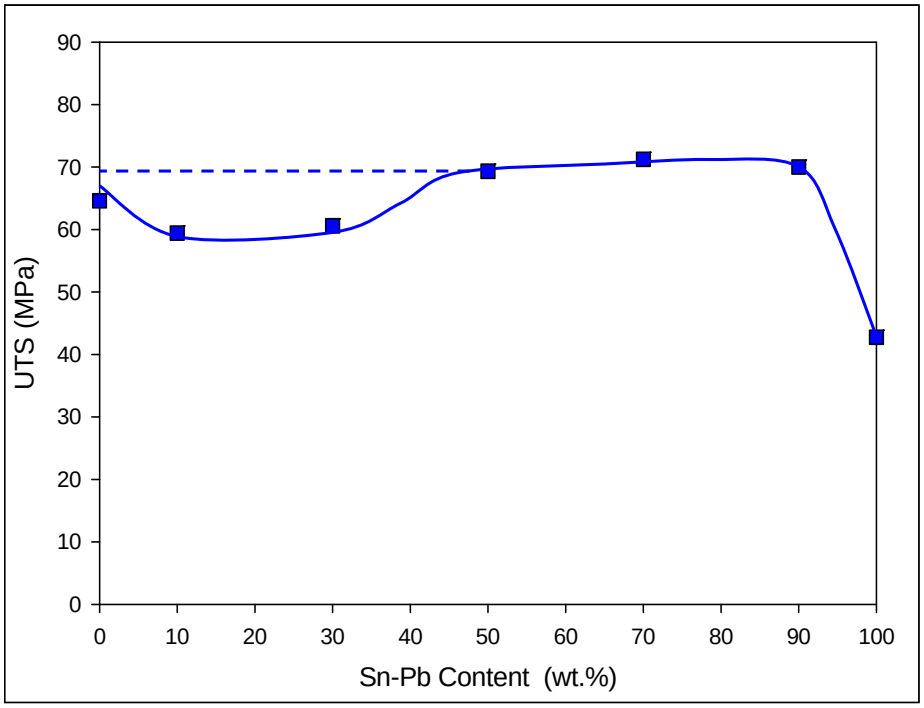

(a) Variation of UTS with Sn-Pb content [Zhang 2009b]

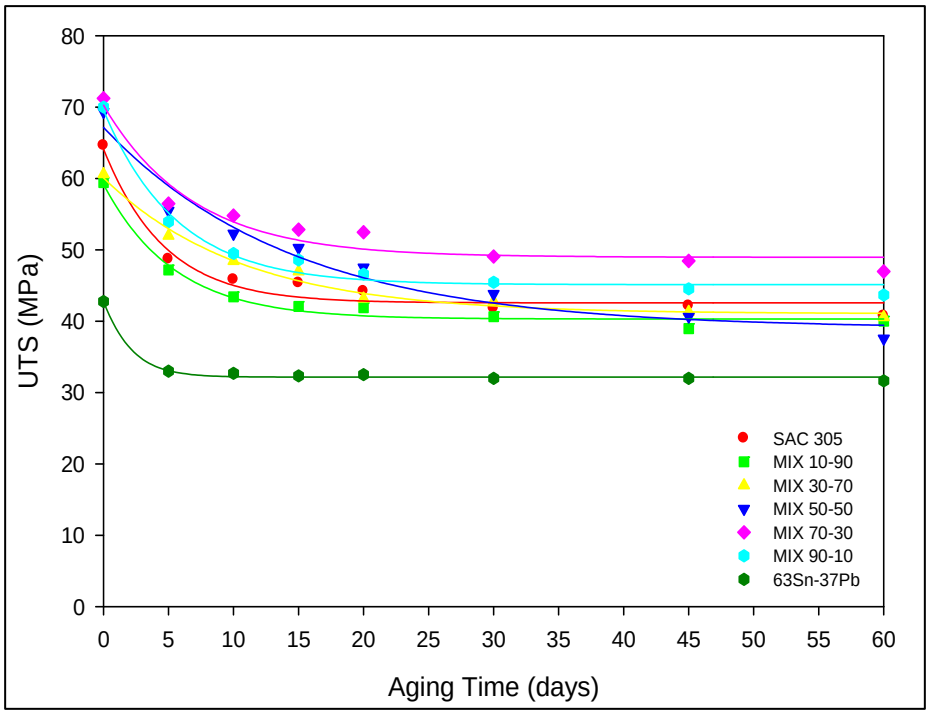

(b) Variation of UTS with Room Temperature Aging [Zhang 2009b]

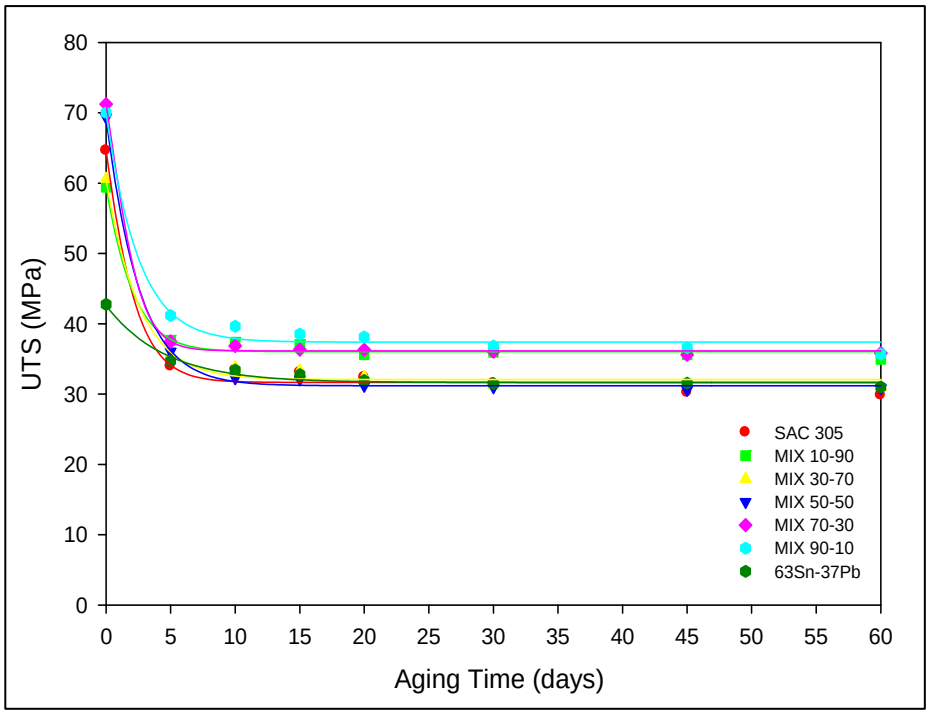

(c) Variation of UTS with room Elevated Temperature aging (100 ^{o}C) [Zhang 2009b]

Figure 4.8 - Variation of UTS of Mixed Formulation Solders

The results in Figure 4.6 demonstrate that the effective elastic modulus remains fairly constant for all mixed formulation solder alloys over a 60-day aging period. The largest changes were observed for SAC 305 that is aged at 100 ^{o}C. The effects of aging were much more dramatic on yield strength and UTS. The majority of the changes occurred during the first 15 days for aging at 25 ^{o}C and first 5 days for aging at 100 ^{o}C. The largest changes were again seen for pure SAC 305 (no Pb), and the smallest changes were seen for pure Sn-Pb alloy (most Pb). Thus Pb aids in resistance to aging induced strength degradations.

4.4 CREEP TESTING RESULTS

4.4.1 Effects of Aging on Solder Creep Response

Uniaxial specimens were formed for the various mixed formulation solder alloys using the methods described in previous chapter, and then aged at T = 25 and 100 ^{o}C for up to 60 days. The specimens for each alloy were prepared in sets of five, which were then subjected to a specific set of aging conditions (aging temperature and aging time). Figures 4.9-4.15 illustrate the typical recorded creep curves for the various solder alloys. In each figure, there are two graphs for the two different aging temperatures (T = 25 and 100 ^{o}C). In each plot, the various creep curves are for different aging times, illustrating the evolution of the creep response with duration of aging. For brevity and clarity of the presentation, only one of the five available creep curves is shown in each plot for each set of aging conditions.

The plots in Figures 4.9-4.15 clearly indicate a dramatic evolution of the creep response for all the solder alloys with aging at elevated temperature (100 ^{o}C). Figure 4.14(a) also demonstrates a significant effect on the creep response for room temperature aging of MIX 90-10. The evolution of the creep response at room temperature is less obvious for other mixed formulations solders and SAC 305 (see graphs in Figures 4.9a-4.13a). However, the evolution is indeed present although it is relatively small compared to the observed variations with elevated temperature aging. The reason the room temperature evolution is not obvious from the plots is due to the fact that common scales were chosen for the vertical (strain) axes in all of graphs in Figures 4.9-4.13. Figure 4.15 shows the analogous plots for eutectic 63Sn-37Pb. As seen clearly, there is almost no change in the creep response for room temperature aging.

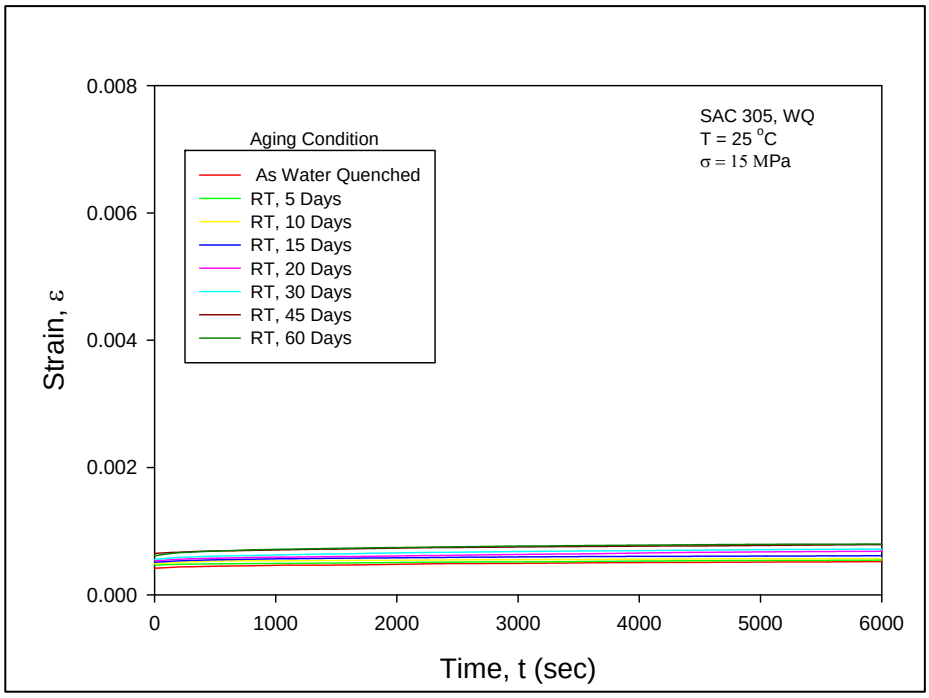

(a) Aging at T = 25 °C

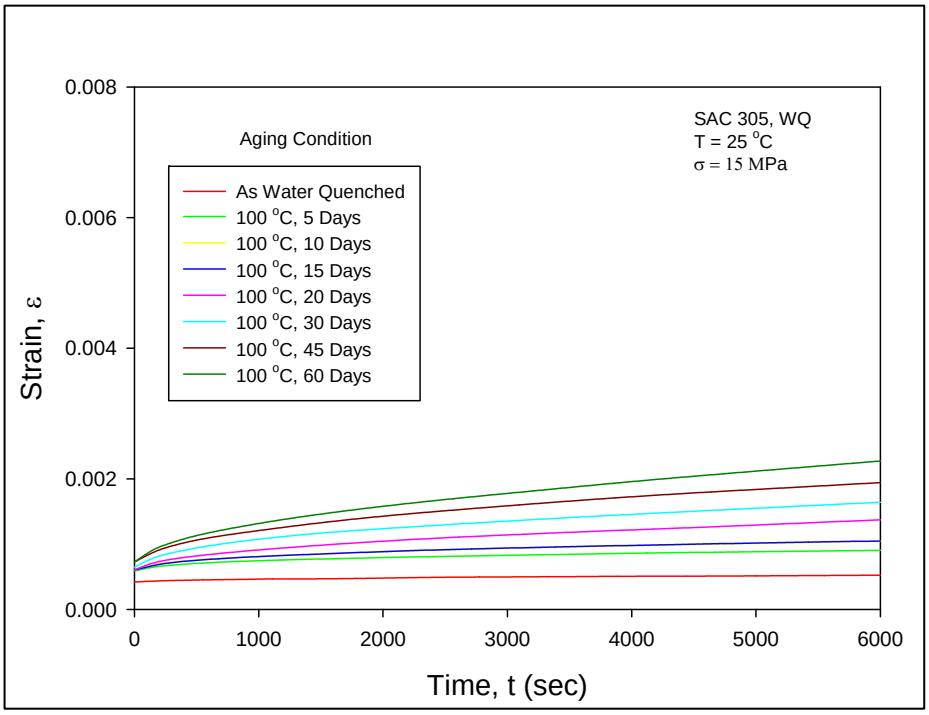

(b) Aging at T = 100 °C

Figure 4.9 - Creep curves for SAC 305 Aging from 0-60 Days

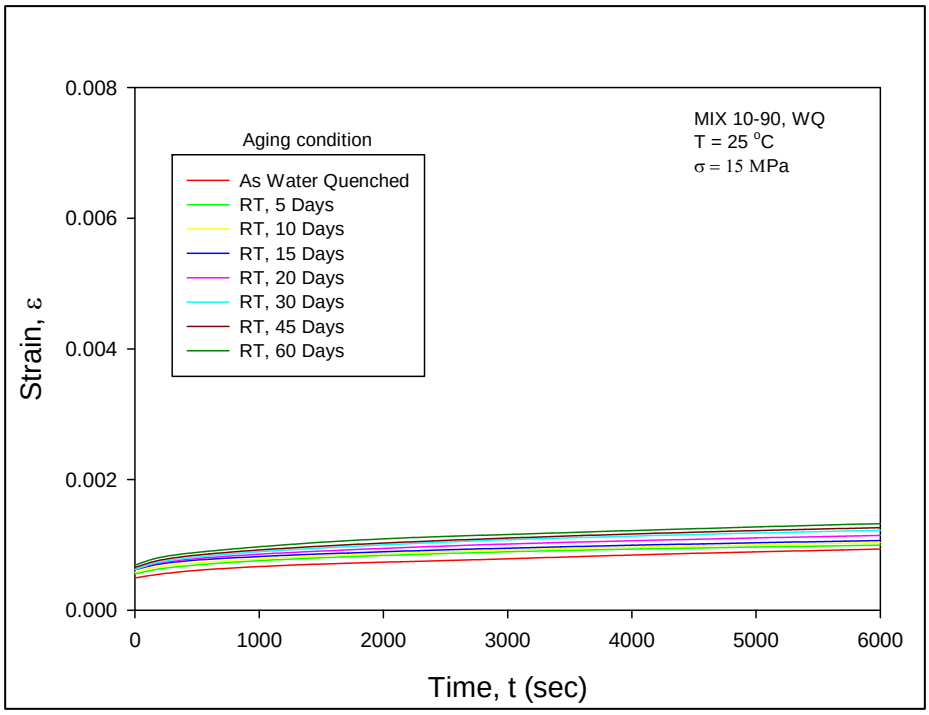

(a) Aging at T = 25 °C

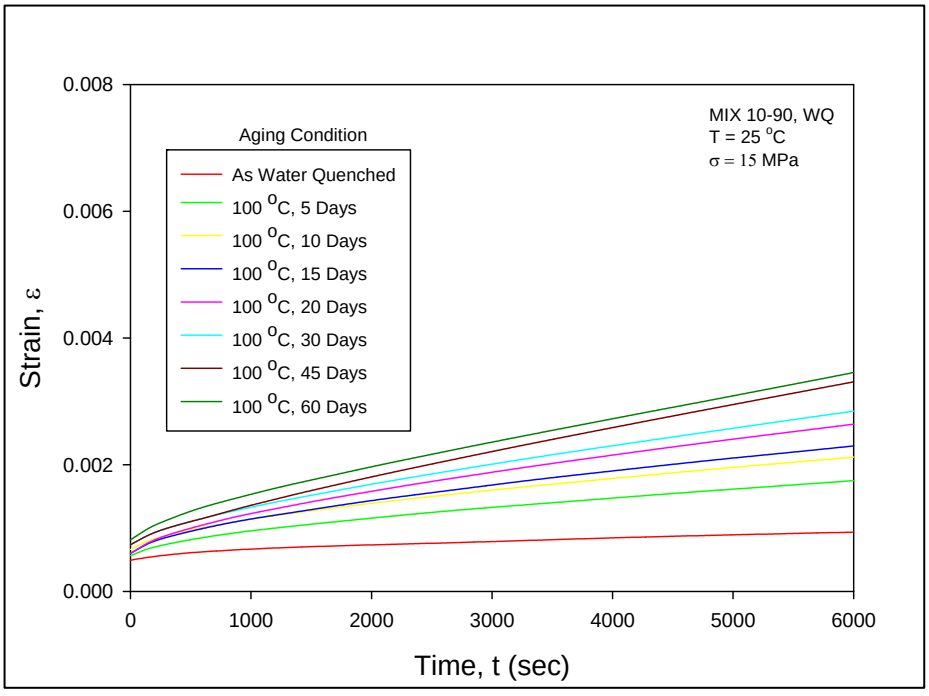

(b) Aging at T = 100 °C

Figure 4.10 - Creep curves for MIX 10-90 Aging from 0-60 Days

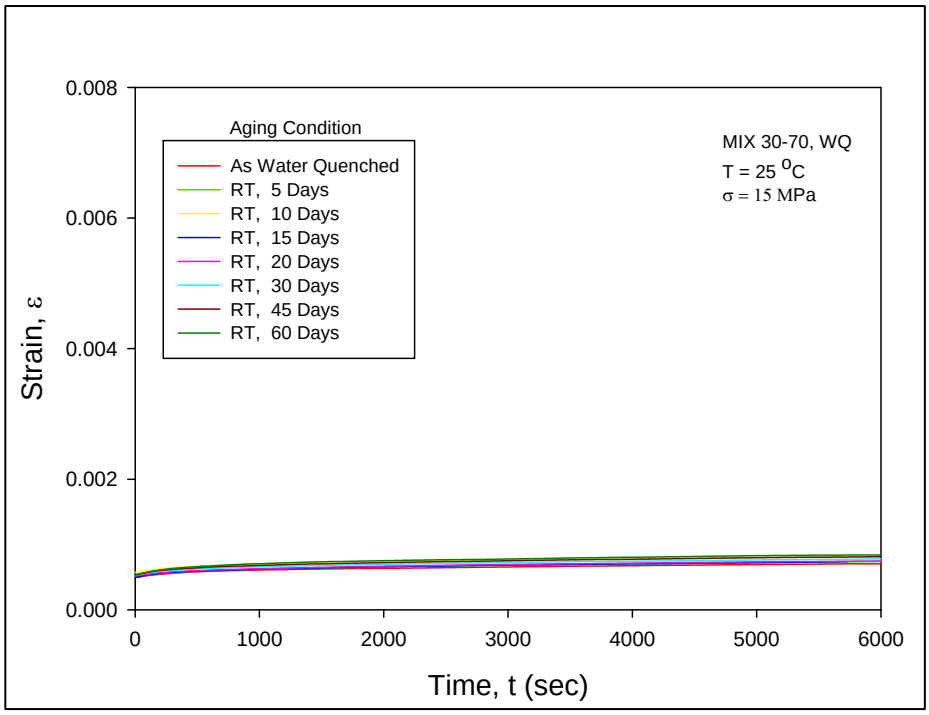

(a) Aging at T = 25 °C

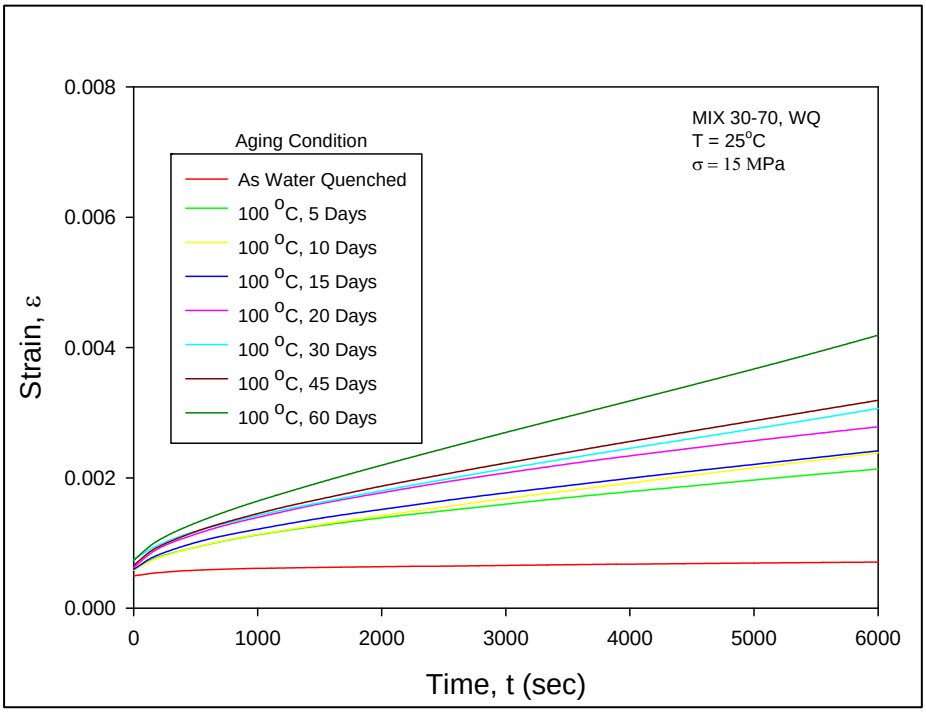

(b) Aging at T = 100 °C

Figure 4.11 - Creep curves for MIX 30-70 Aging from 0-60 Days

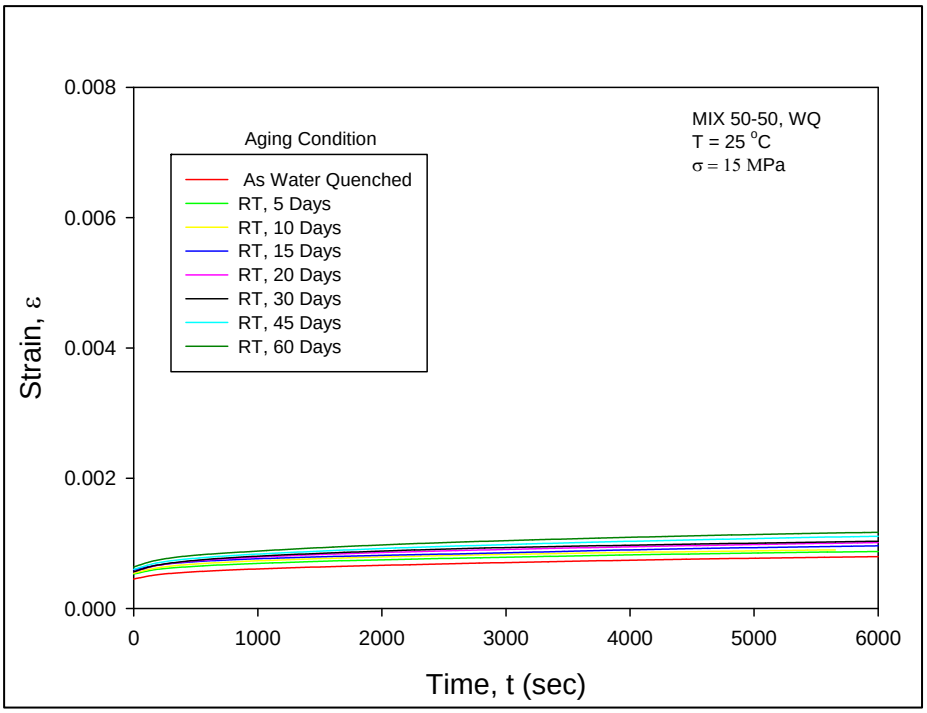

(a) Aging at T = 25 °C

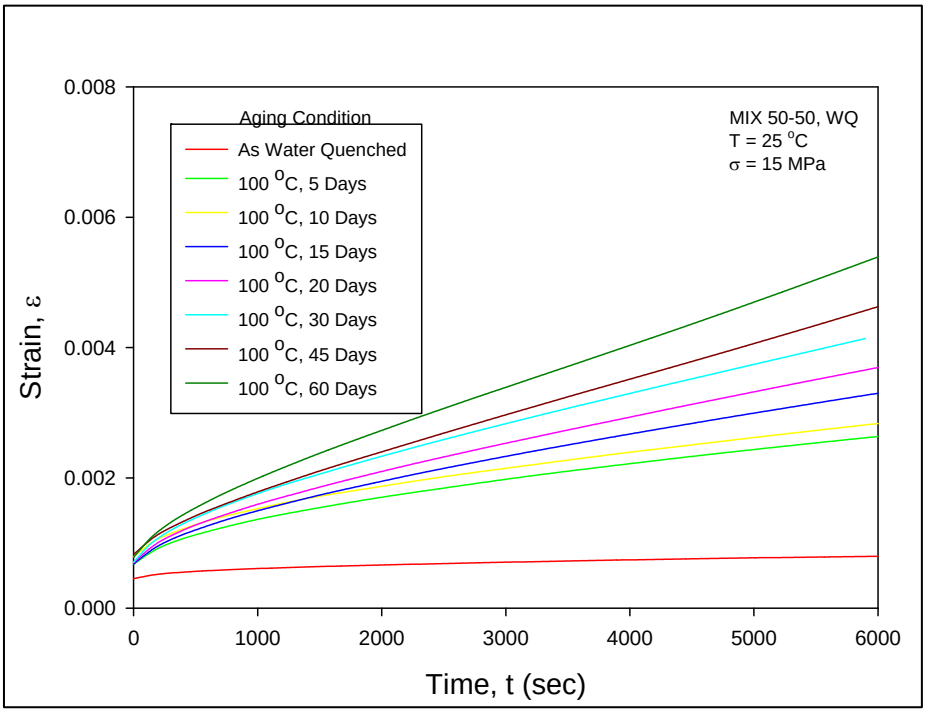

(b) Aging at T = 100 °C

Figure 4.12 - Creep curves for MIX 50-50 Aging from 0-60 Days

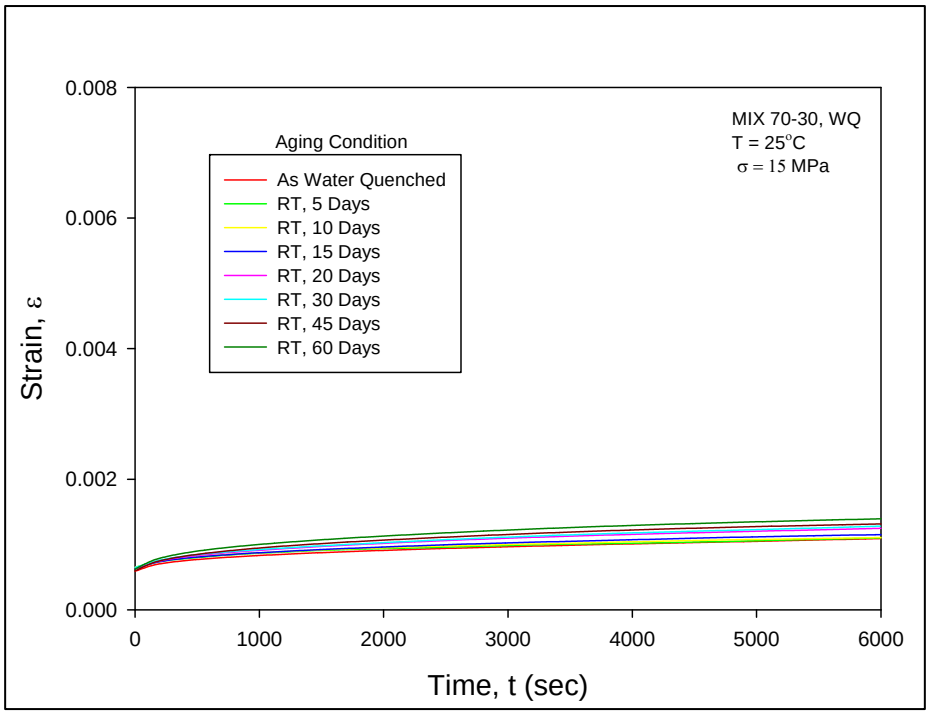

(a) Aging at T = 25 °C

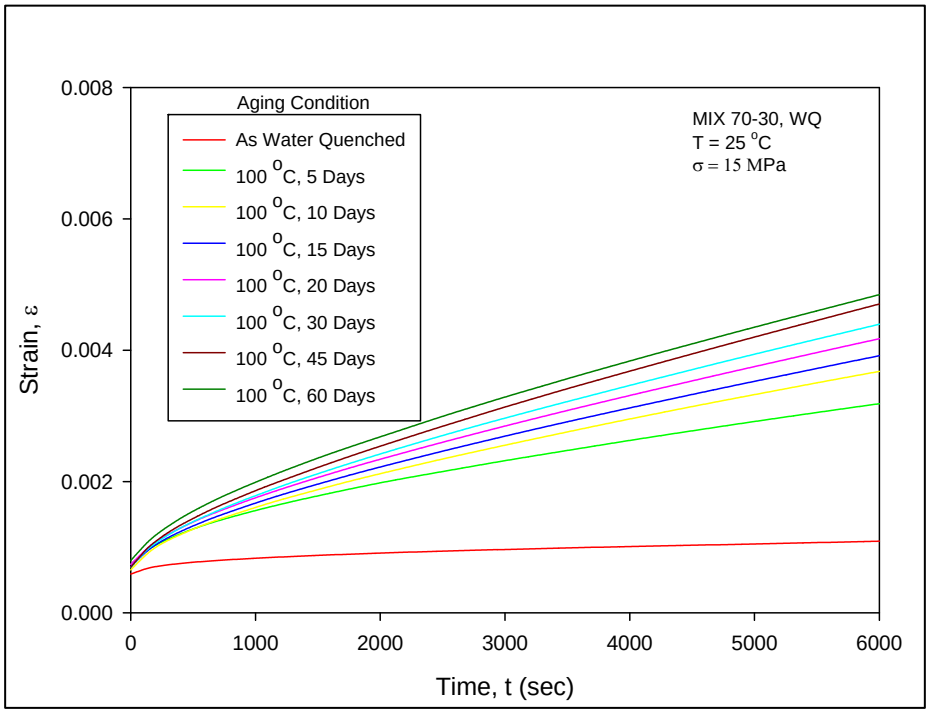

(b) Aging at T = 100 °C

Figure 4.13 - Creep curves for MIX 70-30 Aging from 0-60 Days

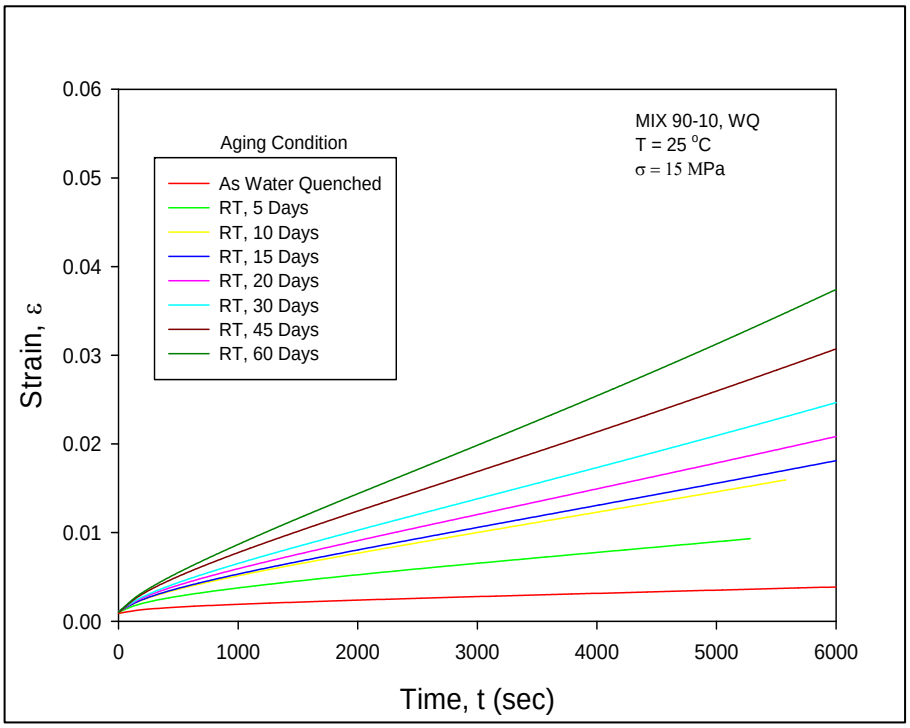

(a) Aging at T = 25 °C

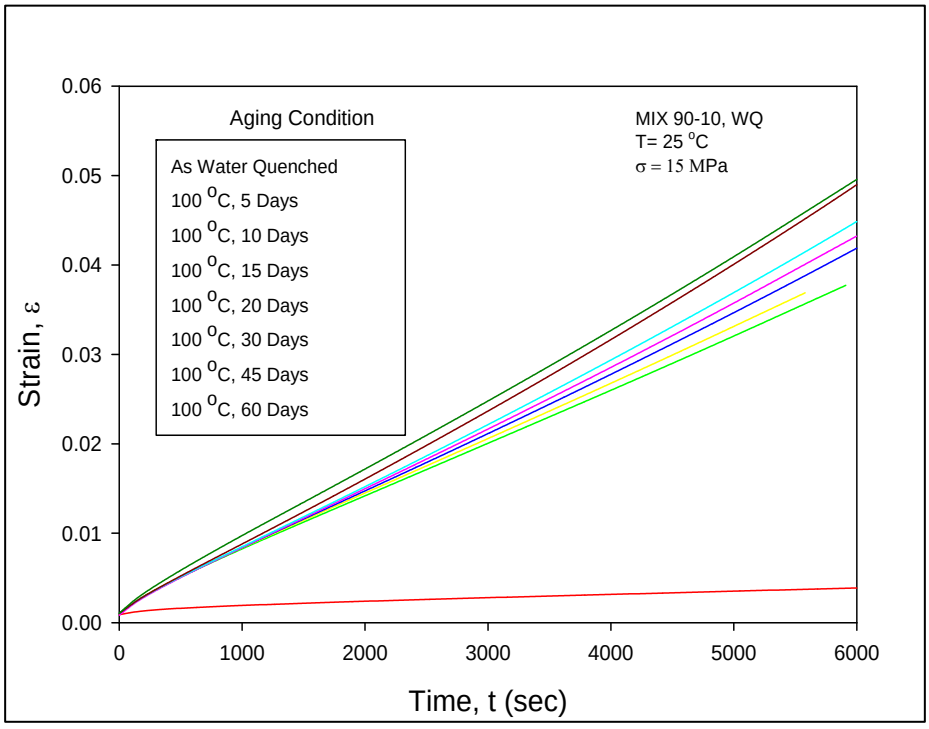

(b) Aging at T = 100 °C

Figure 4.14 - Creep curves for MIX 90-10 Aging from 0-60 Days

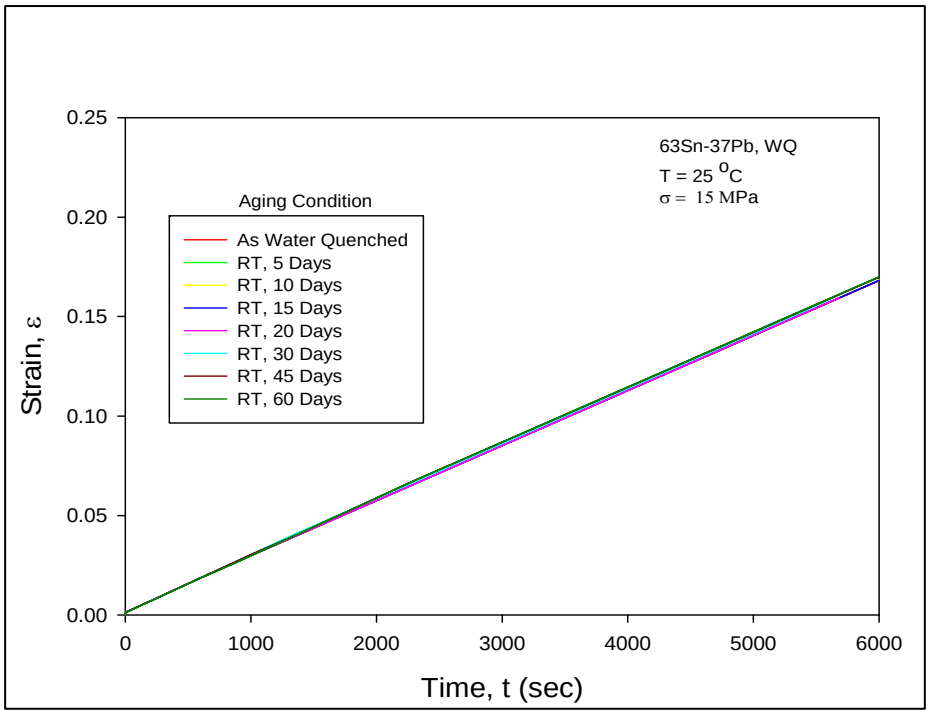

(a) Aging at T = 25 °C

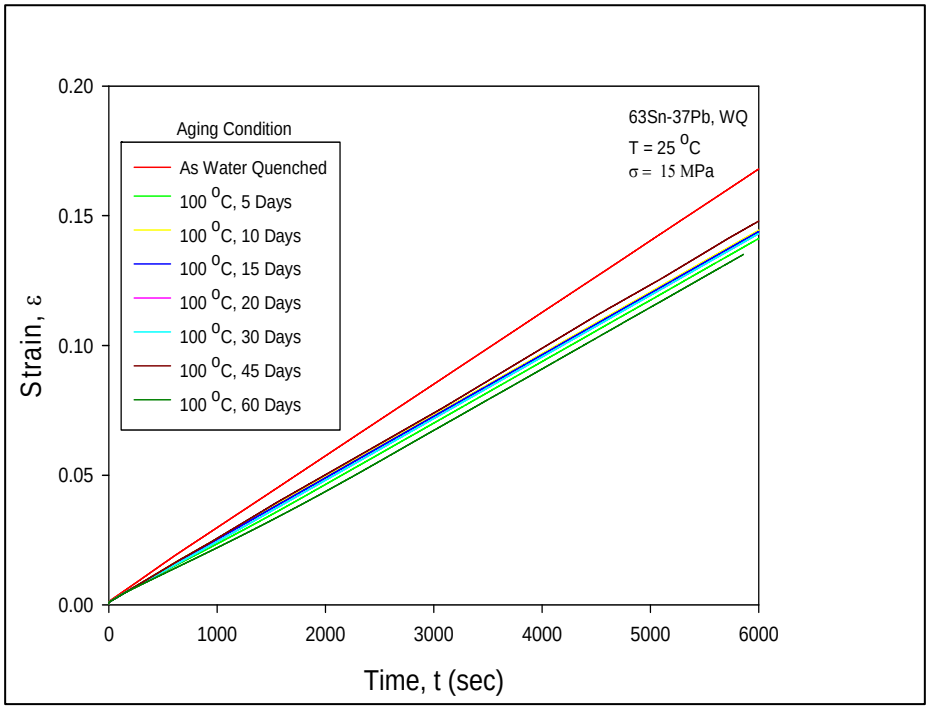

(b) Aging at T = 100 °C

Figure 4.15 - Creep curves for 63Sn-37Pb Aging from 0-60 Days

4.4.2. Evolution of Creep Rate with Aging Exposure

The effects of aging on the creep rate can be better seen by plotting the extracted secondary creep rates versus the aging time for each alloy. Figure 4.16-4.21 illustrate the creep rate evolution as a function of aging time and aging temperature. In each plot, the creep rate evolution is indicated for each of the two aging temperatures. Each data point represents the average creep rate measured for the 5 samples tested at a given set of aging conditions. For each alloy and aging temperature, the data points were fit well with an exponential relationship:

$$\dot{\varepsilon} = e^{C_0 + C_1 t + C_2 (1 - e^{-C_3 t})} \tag{4.1}$$

$$\log \dot{\varepsilon} = C_0 + C_1 t + C_2 (1 - e^{-C_3 t}) \tag{4.2}$$

If the strain rate versus aging time data are plotted with a log scale on the vertical axis (as in Figures 4.16-4.21), constant C_0 is the intercept and constant C_1 is the slope of the linear part of the curve for large aging times. Constants C_2 and C_3 are associated with the nonlinear transition region in the first 30-50 days of aging. Tables 4.1 and 4.2 indicate the material constants for all the solders for room temperature (25 ^{o}C) aging and elevated temperature (100 ^{o}C) aging with the above fitted model.

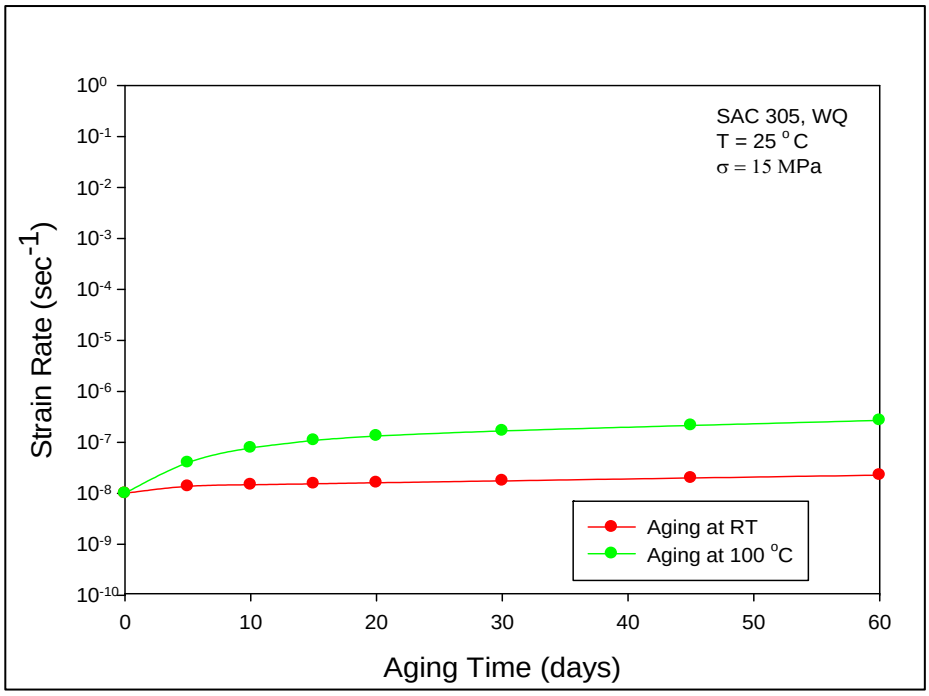

Figure 4.16 - Evolution of Creep Strain Rate with Aging

(SAC305; Aging at 25 and 100 °C)

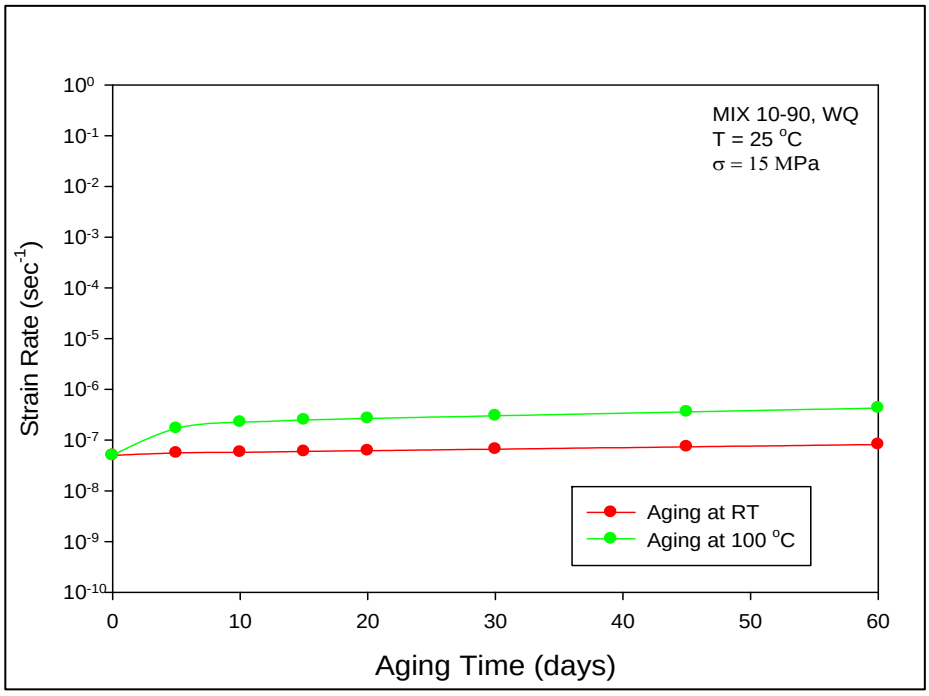

Figure 4.17 - Evolution of Creep Strain Rate with Aging

(MIX 10-90; Aging at 25 and 100 °C)

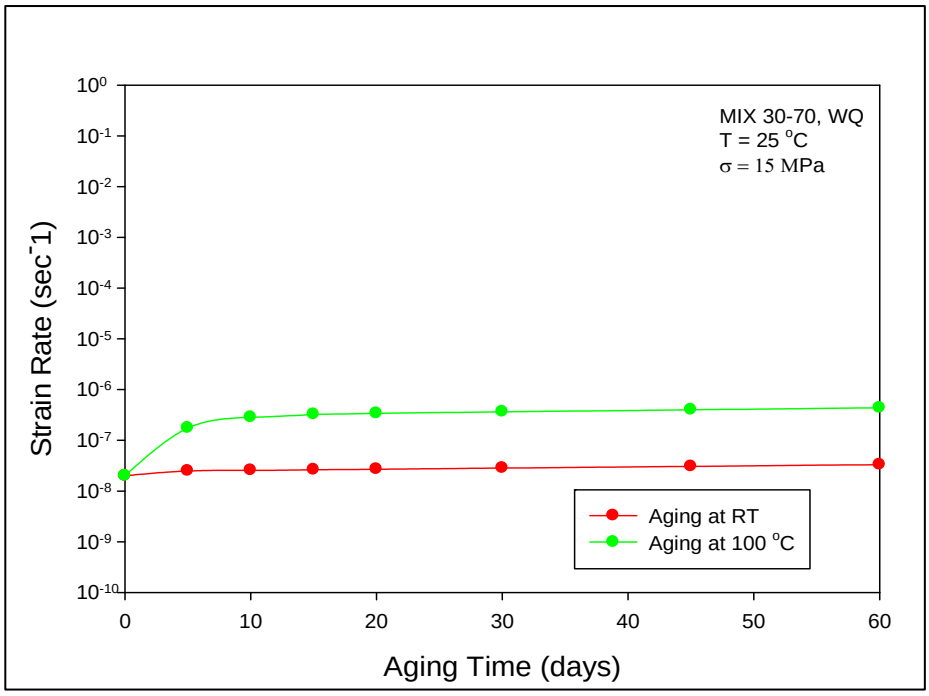

Figure 4.18 - Evolution of Creep Strain Rate with Aging

(MIX 30-70; Aging at 25 and 100 °C)

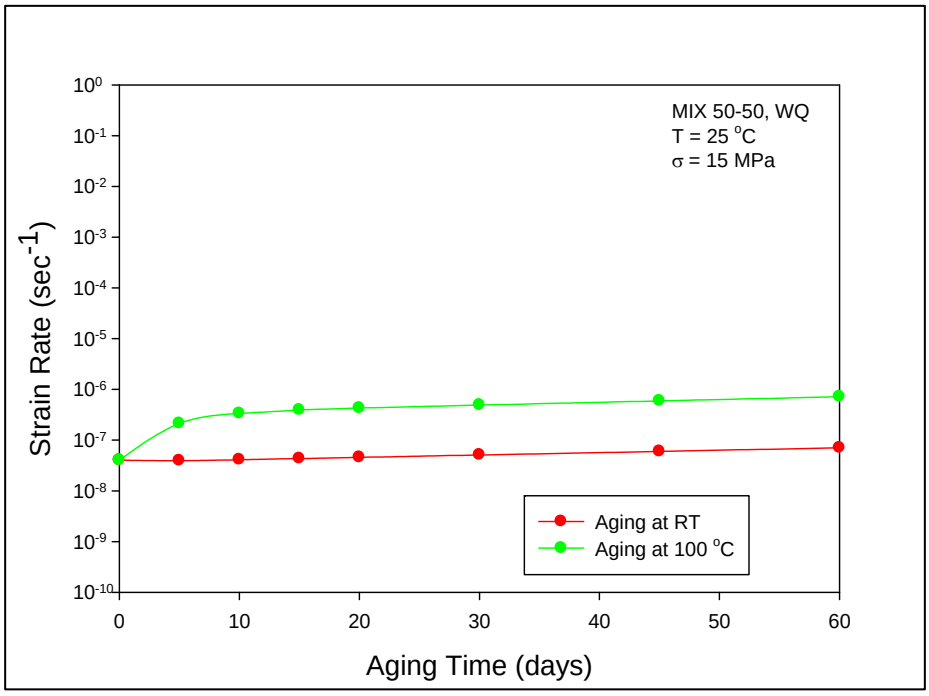

Figure 4.19 - Evolution of Creep Strain Rate with Aging

(MIX 50-50; Aging at 25 and 100 °C)

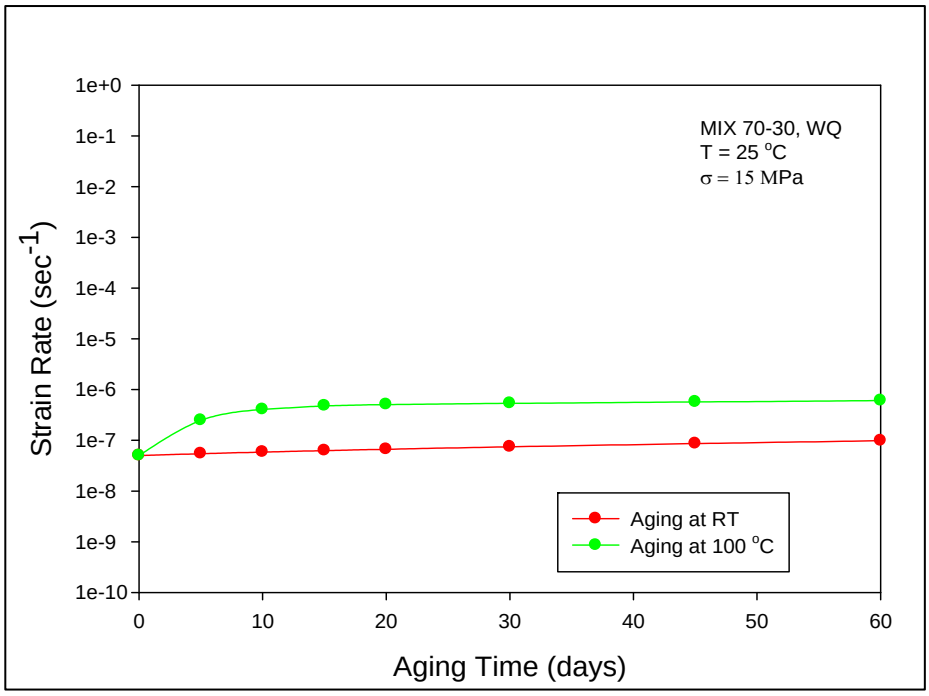

Figure 4.20 - Evolution of Creep Strain Rate with Aging

(MIX 70-30; Aging at 25 and 100 °C)

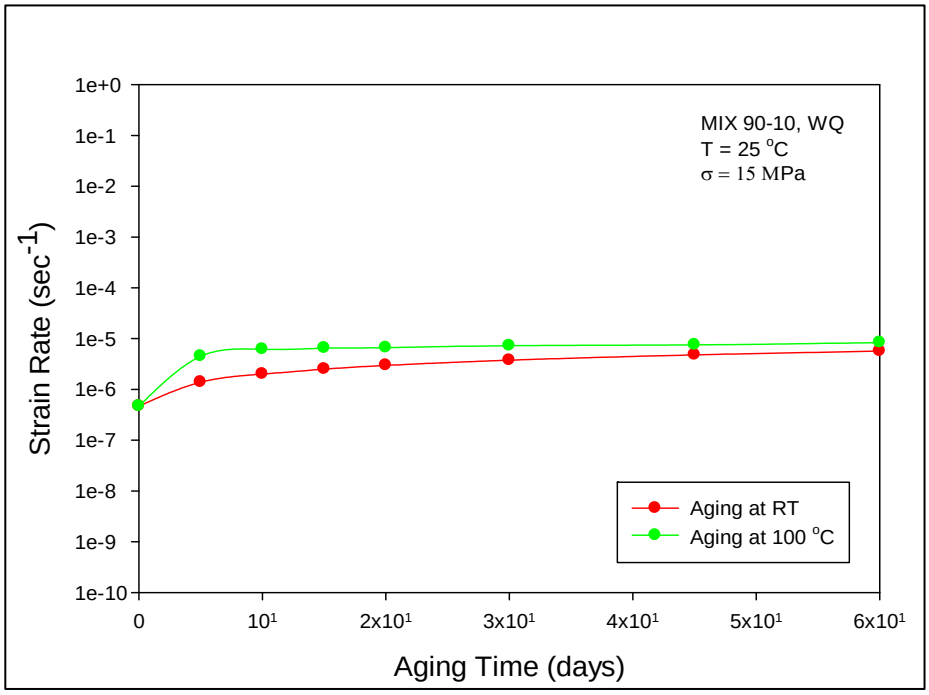

Figure 4.21 - Evolution of Creep Strain Rate with Aging

(MIX 90-10; Aging at 25 and 100 °C)

Solder	C_o	C_1	C_2	C_3
SAC305	-18.4229	0.00862	0.3045	0.4633
MIX 10-90	-16.738	0.00695	0.0044	-1.64E-06
MIX 30-70	-17.5374	0.0052	-0.0693	1.22E-06
MIX 50-50	-17.0324	0.00109	-0.0088	0.4039
MIX 70-30	-16.8101	0.0076	0.2342	0.0408
MIX 90-10	-14.5681	0.0161	1.5566	0.1899
63Sn-Pb37	-10.4477	0.0003	0.0185	0.0683

Table 4.1 - Material Constants for Creep Strain Rate vs. Aging Time (RT, 25 ^{o}C)

Solder	C_o	C_1	C_2	C_3
SAC305	-18.4084	0.0152	2.3713	0.1582
MIX 10-90	-16.775	0.0117	1.407	0.3246
MIX 30-70	-17.7263	0.0061	2.714	0.3085
MIX 50-50	-17.0305	0.0127	2.1202	0.2828
MIX 70-30	-16.963	0.1237	2.3973	7.6394
MIX 90-10	-14.6522	0.0027	2.6727	0.408
63Sn-Pb37	-10.447	0.0012	-0.4361	0.5619

Table 4.2 - Material Constants for Creep Strain Rate vs. Aging Time (100 ^{o}C)

From Figures 4.16-4.21, it is apparent that SAC305 and all the mixed formulation solder alloys experience dramatic changes in their creep rate for elevated temperature aging (8-27X). It is observed that the maximum increase in the creep rate occurs in the first 20 days, after that the strain rate increases linearly for SAC305 and all the mixtures. For the data shown in this work (up to 60 days of aging), there is no indication that an aging saturation point will be reached where the creep rate stabilizes. Table 4.3 contains the numerical values for the minimum creep rates of the non-aged samples and also the values of the maximum creep rates found for the samples aged for 60 days at 100 ^{o}C. The increase in creep rate for SAC 305 and MIX 30-70 are the highest at 27X and 22X. The change for MIX 10-90 was lowest at only 8.6X. This indicates that a lead content of 10% will significantly lower the changes in the creep rate during elevated temperature aging.

Alloy	Minimum Strain Rate	Maximum Strain Rate (After aging for 60 days at 100 ^{o}C)	Increase Ratio
SAC305	9.98E-09	2.69E-07	27.0X
MIX 10-90	5.00E-08	4.28E-07	8.6X
MIX 30-70	2.00E-08	4.36E-07	21.9X
MIX 50-50	4.01E-08	7.15E-07	17.8X
MIX 70-30	5.00E-08	6.05E-07	12.1X
MIX 90-10	4.67E-07	8.33E-06	17.8X

Table 4.3 - Increase in Creep Strain Rate with Aging (60 days at 100 ^{o}C)

4.4.3 Comparison of Mixed Formulation Solder to SAC305 and 63Sn-Pb37

As seen in the Figures 4.22 and 4.23, the aging induced changes in the creep strain rates of the mixed formulation alloys are much larger than the analogous changes observed for conventional eutectic 63Sn-37Pb solder, and they are slightly lower than that of SAC305. It is observed that the creep rates for 63Sn-Pb37 are restricted to a very narrow range of values between $\dot{\varepsilon} = 2 \times 10^{-5}$ and $\dot{\varepsilon} = 3 \times 10^{-5}$. For the same stress level, Figures 4.22 and Figure 4.23 illustrate that the mixed formulation and SAC305 solders begin with creep rates much lower than Sn-Pb solder. As the aging progresses, the creep rates of these alloys increase continuously, and they can approach the creep rates of Sn-Pb for long term aging (up to 1year). As indicated earlier, the effects of aging are much more pronounced for elevated temperature aging (100 ^{o}C) as compared to room temperature aging.

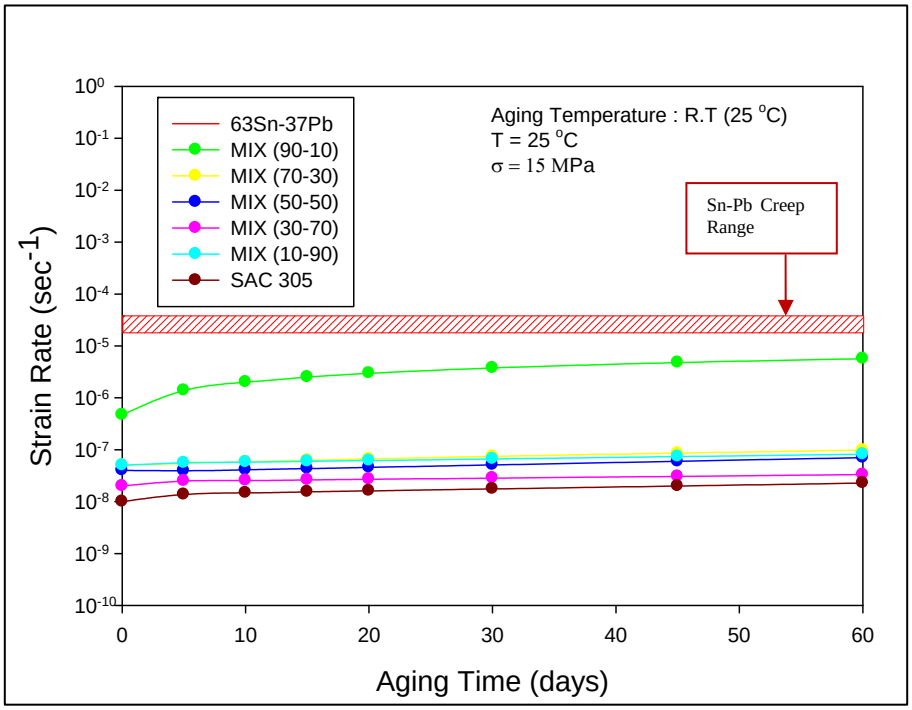

Figure 4.22 - Creep Strain Rate Comparison (Aging at 25 ^{o}C)

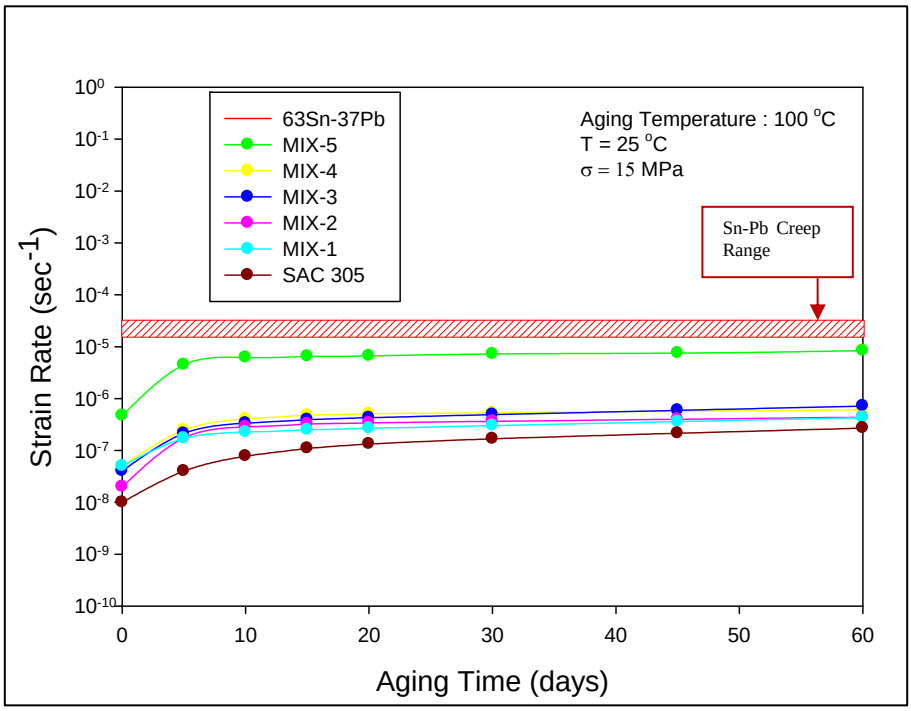

Figure 4.23 - Creep Strain Rate Comparison (Aging at 100 °C)

4.4.4 Influence of Sn-Pb Content on Creep Properties

Figures 4.24-4.26 show the variation of creep strain rate with Sn-Pb content. Abtew, et. al. [Abtew 2006] have shown that there is an appreciable increase in shear strength of mixed solder joints with Pb content of 15% and beyond. A similar trend was observed in this study for creep rates of samples aged at room temperature. The plots in Figures 4.25-4.26 clearly indicate a decrease in creep rate with aging for mixtures with Pb content beyond 10%.

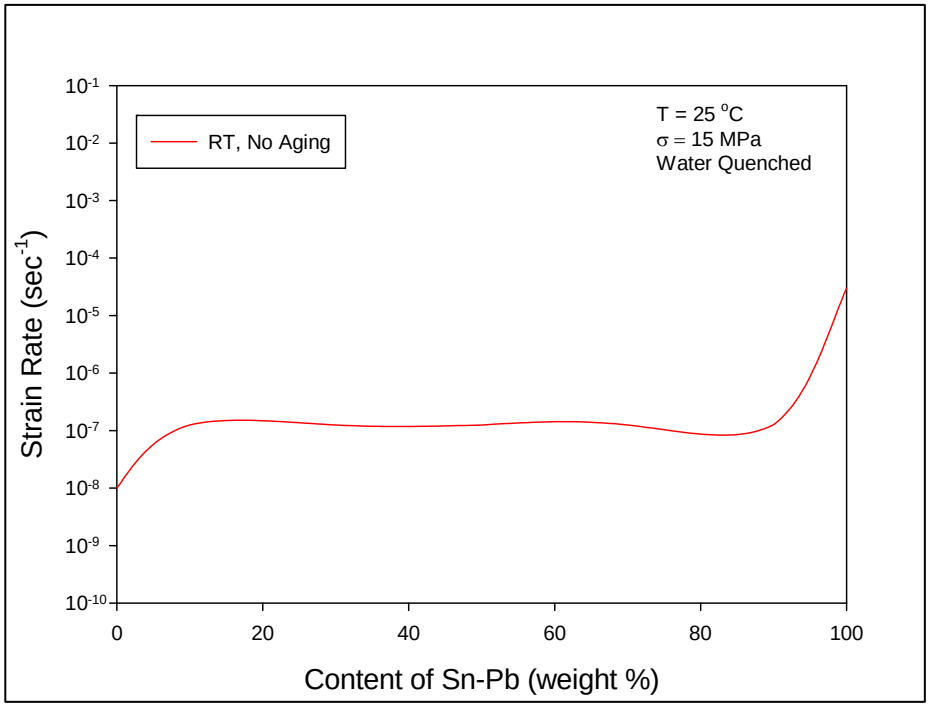

Figure 4.24 - Variation of Creep Strain Rate with Sn-Pb content (No Aging)

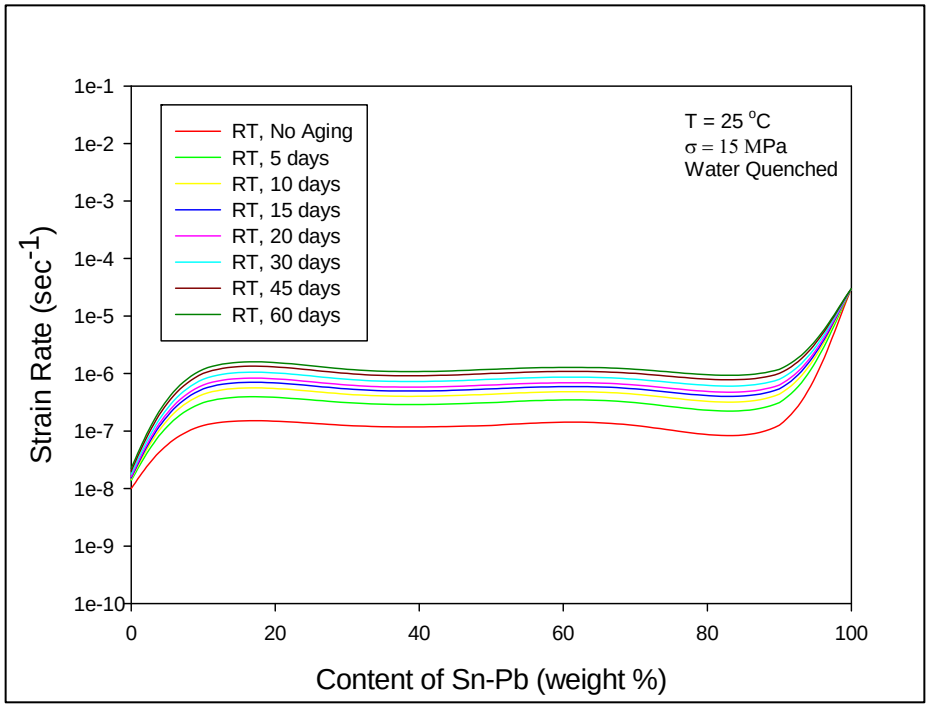

Figure 4.25 - Variation of Creep Strain Rate with Sn-Pb Content (Aging at 25 °C)

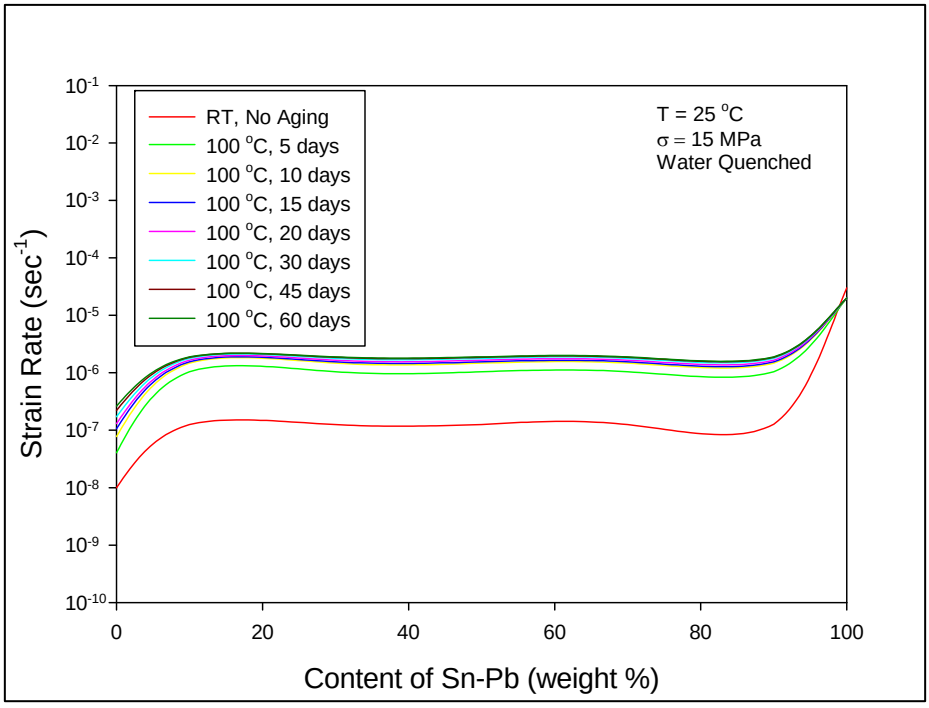

Figure 4.26 - Variation of Creep Strain Rate with Sn-Pb Content (Aging at 100 °C)

4.5 Summary

The microstructure, creep response, and physical properties of mixed solder alloys were investigated. The effects of room temperature and elevated temperature aging on creep rates of mixed solder alloys were investigated for aging up to 60 days. Analogous tests were conducted with eutectic Sn-Pb and SAC305. Thermal aging exacerbates the solder creep, and the effects were much more pronounced at elevated temperature. The major degradation in creep rates occurred in the first 30 days. After that time, the creep rates increase in a linear manner, and they continue to increase even after 60 days of aging. The creep rates of the mixed formulation solders varied in a non-linear manner with Sn-Pb content.

CHAPTER 5

EFFECTS OF TEMPERATURE ON TENSILE PROPERTIES OF SOLDERS

5.1 Introduction

In actual electronic packages, solder joints experience constant CTE mismatch during their course of operation and will be under constant stress at various temperatures. This phenomenon is further exacerbated at large temperature excursions. As mentioned in the literature review, the temperature dependent material properties of solders are not available at extreme low temperatures. This prevents the accurate application of finite element modeling for prediction of low temperature reliability of electronic packages and assemblies. It is therefore important to understand the temperature dependent properties of solders to accurately design the products for specific applications. In this work, the stress-strain behaviors of uniaxial specimens of 63Sn-37Pb and SAC 305 solders have been evaluated for temperatures from -175 ^{o}C to +150 ^{o}C. Testing was conducted at 15 different temperatures, at intervals of 25 ^{o}C. The variation of elastic modulus (E), Yield Strength (YS), and Ultimate Tensile Strength (UTS) have been measured as a function of testing temperature. In this study, all samples were preconditioned at 125 ^{o}C for 50 hours prior to testing to minimize the effects of aging.

5.2 Effects of Temperature on Tensile Properties

In this study, 10 specimens of each solder were tested for each temperature, from -175 ^{o}C to +150 ^{o}C, at intervals of 25 ^{o}C. Figure 5.1 shows a set of sample stress-strain curves, and the fit of the empirical model in eq. (3.2). For brevity and clarity of presentation, only the fitting models are shown in the remaining plots in this chapter. The complete set test results for all of the testing temperatures are included in the Appendix.

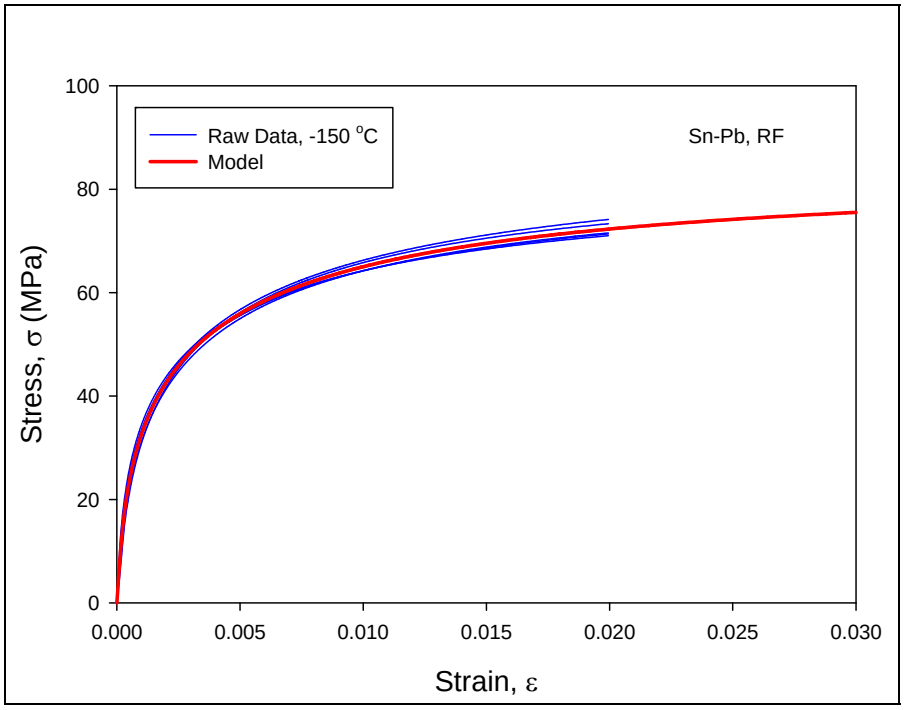

Figure 5.1 - Sample Stress-Strain Curves and the Fitting Model

Figure 5.2 shows the Stress-Strain curves for Sn-Pb tested at various temperatures. Figures 5.3-5.5 illustrate the extracted elastic modulus (Figure 5.3), YS (Figure 5.4), and UTS (Figure 5.5) at the various testing temperatures. The tensile properties of Sn-Pb solder vary linearly with the temperature.

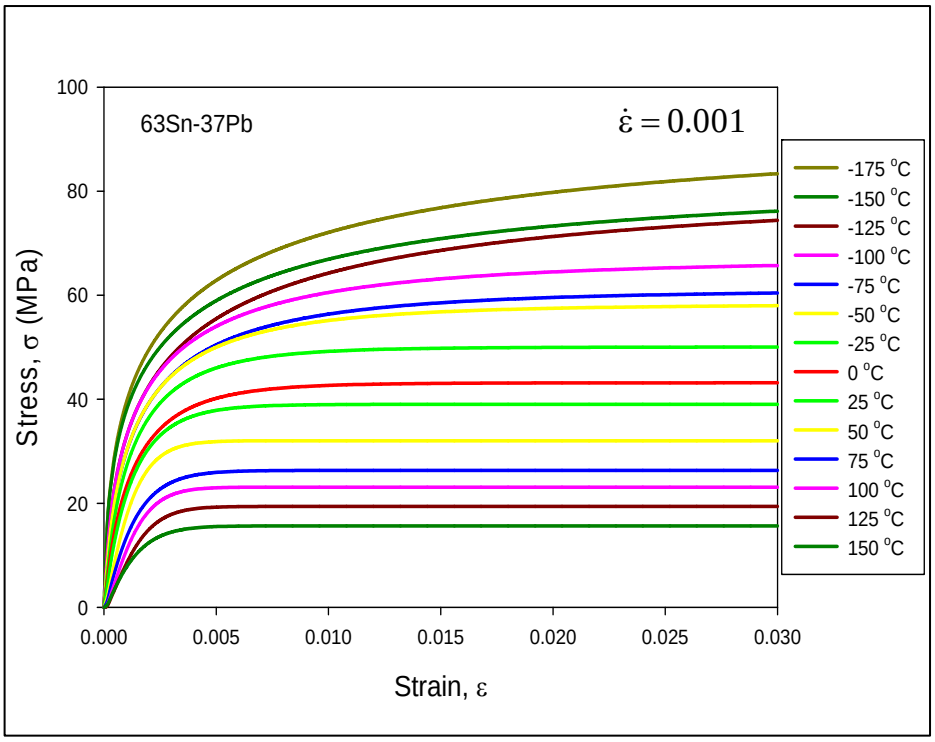

Figure 5.2 - Stress-Strain Curves for 63Sn-37Pb at Various Temperatures

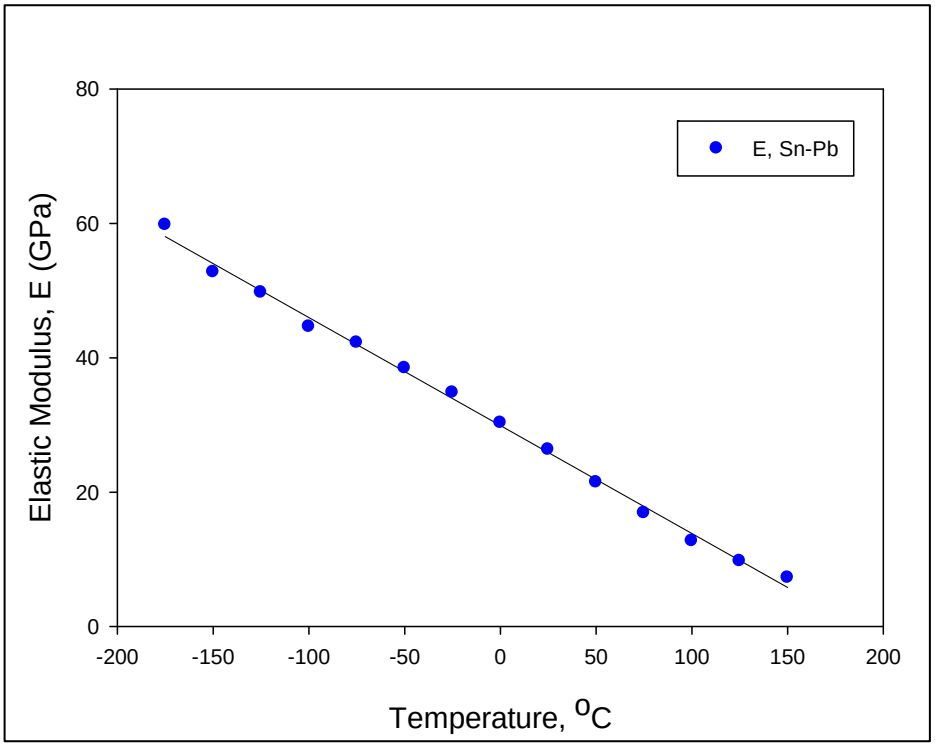

Figure 5.3 - 63Sn-37Pb Elastic Modulus vs. Testing Temperature

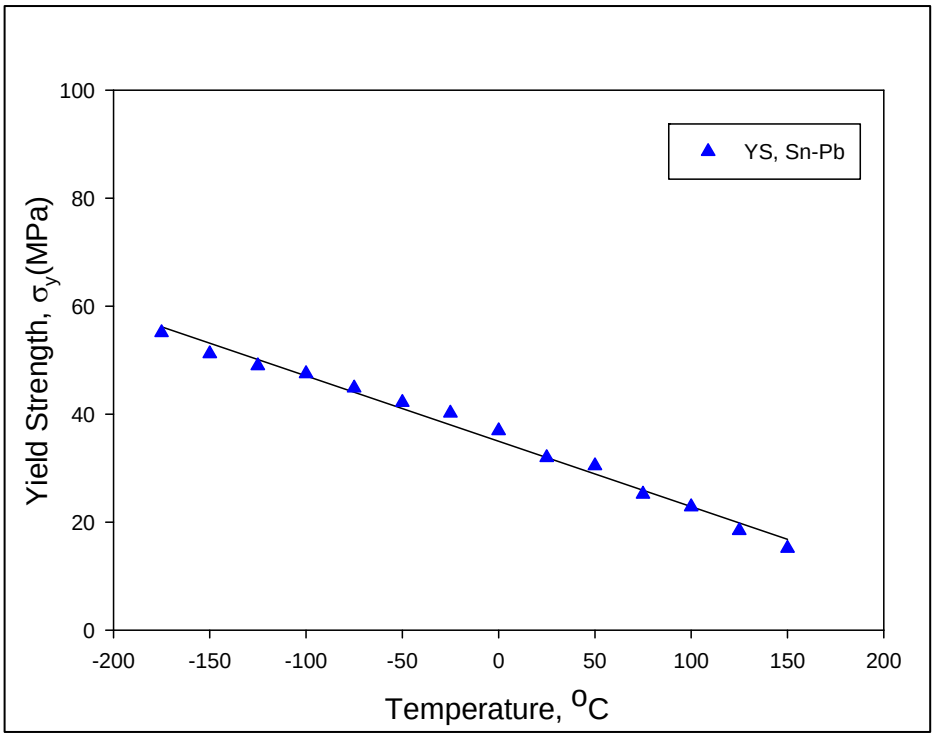

Figure 5.4 - 63Sn-37Pb Yield Strength vs. Testing Temperature

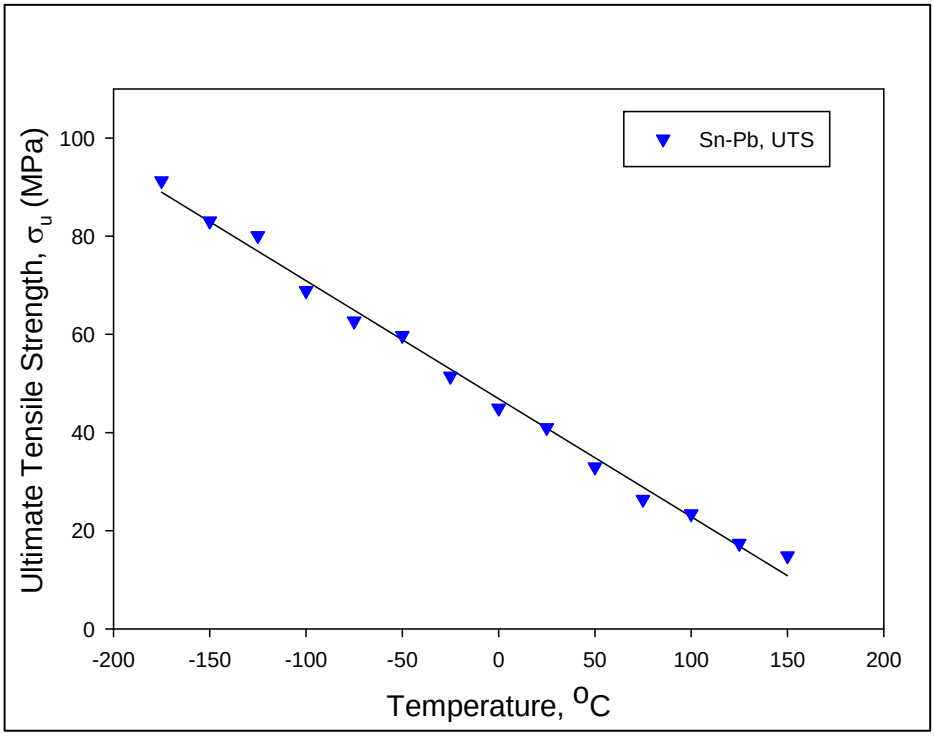

Figure 5.5 - 63Sn-37Pb UTS vs. Testing Temperature

The corresponding tensile data for SAC 305 were also collected at the same temperature intervals. Figure 5.5 shows the stress-strain curves for SAC 305 tested at various temperatures. The stress-strain curves follow a similar trend to those for Sn-Pb. The tensile properties of SAC 305 also vary linearly with temperature as shown in Figures 5.7-5.9. The linear relations for the material properties with the temperature are summarized in Table 5.1. Figure 5.8 indicates that UTS of SAC 305 is more sensitive to temperatures than UTS of Sn-Pb.

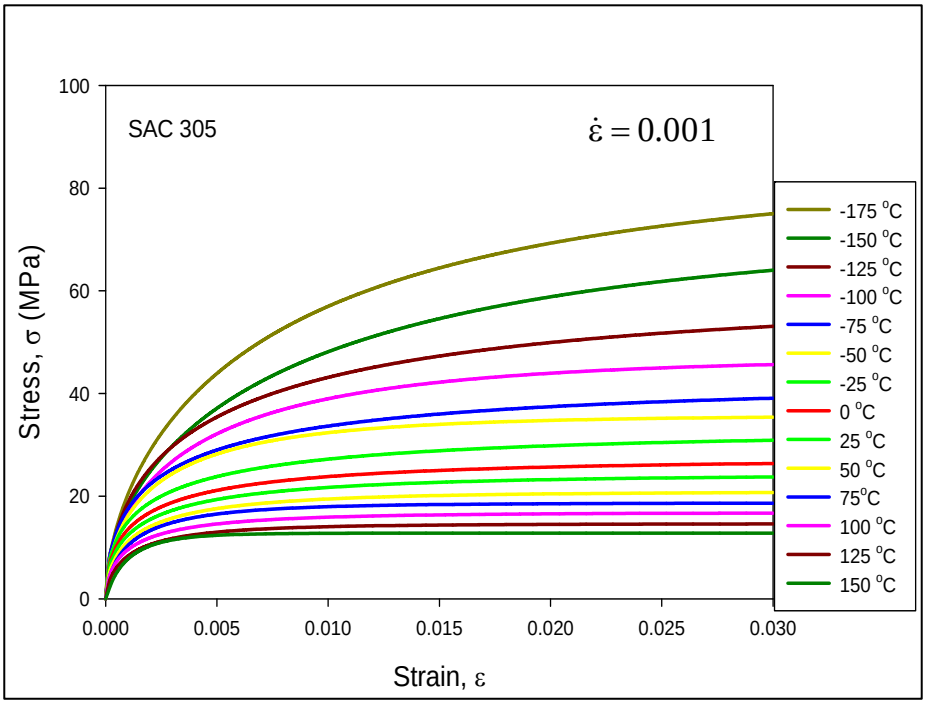

Figure 5.6 - Stress-Strain Curves for SAC 305 at Various Temperatures

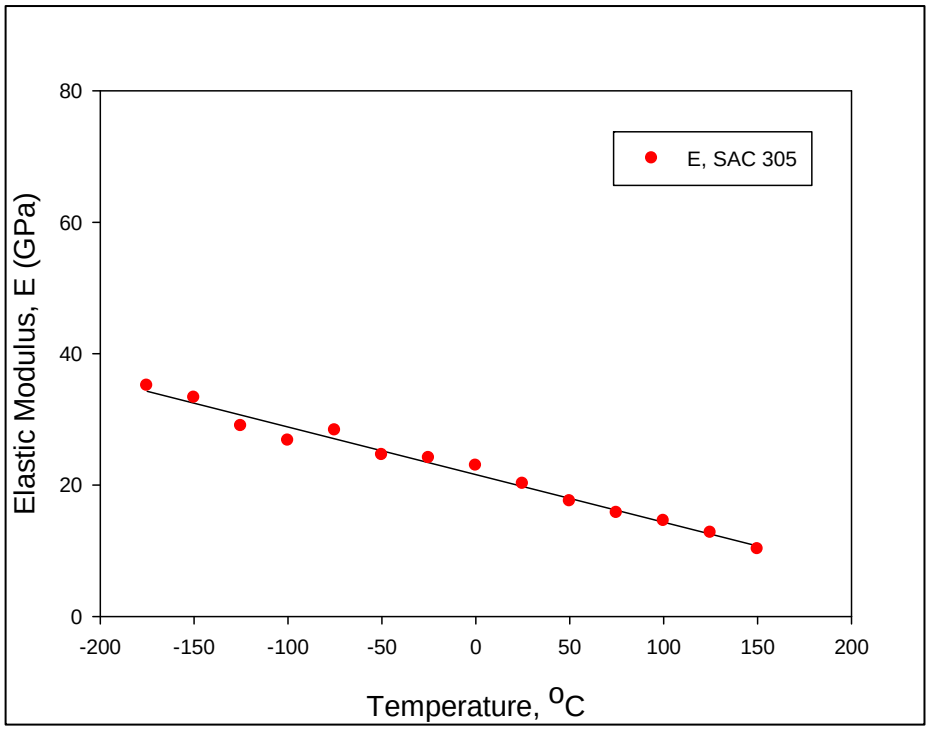

Figure 5.7 - SAC 305 Elastic Modulus vs. Testing Temperature

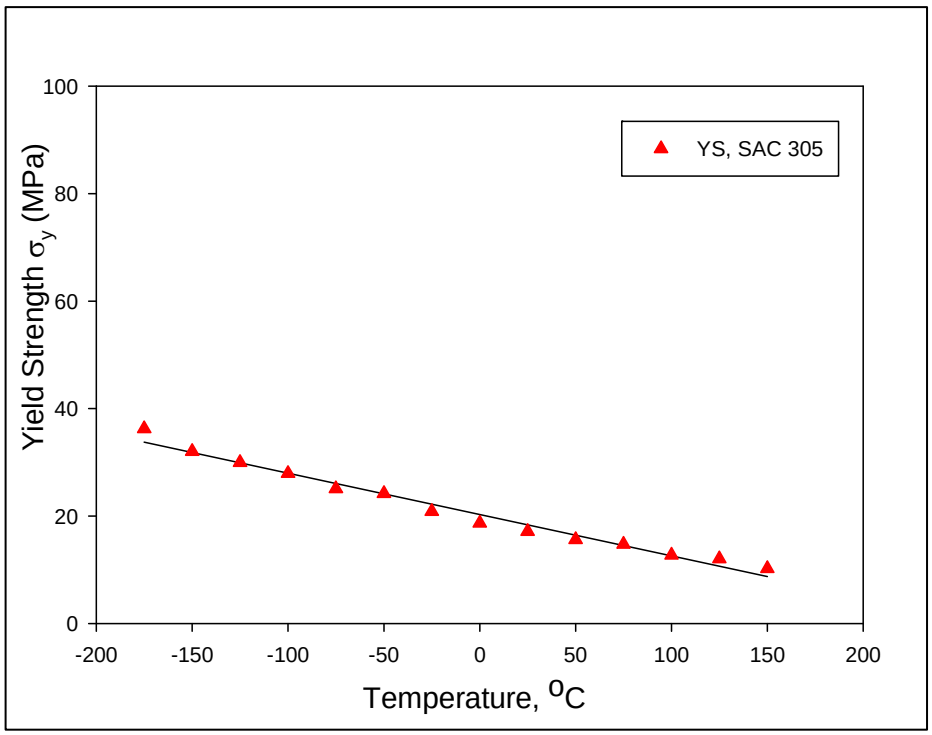

Figure 5.8 - SAC 305 Yield Strength vs. Testing Temperature

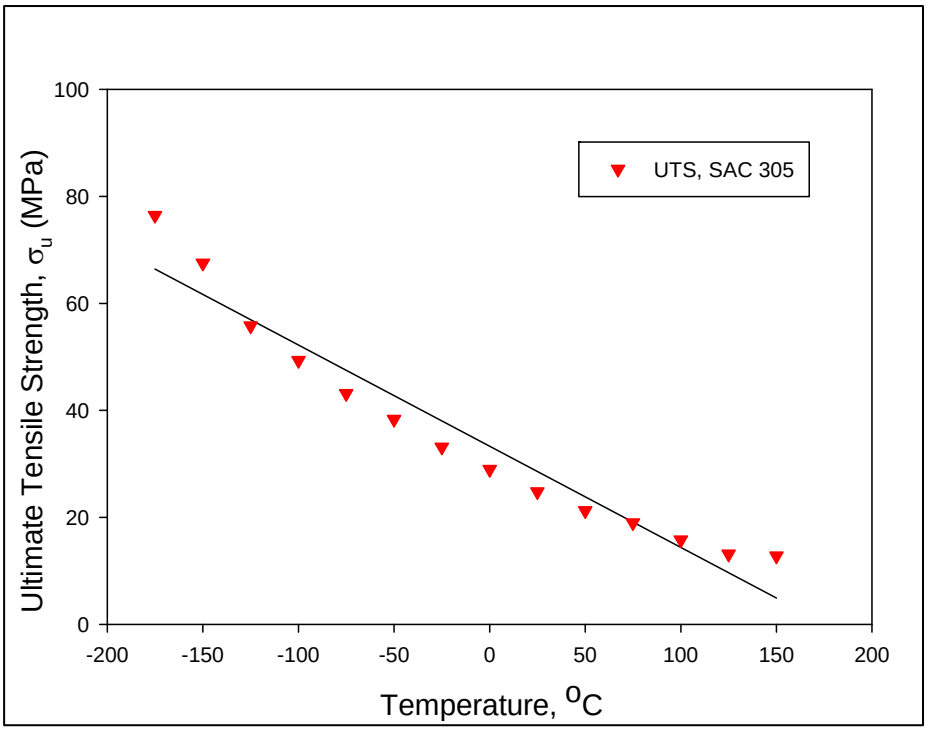

Figure 5.9 - SAC 305 UTS vs. Testing Temperature

Solder Alloy	Tensile properties	Temperature Dependence	R^2
63Sn-37Pb	E	-0.1606T+29.917	0.9966
	YS	-0.121T+34.982	0.9883
	UTS	-0.2403T+46.882	0.993
SAC 305	E	-0.0725T+21.588	0.982
	YS	-0.077T+20.285	0.9792
	UTS	-0.1892T+33.303	0.9402

Table 5.1 - Temperature Dependent Tensile Properties of 63Sn-37Pb and SAC 305

CHAPTER 6

SUMMARY AND CONCLUSION

6.1 Material behavior of Mixed Formulation Solders

In this work, the physical properties and mechanical behavior of mixed formulation solder materials were explored. Seven different mixture ratios of 63Sn-37Pb and SAC305 solder materials have been formed, which include five carefully controlled mixtures of the two solder alloys (by weight percentage) and the two extreme cases (pure Sn-Pb and pure SAC). For the various percentage mixtures, the melting point, pasty range, and creep curves have been characterized.

The melting point of the mixed solders decreased as expected until 30% of the alloy was Sn-Pb. At that point, the melting temperature was approximately constant (at or slightly below the Sn-Pb level of 183 ^{o}C). It was also observed that the pasty range of the mixed solders became large as the mixture neared the two extreme compositions of pure SAC or pure Sn-Pb. For mixtures between 30-70% Sn-Pb, the pasty range was very small (less than 2 ^{o}C). The microstructures realized with the various mixtures were found, and the various shapes and compositions of the intermetallic phases were identified and correlated to the mechanical measurements.

The variations of the creep rates with aging at room temperature (25 C) and elevated temperature (100 C) have also been measured. The creep rates of mixed

formulation solders were strongly dependent on mixed ratio. Eutectic Sn-Pb solder was found to be insensitive to aging (only small changes in creep rates with aging). All of the mixed formulation solders and pure SAC305 show dramatic effects with aging (large changes in creep rate) for elevated temperature aging at 100 ^{o}C. The largest relative changes were again seen for the pure SAC305 alloy (no Pb), while the smallest relative changes were seen for the pure Sn-Pb alloy (most Pb), indicating that Pb aids in resistance to aging induced degradation.

6.2 Temperature Effects on Tensile properties of Solders

The mechanical properties of solders are temperature dependent due to their high homologous temperature. In this study the effects of temperature were investigated on lead free SAC 305 and Sn-Pb solders. Linear relationships were found for the variation of the material properties with temperature.

BIBLIOGRAPHY

Abtew, M., and Kinyanjui, R., "Effect of Inert Atmosphere Reflow and Solder Paste Volume on the Microstructure and Mechanical Strength of Mixed Sn-Ag-Cu and Sn-Pb Solder Joints," *Proceedings of the SMTA International Conference*, pp. 74-78, 2006.

Bath, J., Hu, L., and Chiang, D., "Reliability Evaluation Of Lead-Free SnAgCu PBGA676 Components Using Tin-Lead and Lead-Free SnAgCu Solder Paste," *Proceedings of the SMTA International Conference*, pp. 891-901, 2005.

Cadek, J., *Creep in Metallic Materials*, Elsevier Science Publisher, 1988.

Chatterji, I., "Backward Compatibility, Are We Ready - A Case Study", *Proceedings of the SMTA International Conference*, pp. 416-424, 2006.

Chilton, A. C., Whitmore, M. A., and Hampshire, W. B., "Fatigue Failure in a Model SMD Joint," *Soldering and Surface Mount Technology*, Vol. 3, pp. 21-24, 1989.

Coyle, R. J., Solan, P. P., Serafino, A. J., and Gahr, S. A., "The Influence of Room Temperature Aging on Ball Shear Strength and Microstructure of Area Array Solder Balls," *Proceedings of the 50th Electronic Components and Technology Conference*, pp. 160-169, 2000.

Chiu, T. C., Zeng, K., Stierman, R., Edwards, D., and Ano, K., "Effect of Thermal Aging on Board Level Drop Reliability for Pb-free BGA Packages," *Proceedings of the 54th Electronic Components and Technology Conference*, pp. 1256-1262, 2004.

Choubey, A., and Menschow, D., "Effect of Aging on Pull Strength of SnPb, SnAgCu, and Mixed Solder Joints in Peripheral Surface Mount Components," *Journal of SMTA*, Vol. 19(2), pp. 33-37, 2006.

Chou, G. J. S., "Microstructure Evolution of SnPb and SnAgCu BGA Solder Joints During Thermal Aging," *Proceedings of the 8th Symposium on Advanced Packaging Materials*, pp. 39-46, 2002.

Chung, C. K., Aspandiar, R., Leong, K. F., Tay, C. S., "The Interactions of Lead (Pb) in Lead Free Solder (Sn/Ag/Cu) System," *Proceeding of 52nd Electronic Components and Technology Conference*, pp. 168-175, 2002.

Clech, J. P., "Lead-Free and Mixed Assembly Solder Joint Reliability Trends," *Proceedings of APEX 2004*, Paper S28-3, pp. 1-14, 2004.

Suh, D., Kim, D. W., Liu, P., Kim, H., Weninger, J. A., Kumar, C. M., Prasad, A., Grimsley, B. W., Tejada, H. B., "Effects of Ag content on fracture resistance of Sn–Ag–Cu lead-free solders under high-strain rate conditions", *Materials Science and Engineering* A 460–461 (2007) 595–603

Dai, L. H., Lee, S. R., "Characterization of Strain Rate-Dependent Behavior of 63Sn-37Pb Solder Alloy," Proceeding of the ASME InterPACK'05, pp. 307-313, 2001

Darveaux, R., "Shear Deformation of Lead Free Solder Joints," *Proceedings of the 55th Electronic Components and Technology Conference*, pp. 882-893, 2005

Wiese, S., and Wolter, K. J., "Creep of Thermally Aged SnAgCu Solder Joints," *Microelectronics Reliability*, Vol. 47, pp. 223-232, 2007.

Ding, Y., Wang, C., Tian, Y., and Li, M., "Influence of Aging on Deformation Behavior of 96.5Sn3.5Ag Lead Free Solder Alloy During In Situ Tensile Tests," *Journal of Alloys and Compounds*, Vo. 428, pp. 274-285, 2007.

Ding, Y., Wang, C., Li, M., and Bang, H. S., "Aging Effects on Fracture Behavior of 63Sn37Pb Eutectic Solder During Tensile Tests Under the SEM," *Materials Science and Engineering*, Vol. A384, pp. 314-323, 2004.

Dutta, I., Pan, D., Marks, R. A., Jadhav, S. G., "Effect of Thermo-mechanically Induced Microstructural Coarsening on the Evolution of Creep Response of SnAg-based Microelectronic Solders," *Materials Science and Engineering*, A 410-411, pp. 48-52, 2005.

Evans, J. L., Mitchell, C., Bozack, M., and Payton, L. N., "Reliability of SAC BGA Using SnPb Paste for Harsh Environment Electronics," *Proceedings of the SMTA International Conference*, 2005

Gagliano, R. A., Fine, M. E., Vaynman, S., and Stolkarts, V., "Shear Testing of Solder Joints: The Effect of Various Parameters on the Maximum Shear Stress of Eutectic Tin-Lead Solder," *Advanced Materials for the 21st Century: Proceedings of the 1999 Julia R. Weertman Symposium*, pp. 107-116, Cincinnati, OH, Oct. 31-Nov. 4, 1999.

Garofalo, F., *Fundamentals of Creep and Creep-Rupture in Metals*, The Macmillan Company, 1966.

Handwerker, C., "Transitioning to Lead-Free Assemblies," *Printed Circuit Design and Manufacture*, pp. 17-23, 2005.

Hasegawa, K., Noudou, T., Takahashi, A., and Nakaso, A., "Thermal Aging Reliability of Solder Ball Joint for Semiconductor Package Substrate," *Proceedings of the 2001 SMTA International*, pp. 1-8, 2001.

Hertzberg, R. W., *Deformation and Fracture Mechanics of Engineering Materials*, John Wiley & Sons Inc, 4th edition, 1996.

Hillman, D., Wells, M., Cho, K., and Collins, R., "The Impact of Reflowing a Pbfree Solder Alloy Using a Tin/Lead Solder Alloy Reflow Profile on Solder Joint Integrity," *Proceedings of the Lead-Free Conference*, CMAP Toronto, pp. 1-9, 2005.

Hua, F., Aspandiar, R., Clemons, G., and Chung, C. K., "Solder Joint Reliability Assessment of Sn-Ag-Cu BGA Components Attached with Eutectic Pb-Sn Solder," *Proceedings of the SMTA International Conference*, pp. 246-252, 2005.

Hua, F., Aspandiar, R., Rothman, T., and Anderson, C., "Solder Joint Reliability of Sn-Ag-Cu BGA Components Attached with Eutectic Pb-Sn Solder Paste," *Proceedings of the SMTA International Conference*, 2001.

Hunt, C., Nottay, J., Brewin, A., and Dinsdale, A., "Predicting Microstructure of Mixed Solder Alloy System", *NPL Report*, MATC(A) 83, April 2002.

Jiang, T. B., Du, C., and Xu L. H., "Finite Element Analysis and Fatigue Life Prediction of BGA Mixed Solder Joints," *Proceedings of High Density Packaging and Microsystem Integration - HDP '07*, pp. 1-6, 2007.

Jones, W. K., Liu, Y., Zampino, M. A., Gonzalez, G., Shah, M., Design and Reliability of Solders and Solder Interconnections, TMS, 1997a.

Jones, W. K., Liu, Y., Zampino, M. A., Gonzalez, G., "The At-Temperature Mechanical Properties of Lead-Tin Based Alloys," Advanced Microelectronics, pp. 30-34, 1997b.

Kannabiran, A., Elavarasan, T., Pannerselvam, and S., Ramkumar, M., "Investigation of the Forward And Backward Compatibility of Solder Alloys with Component Finishes For HASL and OSP PCB Finish," *Proceedings of the SMTA International Conference*, pp. 566-570, 2006.

Lampe, B. T. "Room Temperature Aging Properties of Some Solder Alloys," *Welding Journal*, Vol. 55(10), pp. 330s-340s, 1976.

Lang, R., Tanaka, H., Munegata, O., Taguchi, T., Narita, T., "The Effect of Strain Rate and Temperature on the Tensile Properties of Sn-3.5Ag Solder," Materials Characterization, Vol. 54, pp. 223-229, 2005.

Law, C. M. T., and Wu, C. M. L., "Microstructure Evolution and Shear Strength of Sn-3.5Ag-RE Lead Free BGA Solder Balls," *Proceedings of HDP'04*, pp. 60-65, 2004.

Lee, S. W., Tsui, Y. K., Huang, X., and Yan, C. C., "Effects of Room Temperature Storage Time on the Shear Strength of PBGA Solder Balls," *Proceedings of the 2002*

ASME International Mechanical Engineering Congress and Exposition, Paper IMECE2002-39514, pp. 1-4, 2002.

Li, M., Lee, K. Y., Olsen, D. R., Chen, W. T., Tan, B. T. C., and Mhaisalkar, S., "Microstructure, Joint Strength and Failure Mechanisms of SnPb and Pb-Free Solders in BGA Packages," I*EEE Transactions on Electronics Packaging*, Vol. 25(3), pp. 185-192, 2002.

Ma, H., "Constitutive Models of Creep for Lead-free Solders," *Journal of Material Science*, June 2009, pp. 3841-3851.

Ma, H., Suhling, J. C., Lall P., Bozack, M. J., "Reliability of the Aging Lead-free Solder Joint," *Proceeding of the 56th Electronic Components and Technology Conference*, pp. 49-864, San Diego, California, May 30-June 2, 2006.

Ma, H., Suhling, J. C., Zhang, Y., Lall, P., and Bozack, M. J., "The Influence of Elevated Temperature Aging on Reliability of Lead Free Solder Joints," *Proceedings of the 57th IEEE Electronic Components and Technology Conference*, pp. 653-668, Reno, NV, May 29-June 1, 2007.

Ma, H., Zhang, Y., Cai, Z., Suhling, J. C., Lall, P., and Bozack, M. J., "Aging Induced Evolution of Free Solder Material Behavior," *Proceedings of the EuroSimE 2008*, pp. 1-12, Freiburg, Germany, April 20-23, 2008.

McCormick, H., Snugovsky, P., Bagheri, Z., "Mixing Metallurgy: Reliability of SAC Balled Area Array Packages Assembled Using SnPb Solder", *Proceedings of the SMTA International Conference*, pp. 425-432, 2006.

Medvedev, A. S., "Aging of Tin-Lead Solders and Joints Soldered by Them," *Metallovedenie i Obrabotka Metallov,* No. 7, pp. 16-23, 1956.

Miyazawa, Y., and Ariga, T., "Microstructural Change and Hardness of Lead Free Solder Alloys," *Proceedings of the First International Symposium on Environmentally Conscious Design and Inverse Manufacturing*, pp. 616-619, 1999.

Miyazawa, Y., and Ariga T., "Influences of Aging Treatment on Microstructure and Hardness of Sn-(Ag, Bi, Zn) Eutectic Solder Alloys," *Materials Transactions of the Japan Institute of Metals*, Vol. 42(5), pp. 776-782, 2001.

Nandagopal, B., "Study on Assembly, Rework Process, Microstructures and Mechanical Strength of Backward Compatible Assembly," *Proceedings of the SMTA International Conference*, pp. 861-870, 2005.

Nandagopal, B., Mei, Z., and Teng, S., "Microstructure and Thermal Fatigue Life of BGAs with Eutectic Sn-Ag-Cu Balls Assembled at 210 C with Eutectic Sn-Pb Solder

Paste," *Proceeding of the 56th Electronic Components and Technology Conference*, pp. 875-883, 2006.

Nguyen, J., Geiger, D., Rooney, D., and Shangguan, D., "Reliability Study of Lead-Free Area Array Packages with Tin-Lead Soldering Processes", *Proceedings of the SMTA International Conference*, pp. 433-438, 2006.

Nguyen, J., and Shangguan, D., "Solder Joint Characteristics and Reliability of Lead-Free Area Packages Assembled Under Various Tin-Lead Soldering Process Conditions," *Proceeding of 57th Electronic Components and Technology Conference*, pp. 1340-1349, 2007.

Nose, H., Sakane, M., Tsukada, T., Nishimura, H., "Temperature and Strain Rate Effects on Tensile Strength and Inelastic Constitutive Relationship of Sn-Pb Solders," Journal of Electronic Packaging, Vol. 124, pp. 59-66, 2003.

Oliver, J., Nylen, M., Rod, O., and Markou, C., "Fatigur Properties of Sn3.5Ag0.7Cu Solder Joints and Effects of Pb-Contamination," *Proceedings of the SMTA International Conference*, pp. 246-252, 2002.

Pang, J. H. L., Low, T. H., Xiong, B. S., Xu, L., and Neo, C. C.., "Thermal cycling aging effects on Sn–Ag–Cu solder joint microstructure, IMC and strength," *Thin Solid Films*, Vol. 462-463, pp. 370-375, 2004.

Plumbridge, W. J., Gagg. C. R., "Effects of Strain Rate and Temperature on the Stress-strain Response of Solder Alloys," Journal of Materials Science: Materials in Electronics, Vol. 10, pp. 461-468, 1999.

Shi, X. Q., Zhou, W., Pang, H. L. J., Wang, Z. P., "Effect of Temperature and Strain Rate on Mechanical Properties of 63Sn/37Pb Solder Alloy," Journal of Electronic Packaging, Vol. 121 (3), pp. 179-185, 1999.

Sun, F., "Solder Joint Reliability of Sn-Ag-Cu BGA and Sn-Pb Solder Paste," *Proceeding of 6th International Conference on Electronic Packaging Technology*, 2006.

Theuss, H., Kilger, T., and Ort, T., "Solder Joint Reliability of Lead-free Solder Balls Assembled with SnPb Paste," *Proceeding of the 53rd Electronic Components and Technology Conference*, pp. 331-337, 2003.

Thornton, P. A., Colangelo V. J., *Fundamentals of Engineering Materials*, Prentice-Hall, Inc., pp. 227-229, 1985.

Tsui, Y. K. , Lee, S. W., and Huang, X., "Experimental Investigation on the Degradation of BGA Solder Ball Shear Strength Due to Room Temperature Aging," *Proceedings of the 4th International Symposium on Electronic Materials and Packaging*, pp. 478-481, 2002.

Xiao, Q.; Bailey, H. J.; and Armstrong, W. D., “Aging Effects on Microstructure and Tensile Property of Sn3.9Ag0.6Cu Solder Alloy,” *Journal of Electronic Packaging*, Vol. 126(2), pp. 208-212, 2004.

Xiao, Q., Nguyen, L., and Armstrong, W. D., “Aging and Creep Behavior of Sn3.9Ag0.6Cu Solder Alloy,” *Proceedings of the 54th Electronic Components and Technology Conference*, pp. 1325-1332, 2004.

Zhang, Y., Cai, Z., Suhling, J. C., Lall, P., and Bozack, M. J., “The Effects of Aging Temperature on SAC Solder Joint Material Behavior and Reliability,” *Proceedings of the 58th IEEE Electronic Components and Technology Conference*, pp. 99-112, Orlando, FL, May 27-30, 2008.

Zhang, Y., Cai, Z., Suhling, J. C., Lall, P., and Bozack, M. J., “The Effects SAC alloy composition on aging resistance and Reliability,” *Proceedings of the 59th IEEE Electronic Components and Technology Conference*, pp. 370-389, San Diego, CA, May 26-39, 2009a.

Zhang, Y., Kurumaddali, K., Suhling, J. C., Lall, P., and Bozack, M. J., “Analysis of the mechanical behavior, microstructure, and reliability of mixed formulation solder joints,” *Proceedings of the 59th IEEE Electronic Components and Technology Conference*, pp. 759-770, San Diego, CA, May 26-39, 2009b.

Zbrzezny, A.R., Snugovsky, P., Lindsay, T., and Lau, R., “Reliability Investigation of Mixed BGA Assemblies,” *IEEE Transactions on Electronics Packaging Manufacturing*, Vol. 29(3), pp. 211-216, 2006

Wable, G. S., Chada, S., Neal, B., and Fournelle, R. A., “Solidification and Shrinkage defects in Electronic Solders,” *Journal of Electronic Materials*, June 2005, pp. 38-42.

APPENDIX

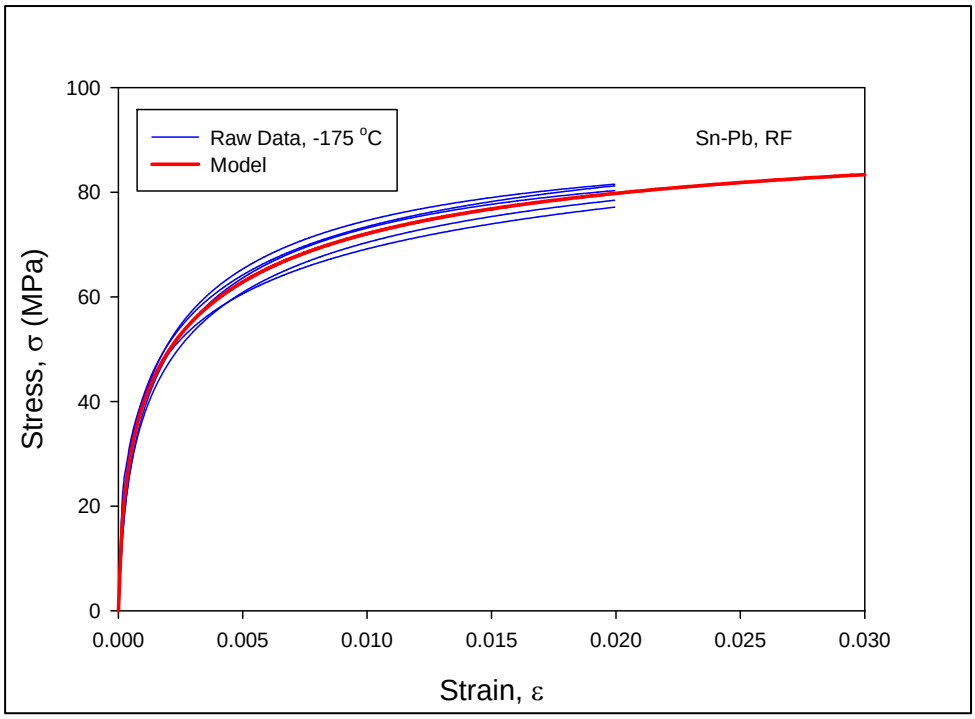

Figure A.1 - Stress-Strain Curves for 63Sn-37Pb at -175 °C

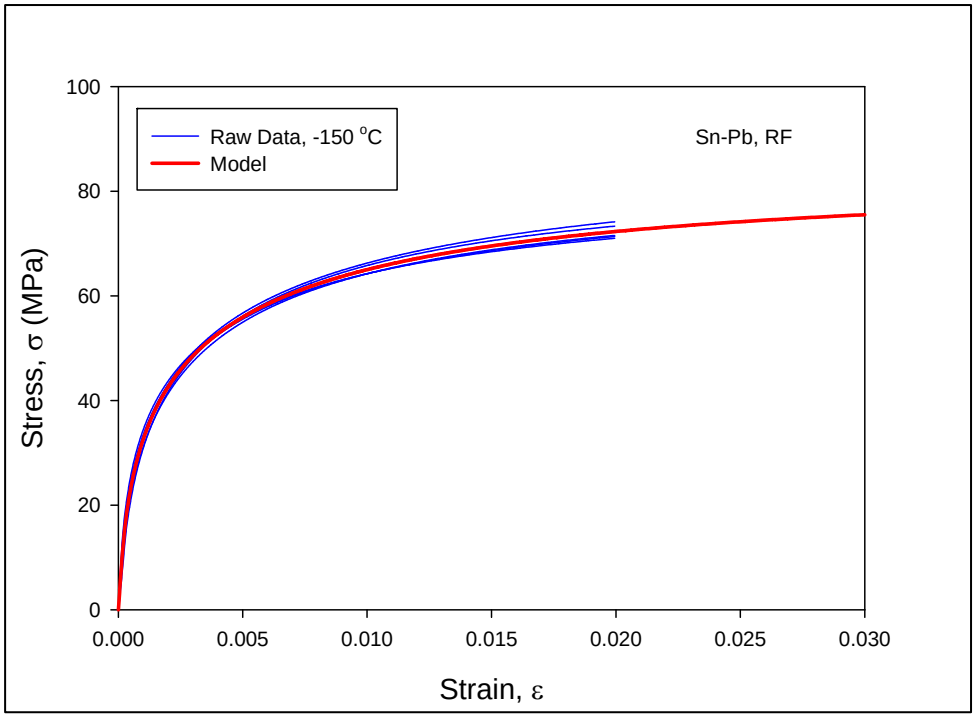

Figure A.2 - Stress-Strain Curves for 63Sn-37Pb at -150 °C

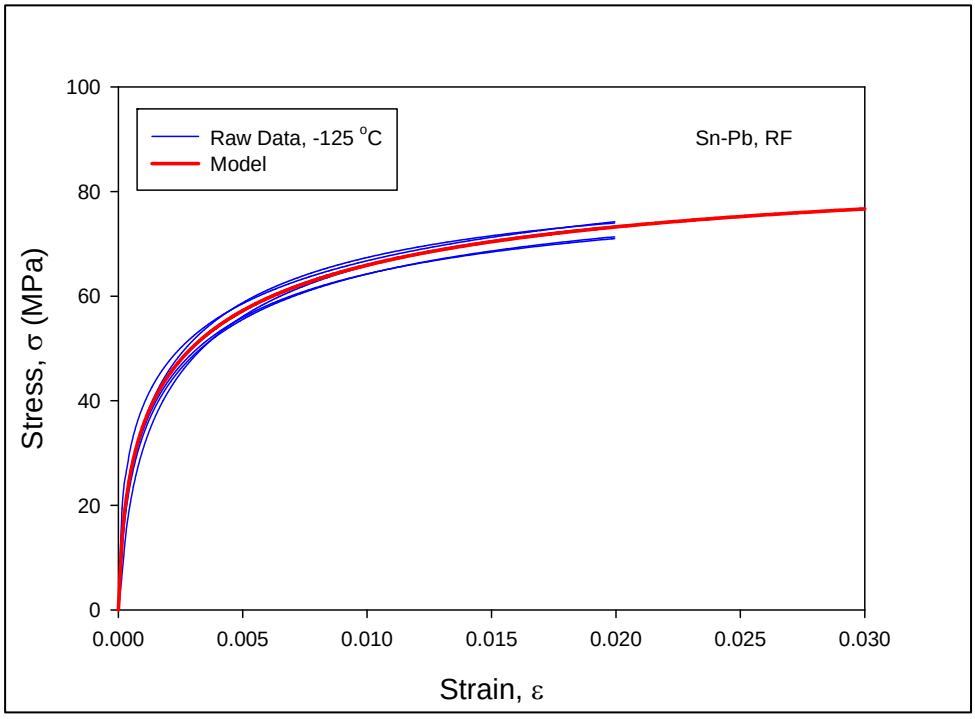

Figure A.3 - Stress-Strain Curves for 63Sn-37Pb at -125 °C

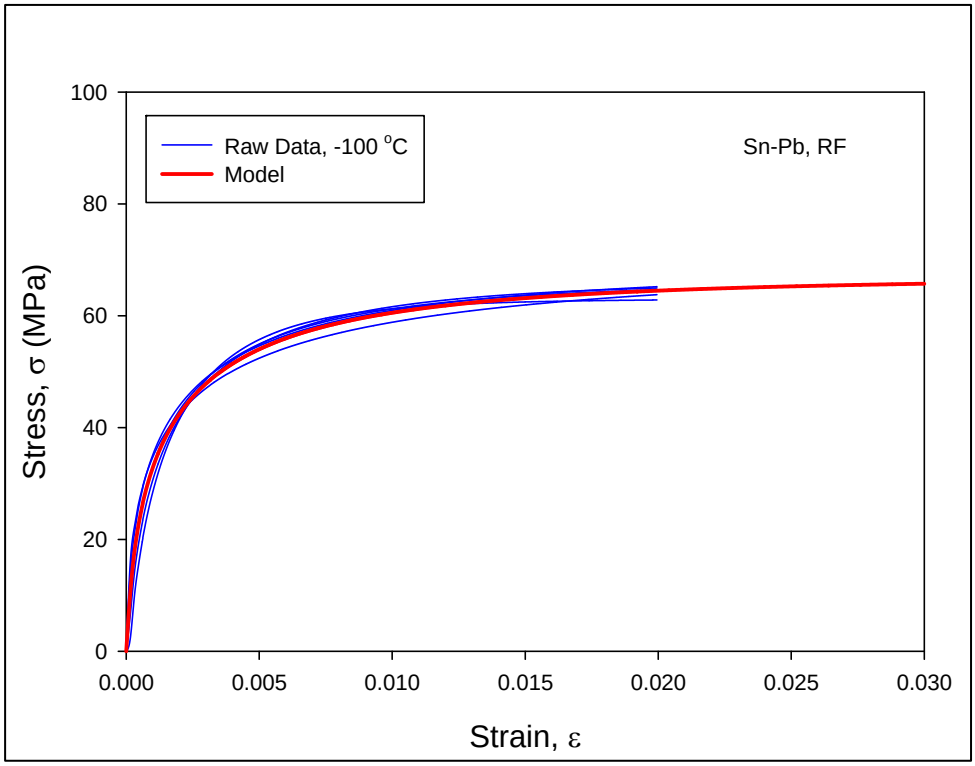

Figure A.4 - Stress-Strain Curves for 63Sn-37Pb at -100 °C

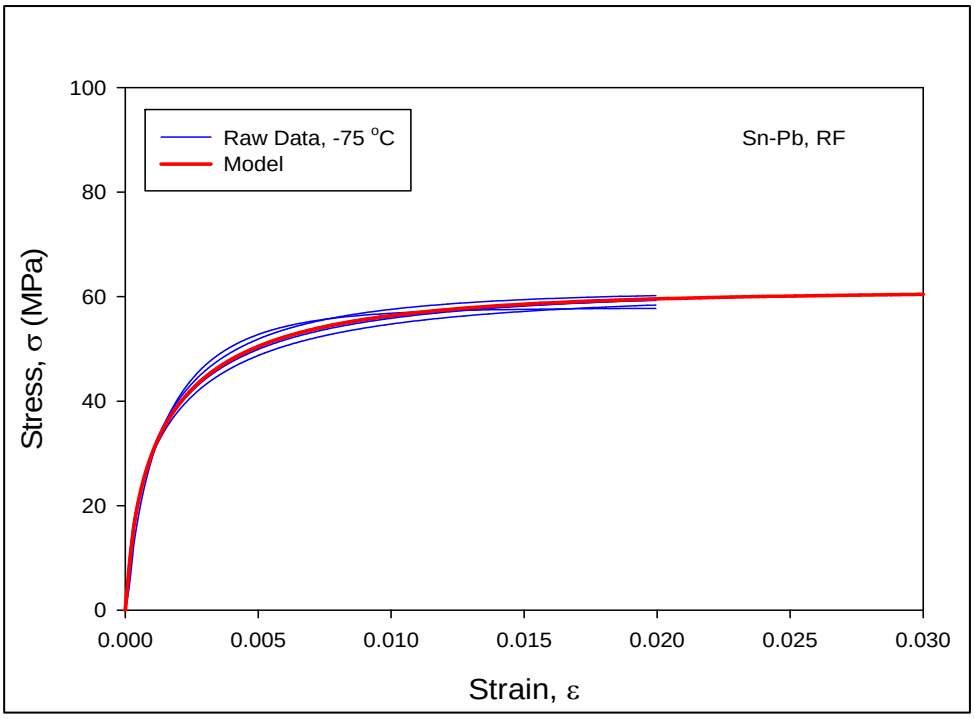

Figure A.5 - Stress-Strain Curves for 63Sn-37Pb at -75 °C

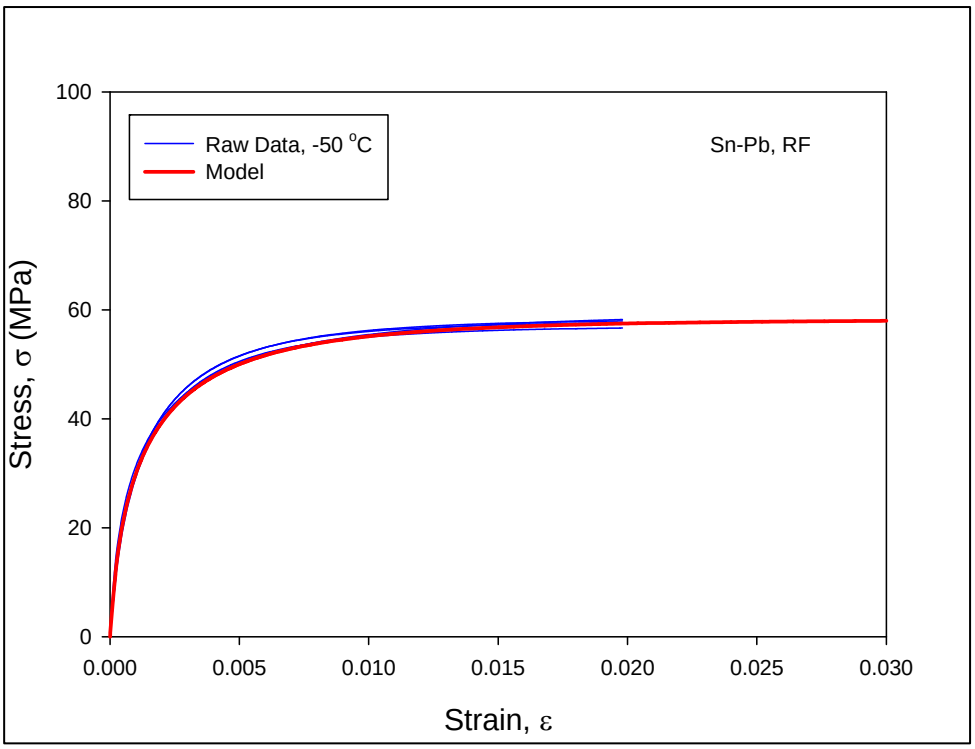

Figure A.6 - Stress-Strain Curves for 63Sn-37Pb at -50 °C

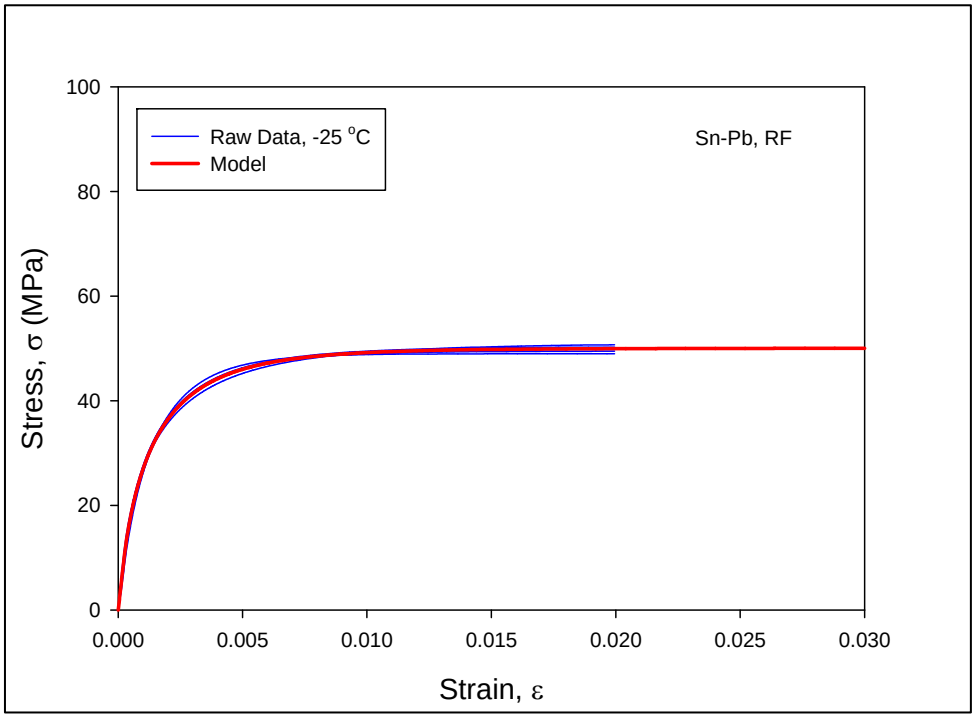

Figure A.7 - Stress-Strain Curves for 63Sn-37Pb at -25 °C

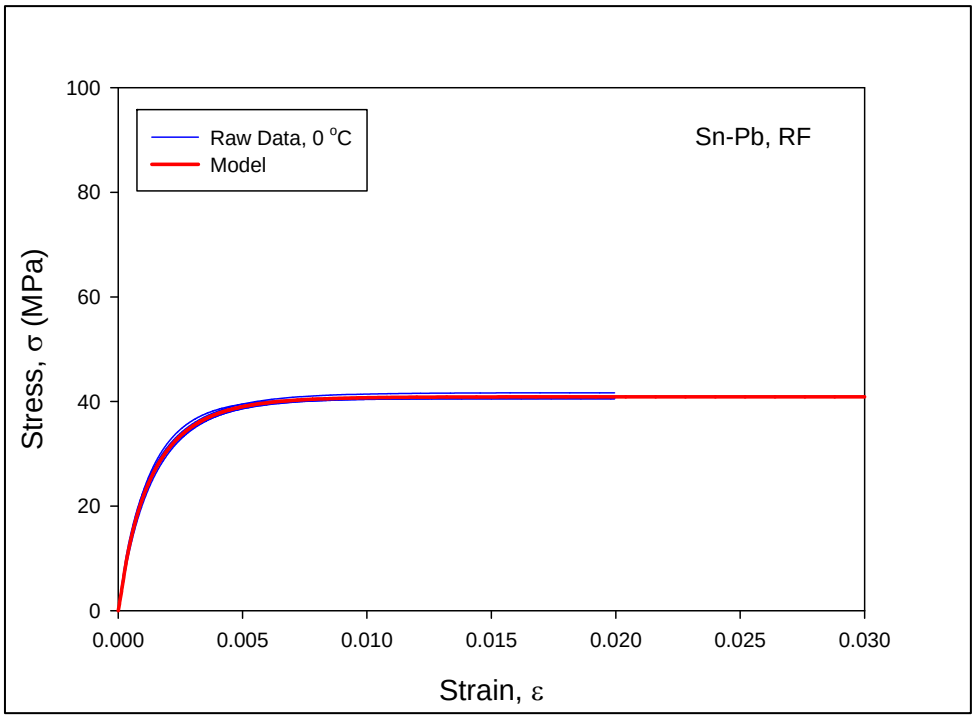

Figure A.8 - Stress-Strain Curves for 63Sn-37Pb at 0 °C

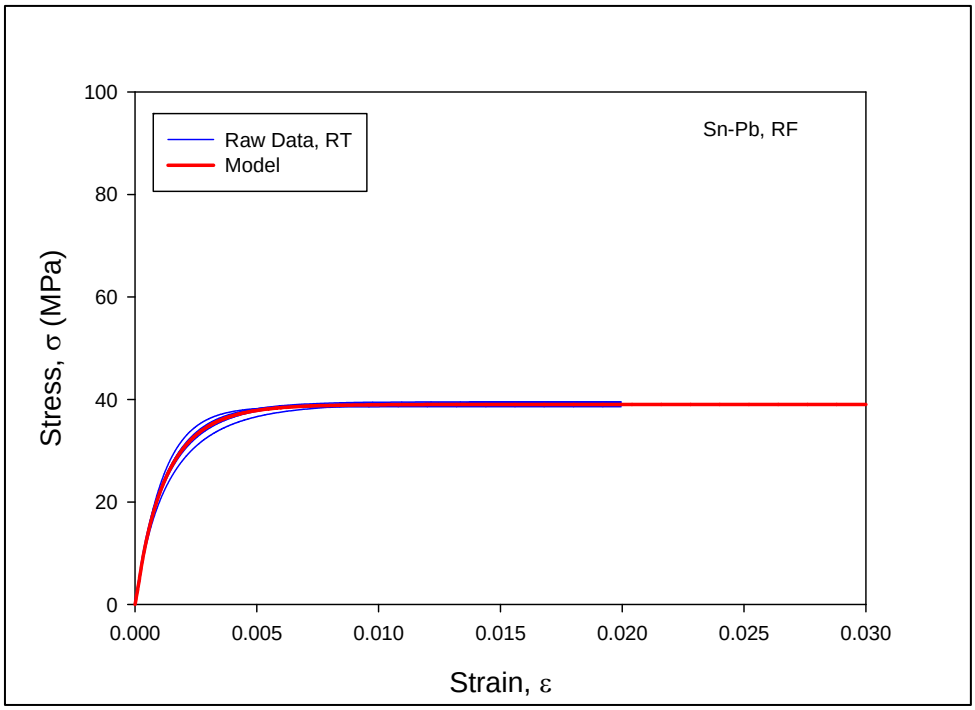

Figure A.9 - Stress-Strain Curves for 63Sn-37Pb at 25 ^{o}C

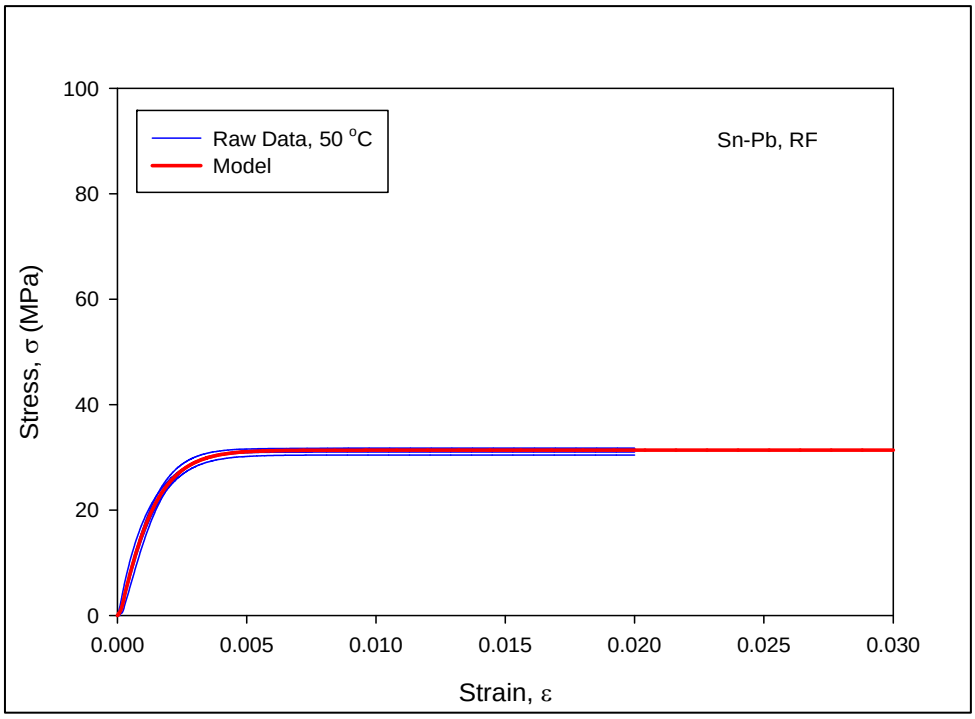

Figure A.10 - Stress-Strain Curves for 63Sn-37Pb at 50 ^{o}C

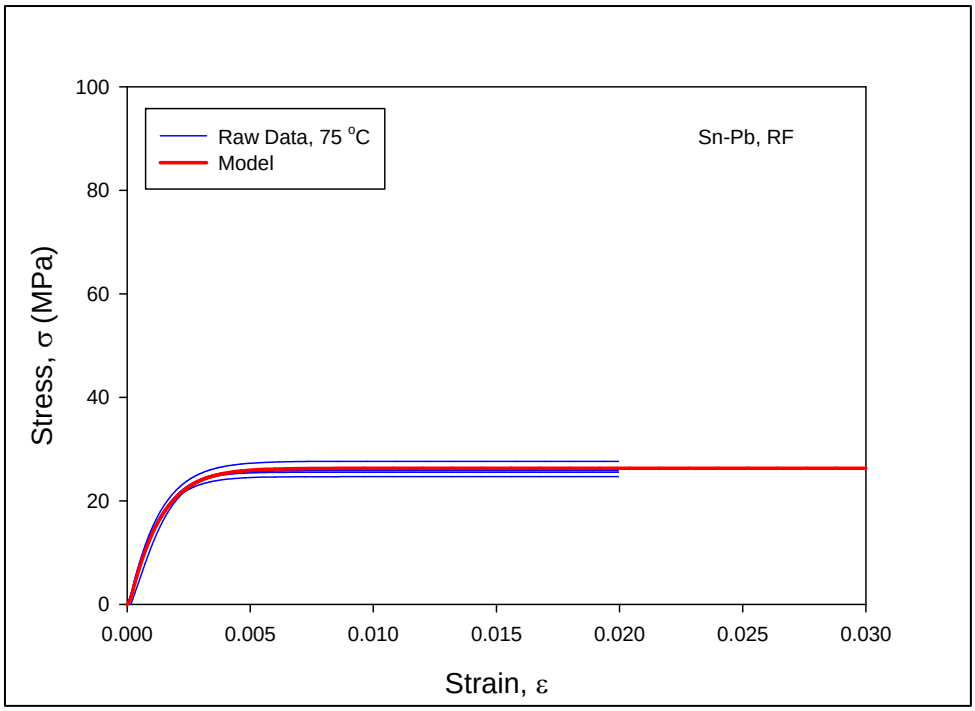

Figure A.11 - Stress-Strain Curves for 63Sn-37Pb at 75 °C

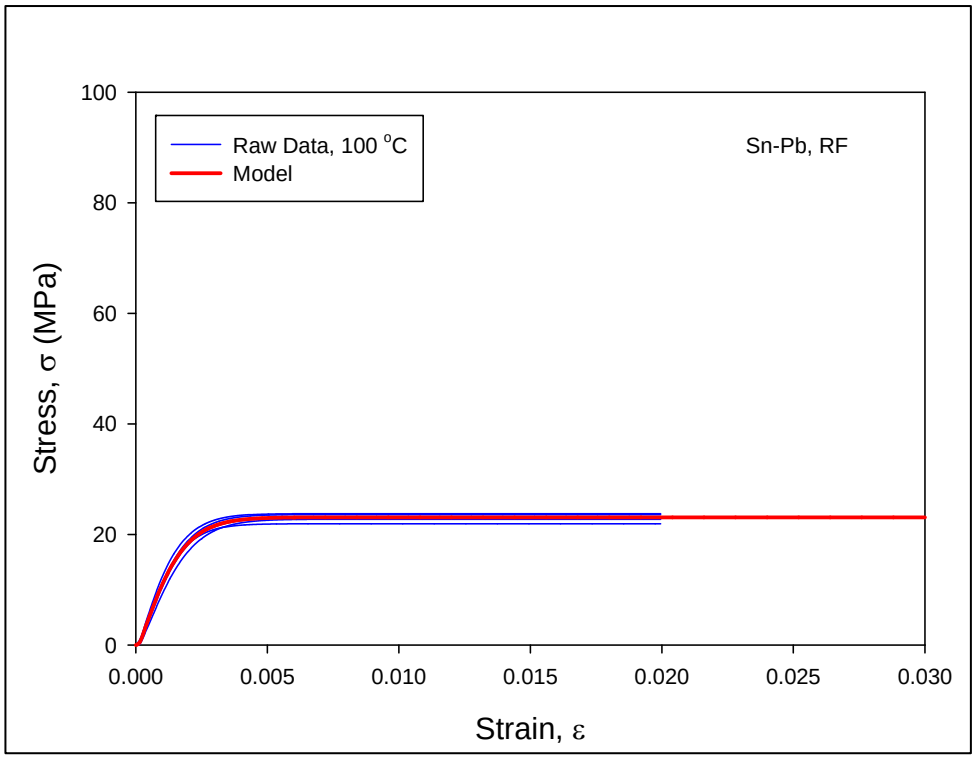

Figure A.12 - Stress-Strain Curves for 63Sn-37Pb at 100 °C

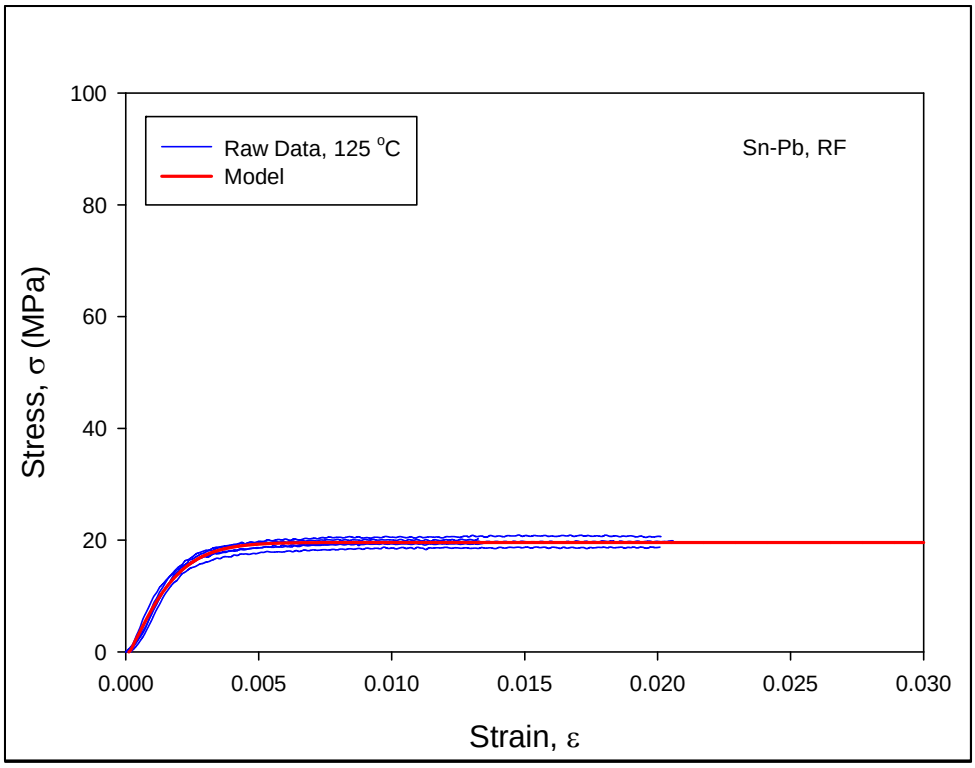

Figure A.13 - Stress-Strain Curves for 63Sn-37Pb at 125 °C

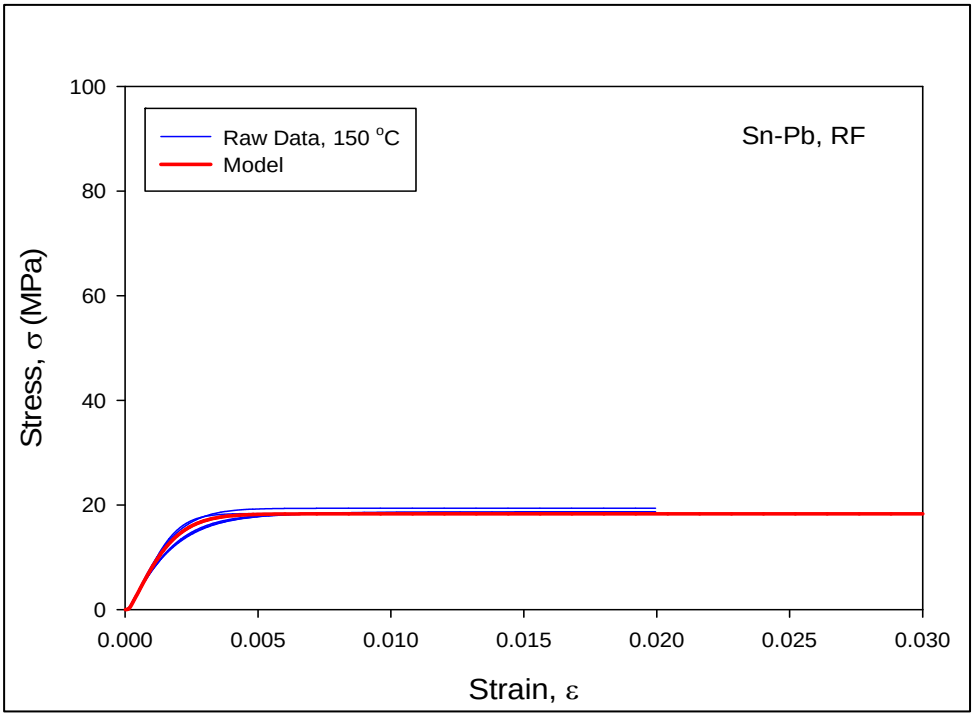

Figure A.14 - Stress-Strain Curves for 63Sn-37Pb at 150 °C

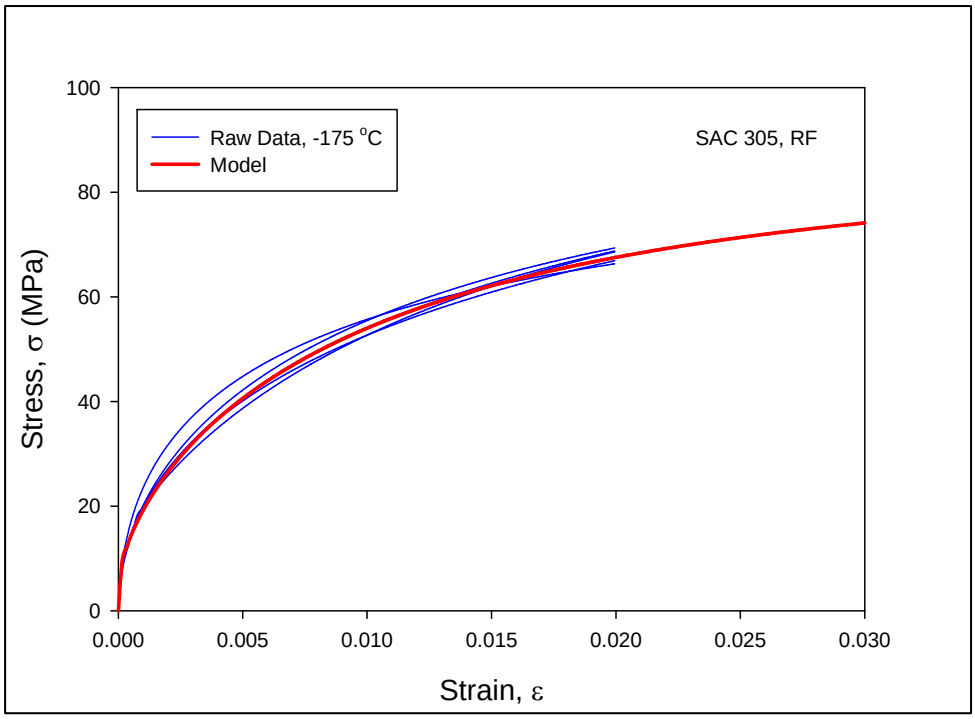

Figure A.15 - Stress-Strain Curves for SAC 305 at -175 °C

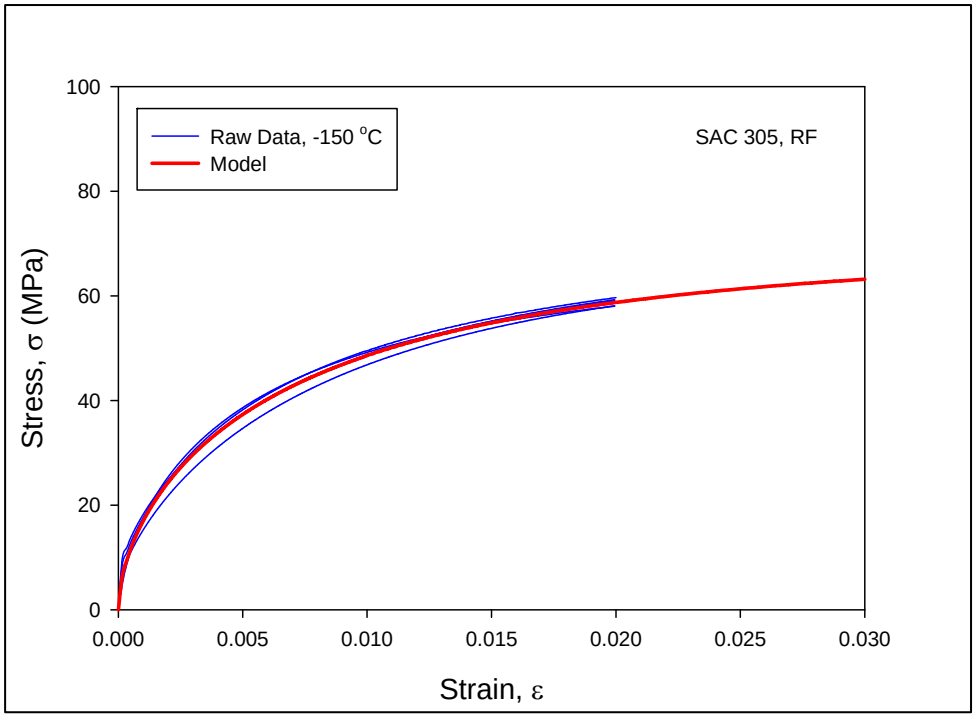

Figure A.16 - Stress-Strain Curves for SAC 305 at -150 °C

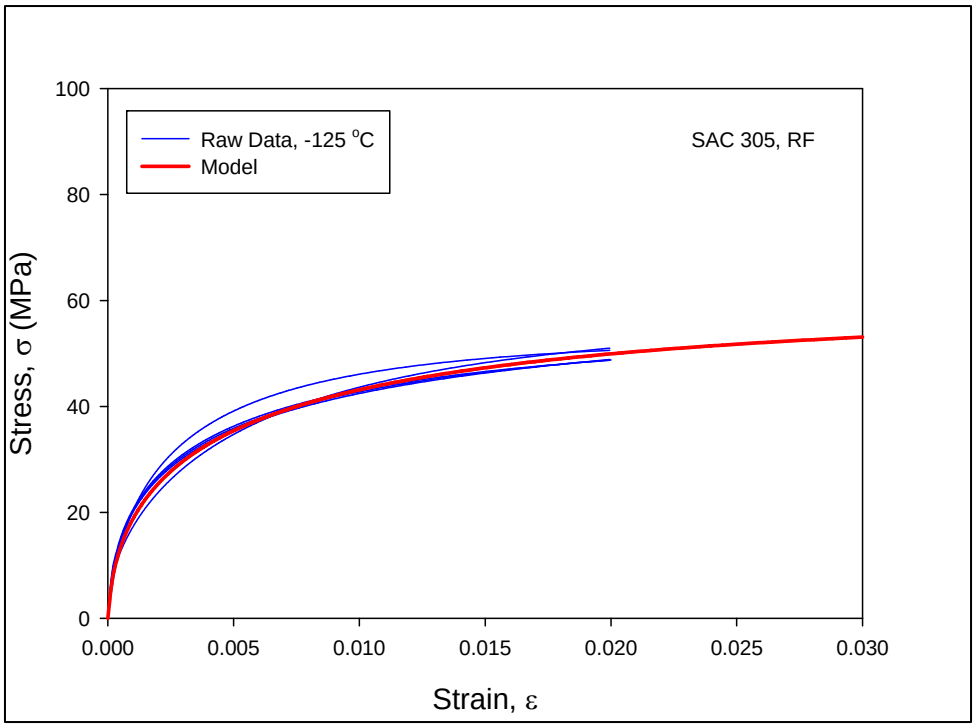

Figure A.17 - Stress-Strain Curves for SAC 305 at -125 °C

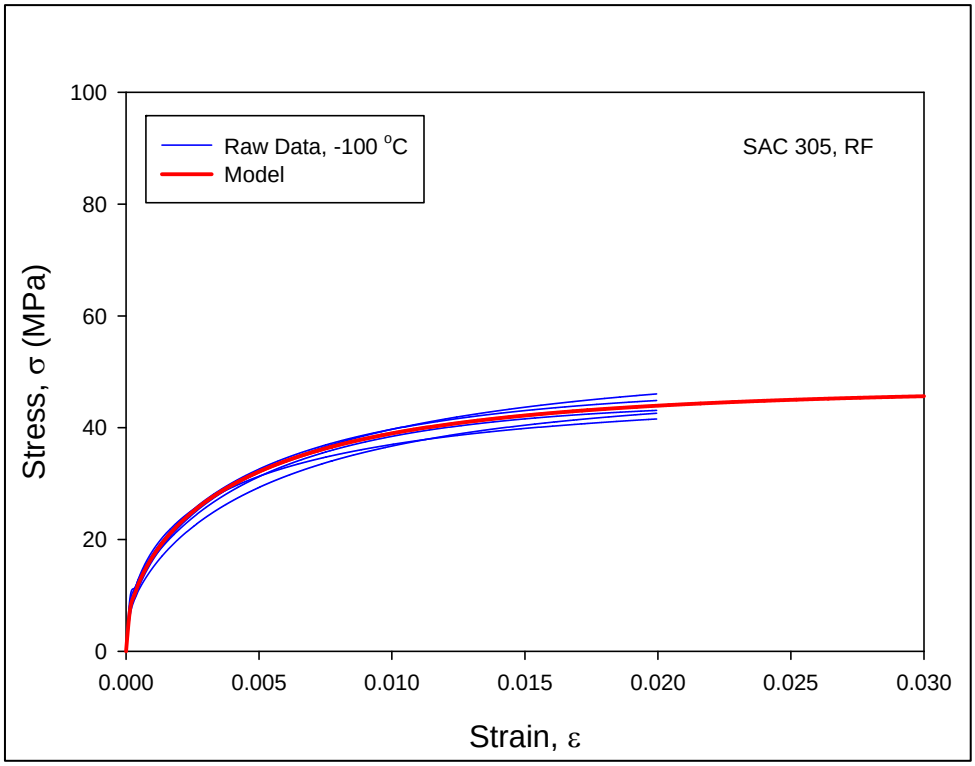

Figure A.18 - Stress-Strain Curves for SAC 305 at -100 °C

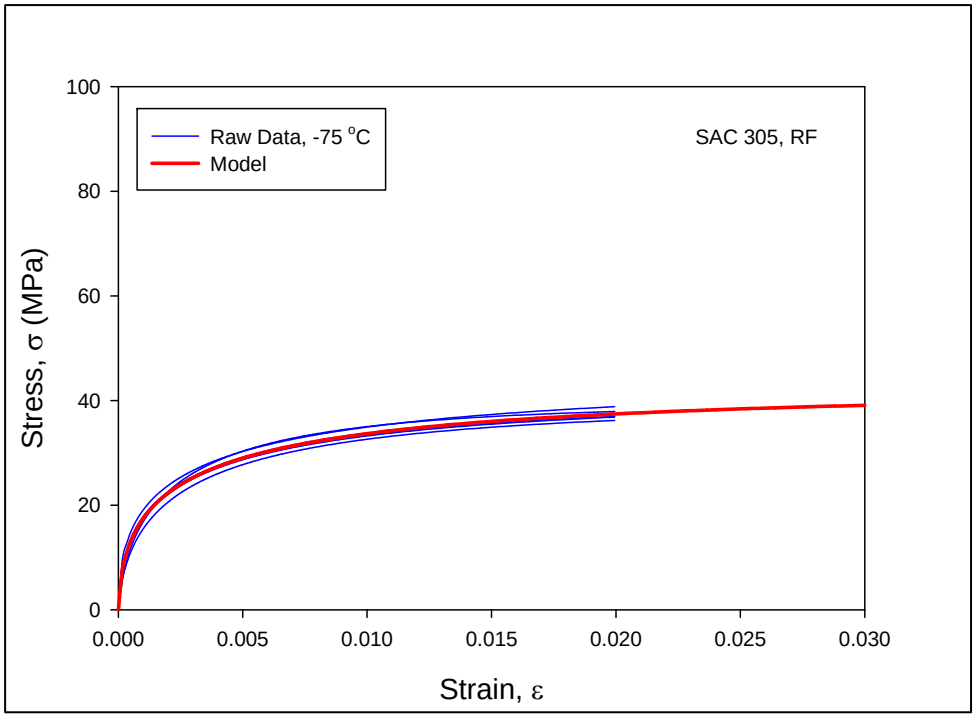

Figure A.19 - Stress-Strain Curves for SAC 305 at -75 °C

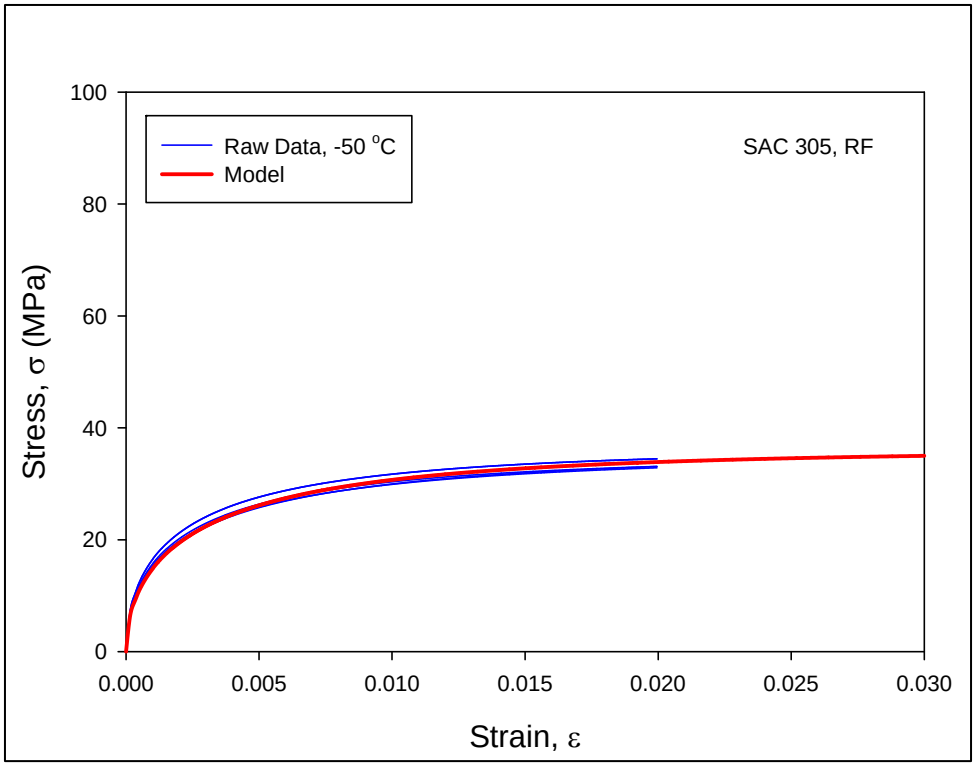

Figure A.20 - Stress-Strain Curves for SAC 305 at -50 °C

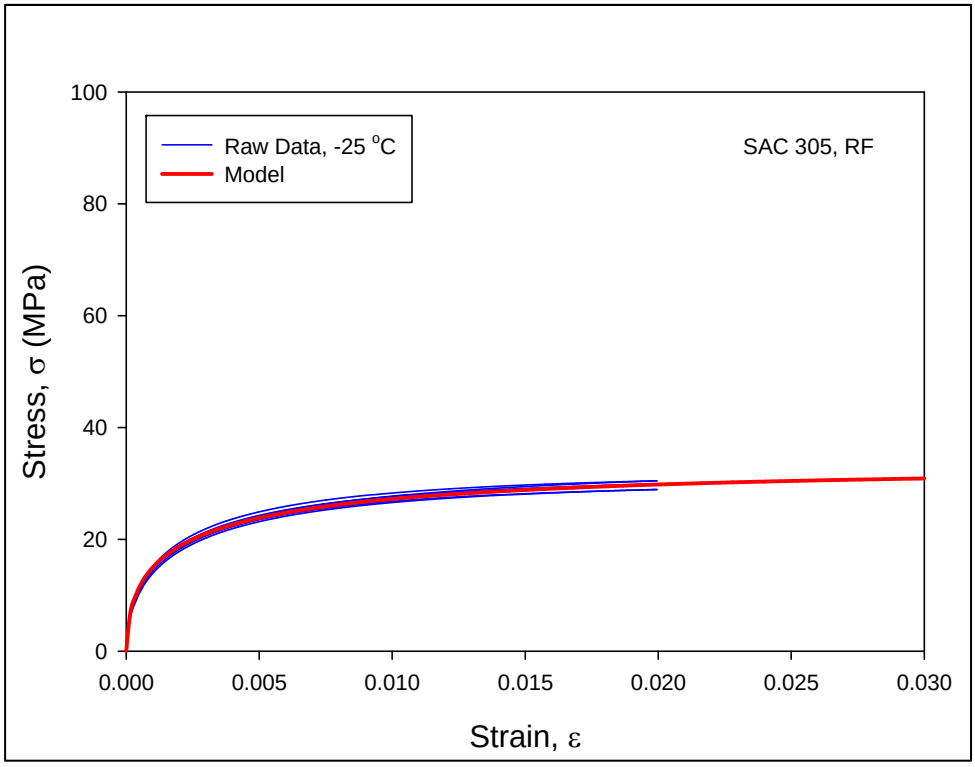

Figure A.21 - Stress-Strain Curves for SAC 305 at -25 °C

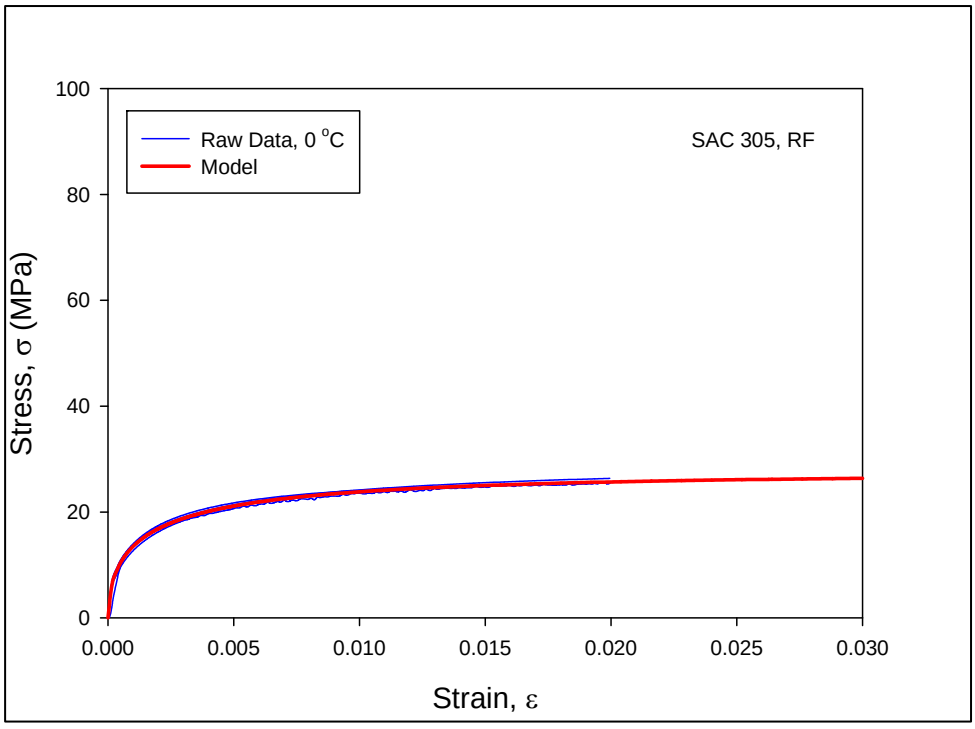

Figure A.22 - Stress-Strain Curves for SAC 305 at 0 °C

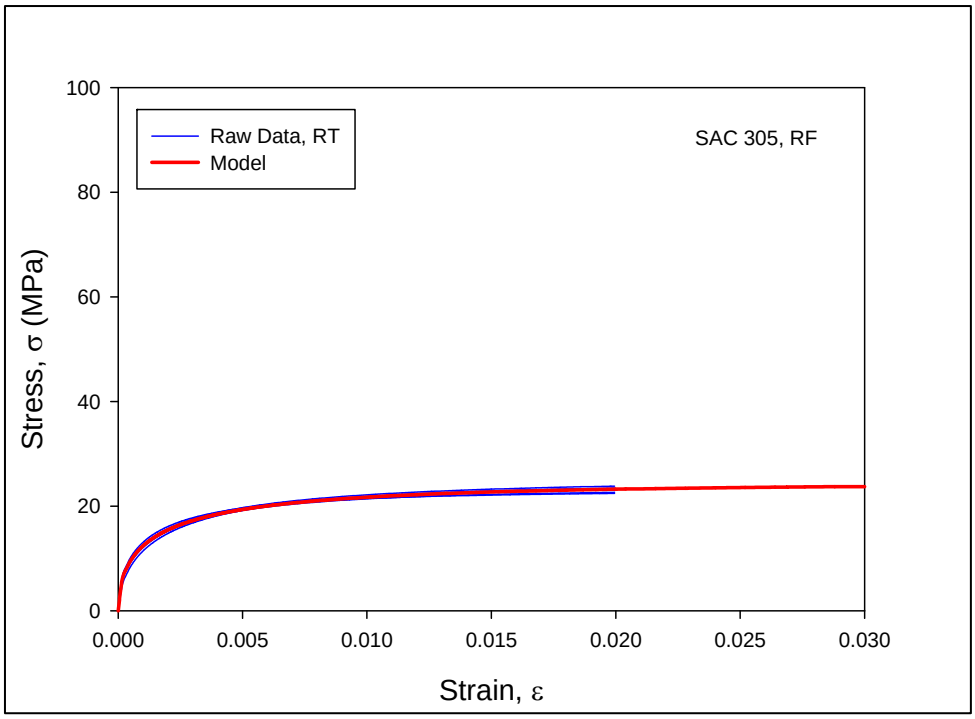

Figure A.23 - Stress-Strain Curves for SAC 305 at 25 ^{o}C

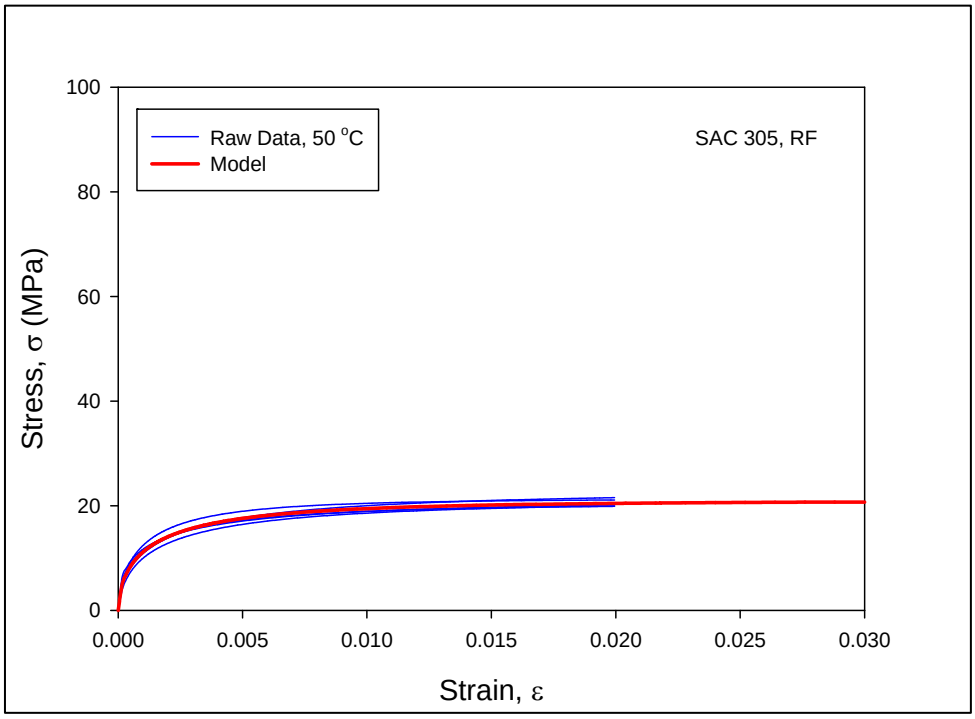

Figure A.24 - Stress-Strain Curves for SAC 305 at 50 ^{o}C

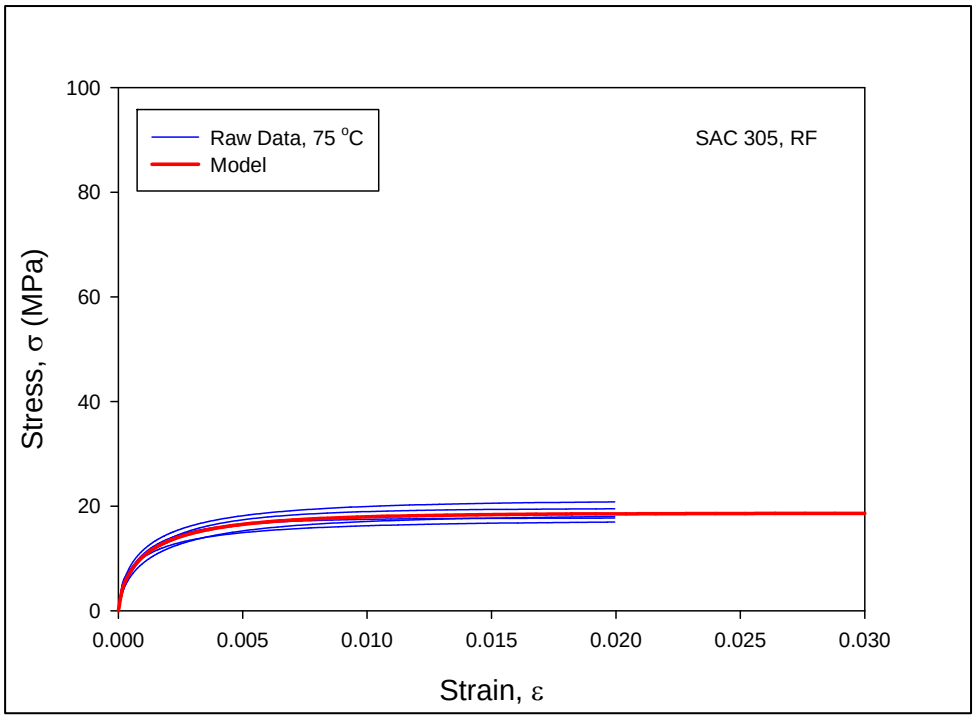

Figure A.25 - Stress-Strain Curves for SAC 305 at 75 °C

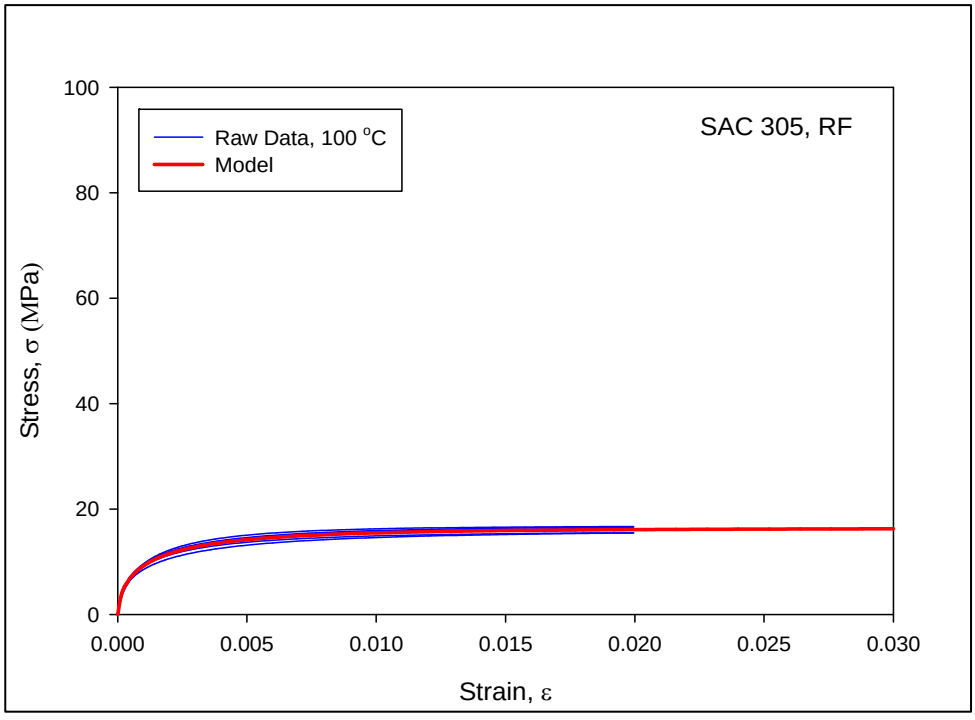

Figure A.26 - Stress-Strain Curves for SAC 305 at 100 °C

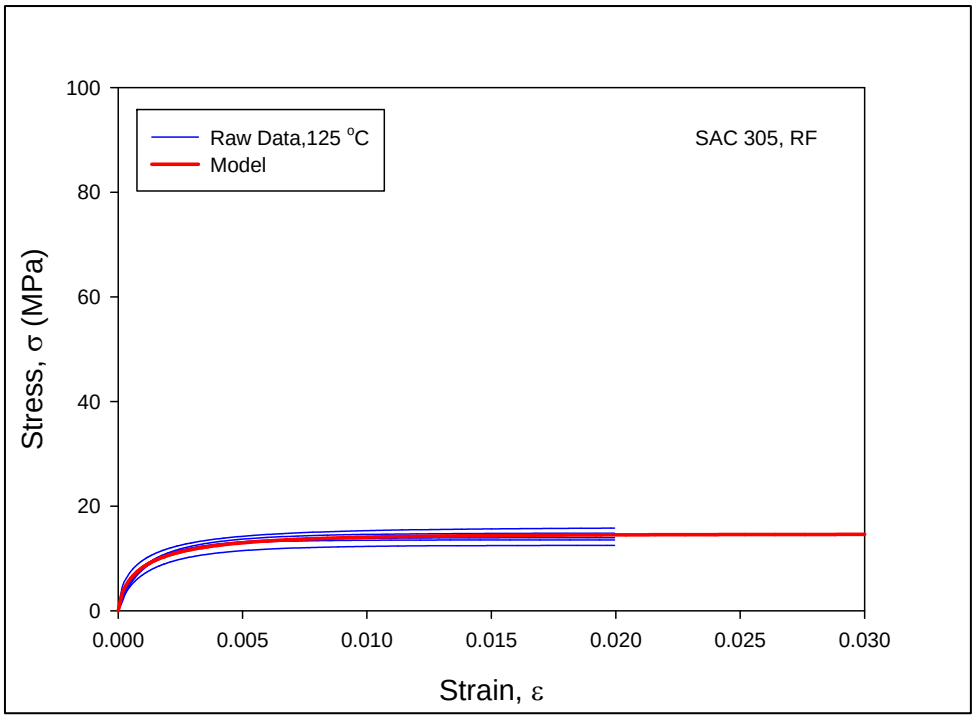

Figure A.27 - Stress-Strain Curves for SAC 305 at 125 °C

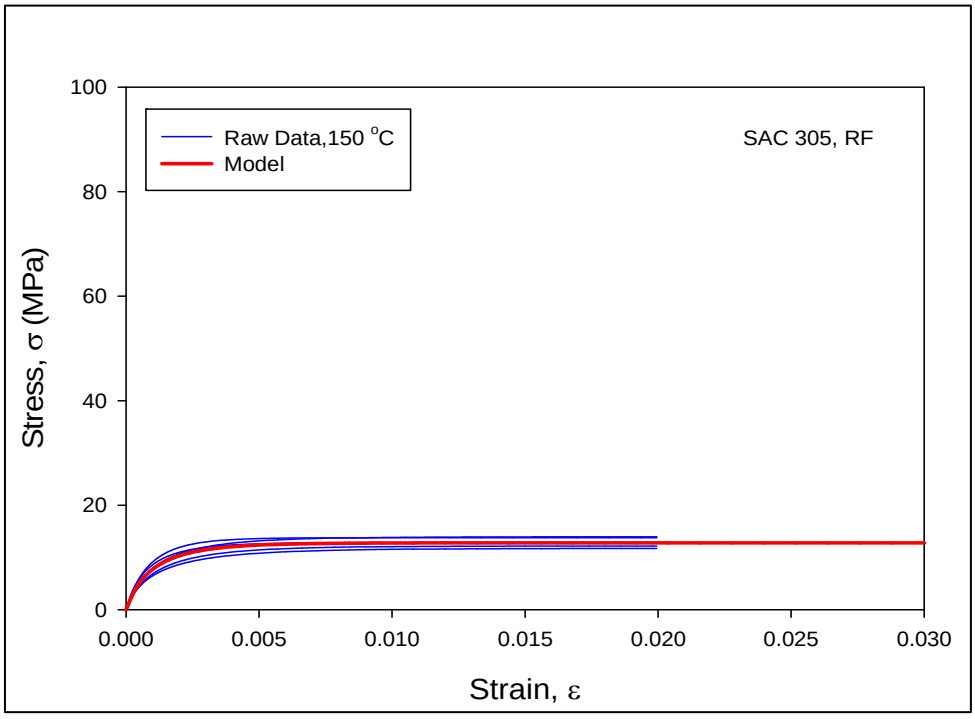

Figure A.28 - Stress-Strain Curves for SAC 305 at 150 °C